The University Of Sheffield.

Conventional and Microwave Pyrolysis of Empty Fruit Bunch and Rice Husk Pellets

By:

Noor Afiqah Binti Mohd

A Thesis Submitted
For the Degree of Doctor of Philosophy

Department of Chemical & Biological Engineering

University of Sheffield

February 2017

Executive Summary

In recent years, microwave pyrolysis has been the focus of intense research due to the claim that it produced better quality products at a lower power input compared to the electrical furnace pyrolysis system. This study aimed to investigate the influence of both pyrolysis methods on yield and product composition obtained from Malaysian biomass, *i.e.*: empty fruit bunch and rice husk pellets. They represent lignocellulosic biomass procured as by-products of the milling process.

In the first part of the thesis, an initial characterisation of biomass was conducted to determine the chemical composition. It was found that the biomass in this study has moisture and volatiles content at around 5.4 wt.% and 70 wt.%, respectively which makes them ideal for the pyrolysis process. 200g of biomass was loaded into a 15.8kW fixed-bed pyrolysis reactor once the reactor had reached the set temperature. Typically, 40g of biomass was pyrolysed in a specially designed 1000W multi-mode microwave oven, where microwaves were fed into the oven cavity through a bottom-feed waveguide.

It was found that microwave pyrolysis gave a higher bio oil and char yield than conventional pyrolysis at a similar reaction temperature. Up to 8.40% increase in bio oil yield was observed when rice husk pellets were pyrolysed under microwave radiation at 800ºC. GC-MS analysis revealed a greater content of mono-aromatics compounds obtained from microwave pyrolysis oils with negligible Polycyclic Aromatic Hydrocarbons (PAH) than conventional pyrolysis oils. Similarly, greater cracking of heavier hydrocarbons at high temperature resulted in up to 44% increase in phenol formation from microwave pyrolysis oils.

A maximum surface area of 410m^2/g was also recorded during microwave pyrolysis of rice husk pellets at 500ºC, where this value reduces with an increase in pyrolysis temperature. Moreover, microwave pyrolysis resulted in up to 29% increase in syngas (H_2+CO) evolution and about 42% lower greenhouse gases (CH_4+CO_2) than conventional pyrolysis. These differences can be attributed to internal heat generation during microwave processing in contrast to conduction from the surface inwards during conventional heating. Energy yield analysis suggested that microwave pyrolysis can be optimised for the production of high quality char and bio oil. Meanwhile, conventional pyrolysis can be optimised to enhance syngas production.

The second part of this thesis looks into the effect of waveguide position and biomass bed height on the electric field and its corresponding temperature distribution. Numerical modelling has shown that higher temperature rise can be generated in a larger load due to greater microwave power deposited. Moreover, an increase in relative permittivity was observed as biomass was converted into char during pyrolysis. This showed that microwave pyrolysis of biomass can be a self-sustaining process, without any addition of microwave absorber.

It was concluded that viable industrial application of microwave pyrolysis is very promising

Acknowledgements

I wish to express sincere gratitude to my supervisors; Professor Jim Swithenbank, Dr. Vida Sharifi and Dr. Grant Wilson for their endless support and supervision. Many thanks to David Palmer, Mike O'Meara, and Oz MacFarlane for providing technical support. Special thanks to Dr. M Sandhu from the Institute of Microwave and Photonics, Leeds University for assistance with dielectric characterisation. Special thanks to Majlis Amanah Rakyat (MARA) and Universiti Kuala Lumpur (UniKL) for providing financial assistance over the course of my study. To my family and friends, thank you.

Table of Contents

List of Tables

List of Figures

Nomenclatures

Abbreviations

BET	Brunauer-Emmett-Teller
CCGT	Combined Cycle Gas Turbine
CHP	Combined Heat and Power
CP	Conventional Pyrolysis
DTG	Derivative Thermogravimetry
EDS	Energy Dispersive Spectroscopy
EFB	Empty Fruit Bunch
EM	Electromagnetic
FIT	Feed-In Tariff
FTIR	Fourier Transform Infrared
GCV	Gross Calorific Value
GHG	Greenhouse Gases
LPM	Litre Per Minute
MP	Microwave Pyrolysis
PAH	Polycyclic Aromatic Hydrocarbons
RH	Rice Husk
SEM	Scanning Electron Microscopy
SVOC	Semi-Volatile Organic Compounds
TGA	Thermogravimetry Analysis
VOC	Volatile Organic Compounds

Symbol	**Description**	**SI unit**
ΔT	Temperature difference	^oC
B	Magnetic flux density	T
Bi	Biot number	-
C_p	Heat capacity at constant pressure	J/kgK
E	Electric field intensity	V/m
e_1	Correction for heat of formation HNO_3	J
e_2	Correction for heat of formation of H_2SO_4	J
e_3	Correction for heat of combustion of fuse wire	J
E_b	Energy content of biomass	J/kg
E_i	Energy content of pyrolysis product	J/kg

E_s	Source electric field	V/m
f	Frequency	Hz
h	Convective heat transfer coefficient	W/m^2K
H	Magnetic field intensity	A/m
J	Current density	A/m^2
k	Thermal conductivity	W/mK
k_0	Wave number of free space	rad/m
l	Length	m
L_c	Characteristic length	m
m	Mass	kg
N	Complex refractive index	-
P	Partial pressure of N_2	Pa
P_0	Saturation pressure of N_2	Pa
Q_b	Energy content of biomass	J/kg
Q_c	Energy content of pyrolysed char	J/kg
Q_e	Electrical energy	J/kg
Q_g	Energy content of pyrolysis gas	J/kg
Q_{loss}	Energy loss within the system	J/kg
Q_{oil}	Energy content of pyrolysis bio oil	J/kg
r	Radial position	m
T	Temperature	K
t	Time	s
T_0	Initial temperature of biomass	K
T_∞	Bulk temperature	K
$tan\ \alpha$	Loss factor	-
v	Volume of adsorbed gas	L
v_m	Volume of adsorbed gas in a monolayer	L
W	Energy Equivalent	J/ºC
x	Dimensionless distance	-
Y_i	Product yield	-
β	Propagation constant	rad/m
ΔY	Mass loss	kg
ϵ	Emissivity	-
ε	Permittivity	F/m
ϵ'	Dielectric constant	-

ϵ''	Dielectric loss	-
ε_0	Permittivity of free space (8.85×10^{-12})	F/m
ε_r	Relative permittivity	-
η	Efficiency	-
θ	Dimensionless temperature	-
μ	Permeability	H/m
μ_r	Relative permeability	-
ρ	Density	m^3/kg
σ	Stefan-Boltzmann constant (5.67×10^{-8})	W/m^2K^4
τ	Dimensionless time	-
ϕ	Diameter	m
ω	Angular frequency	rad/s
α	Thermal diffusivity	m^2/s

Chemical Compounds

CH_4	Methane
CO	Carbon monoxide
CO_2	Carbon dioxide
H_2	Hydrogen
H_2O	Water
K	Potassium
N_2	Nitrogen
Si	Silica
SiO_2	Silicon Dioxide

1 Introduction

This chapter looks into the current world energy scenario, the accumulation of waste biomass worldwide, and the cost of conversion technologies. It also looks into global warming as an imminent threat to humanity and pyrolysis as a solution to waste management and energy recovery. The aim and objectives of the present work are highlighted, along with thesis outline at the end of this section.

1.1 Current World Energy, Environment and Economy Scenario

The world's energy consumption is projected to increase by 48% between 2012 and 2040 with most demand coming from developing countries outside the Organisation for Economic Cooperation and Development (Doman, 2016). Energy demand is projected to reach above 8.44 x 10^{14} MJ. Emerging markets are projected to grow by 4.7% in 2017, with India as the fastest growing economy at a rate of 7.5%. India for instance, is the world's third largest producer of crude steel at 88.98 MT. This market is expected to grow further driven by growth in infrastructure development and rising demand from automotive industry (India Brand Equity Foundation, 2016). Steel manufacturing is one of the most energy-intensive industries. With this in mind, the nation is required to secure a stable supply of energy to sustain its long-term economic development.

Moreover, global population is projected to hit 9.7 billion mark by 2050, a 9% increase from 6.1 billion in 2000. This represents a serious need to address the solution in terms of food and energy security, resource and waste management to create a sustainable development without compromising the environment. Increasing energy demand would put a strain on the old centralised power generation and distribution.

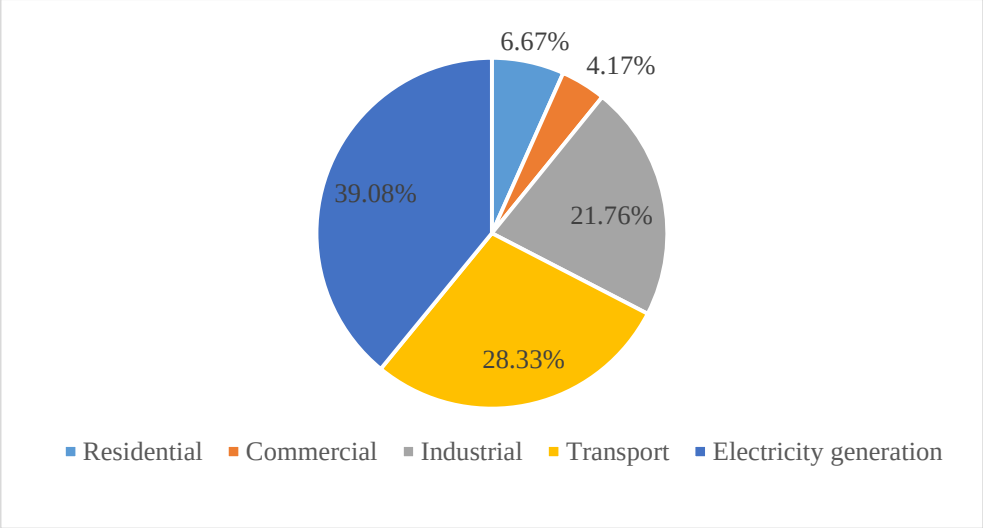

Figure 1-1: Energy consumption by sector in 2015 (Doman, 2016)

Primary energy supplies include coal, oil, and natural gas, along with smaller share of renewables. The breakdown of primary energy consumption is illustrated in *Figure 1-1*. According to the data released by U.S Energy Information and Administration (Doman, 2016), almost 40% or 4.02 x 10^{13} MJ of energy supplies goes into electricity generation. This is followed by transportation sector at 28.33%, fuelled mostly by oil and liquefied natural gas (LNG). The combination of the industrial, residential, and commercial sectors takes up around 32.60% of total energy supplies. Energy consumption and greenhouse gas (GHG) emissions are closely related. The former is driven by factors such as energy demand, climatic conditions, combustion engine inefficiency, and poor building insulation. For example, high energy consumption is expected during cold winter months for commercial and residential heating.

1.2 Greenhouse Gas Emission

Primary constituents of GHG include carbon dioxide, methane, nitrous oxide, chlorofluorocarbons, and hydro chlorofluorocarbons (known collectively as Freon gases). These gases are present in the lower atmosphere, with capability to absorb some of the

outgoing radiation leaving the earth. This in turn helps to keep the earth warm. However, activities such as deforestation, the burning of fossil fuels, and livestock farming are mainly responsible for anthropogenic GHG emissions. Since the beginning of Industrial Revolution, heavy emission of GHG into the atmosphere has altered the equilibrium of the natural carbon cycle.

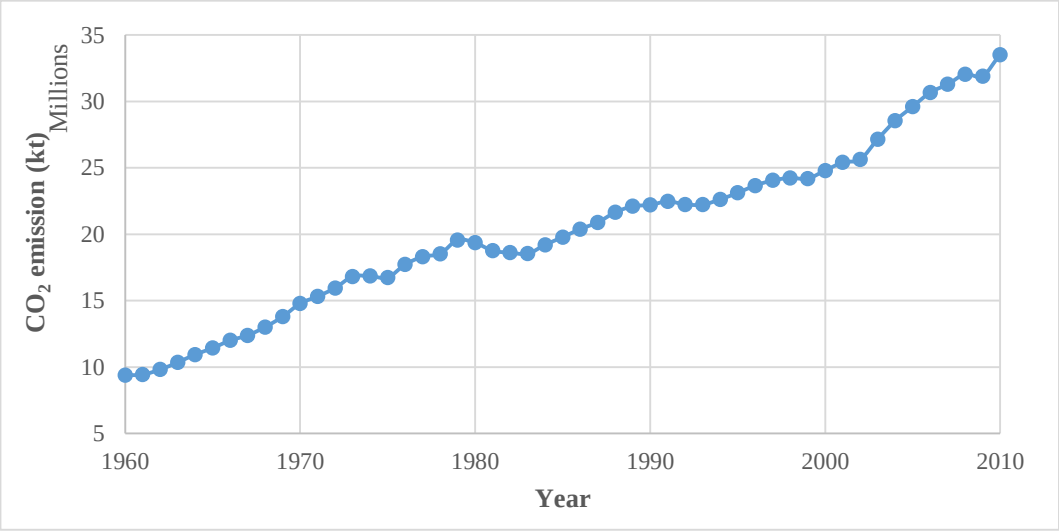

Figure 1-2: CO_2 emission (The World Bank, 2016)

Heavy reliance on traditional fossil fuels to fuel our economic growth has its own set of challenges. Total GHG emission in 2012 stands at 52.8 Giga Tonne (GT) of CO_2 equivalent. Carbon dioxide made up the largest fraction of total emissions at 34.65 GT in 2011, rising by 268.7% from the 1960 levels, as shown in *Figure 1-2*. Fossil fuel combustion, cement and steel manufacturing, and gas flaring are some of the main contributors for increased CO_2. Meanwhile, the concentration of methane in the atmosphere is alarming due to its high global warming potential (GWP). It is a measure of energy absorption of gas emitted, relative to carbon dioxide. In this case, methane is 25 times better at retaining heat than carbon dioxide, within 100 year time frame (United Nations Framework Convention on Climate Change, 2014a). Intensive livestock farming

and poor waste management have resulted in increase of CH_4 concentration. For instance, anaerobic decomposition of waste in landfill produced biogas, which consists around 50-55 vol. % CH_4 and 45-50 vol. % CO_2. However, the release of these gases could be avoided by utilising a proper landfill design with biogas collection. Other impacts of GHG emissions include acid rain, ozone depletion, and the creation of low level ozone.

1.3 Climate Change and Energy Security

Global warming has resulted in the melting of ice caps, rising sea levels, and an erratic global weather pattern. This is indicated by severe drought and increased in hurricane intensity in different parts of the world, which has led to damage incurred by real estate and income losses. Imminent effects of climate change include low crop yield and rising food prices, where poor countries are the most vulnerable. Sir Nicholas Stern in his Stern Review has concluded that the "benefits of early action to mitigate climate change far outweigh the economic costs of not acting". Delaying the actions to mitigate climate change would cost the world 5% of its annual Gross Domestic Product (GDP), due to climate-related damage. This report strongly recommends that the global GHG levels to be stabilised at around 450-550 ppm CO_2e in order to avoid 2°C increase in global surface temperature and mitigate the worst impact of climate change. This would require collective effort to reduce GHG emissions by at least 25% or more below current levels by 2050 (Stern, 2006).

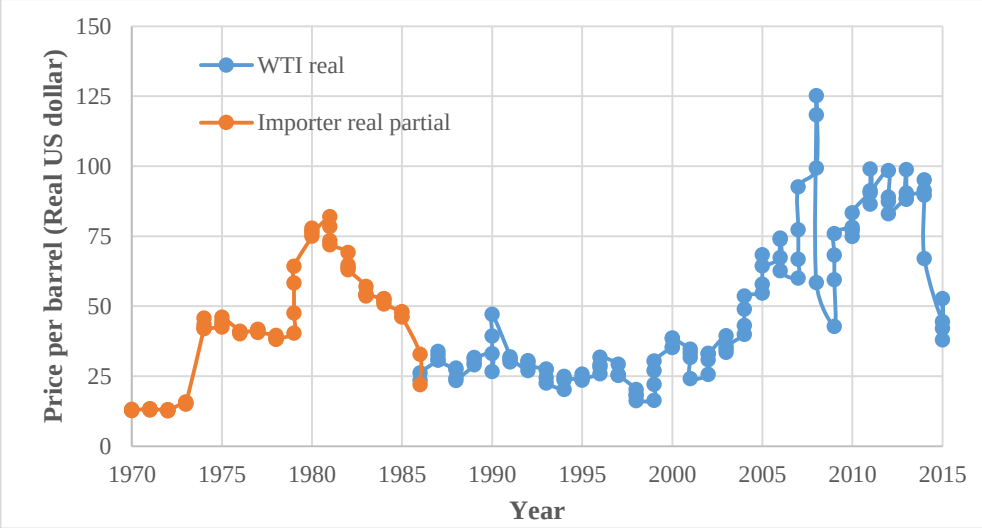

Figure 1-3: Crude oil prices (U.S Energy Information Administration, 2016)

Commodities such as oil and natural gas are traded on the global market. It is subjected to volatility in prices driven by factors such as geopolitical events, spare capacity, demand and supply, and market uncertainty. *Figure 1-3* shows the graph of crude oil prices over the past 45 years. 1973 oil crisis marked the first key event that drove the crude oil price from $15 to $42 (in 2010 USD), a year later. The Iran-Iraq war, global financial collapse, and production cut from OPEC are among key events that influence the global crude oil prices. This prompts the need to secure stable supply of fuels over the next decades.

1.4 Emissions Target

The Kyoto Protocol was adopted in 1997 in the first international joint effort to curb GHG emissions. It is based on a premise that industrialised nations were responsible for GHG released over the past 150 years of economic activity. It bound the 37 industrialised nations to reduce emissions by an average of 5%, from the 1990 level during its first commitment period (2008-2012). This is achieved through Joint Implementation, Clean Development Mechanism, and Emission Trading between developed and developing

countries. Kyoto Protocol is superseded by the Doha Amendment in 2012 for its second commitment period between 2013 and 2020. This amendment is ratified by 66 countries, with binding commitment to reduce GHG emission by 18%, relative to 1990 levels (United Nations Framework Convention on Climate Change, 2014b).

The emissions target, resource depletion, energy security, population growth, and climate change issues have triggered the need to find alternative fuels from renewable energy (RE) to ensure sustainable development. The current fossil-fuel based energy systems are not only environmentally unsustainable, they are also highly inequitable, leaving 1.4 billion people without access to electricity (United Nations Environment Programme, 2016). Renewable energy differs from non-renewables in the way that it replenishes faster for efficient extraction. Sources of renewable energy include wind, tidal, solar, geothermal, hydro, and biomass. With most emissions coming from the combustion of fossil fuels in power and transport sector, it is vital to switch into the low carbon technologies.

1.5 Costs of Technologies

High generation cost is one of the biggest challenges in the implementation of low carbon technologies. It is reflected by high electricity price which is passed on to the end consumer. Levelised cost of electricity (LCOE) is an average cost over the lifetime of generation plant, converted into equivalent unit of cost of generation in (£/MWh). It takes into consideration costs incurred during planning, construction, operating and decommissioning stages. It covers the capital cost, fixed and variable operational cost, fuel cost, and carbon tax. It provides assessment for different conversion technologies without

taking into account revenue streams generated; *e.g.*: sale of electricity. Cost estimates for a project starting in 2018 are presented in *Table 1-1*.

Table 1-1: Levelised cost of electricity for projects starting 2018, at 10% discount rate (Department of Energy & Climate Change, 2012)

Type	**Technologies**	**LCOE (£/MWh)**
Gas	CCGT	85
	CCGT with post comb. CCS	94
Biomass	< 50MW	115
	>50MW	121
Coal	ASC with FGD	113
	ASC with post comb. CCS	116
	IGCC	131
	IGCC with CCS	111
Nuclear		73
Wind	Onshore >5MW, E&W	101
	Onshore >5MW, UK	90
	Offshore R2	103
	Offshore R3	113

Gas and coal-fired power plants are equipped with post-combustion technologies such as Flue Gas Desulphurisation (FGD) and Carbon Capture and Storage (CCS), in an effort to reduce emission of GHG and pollutants, *e*.g.: SO_2 into the atmosphere. Development in high-temperature steel that is capable to withstand super-critical steam has seen the progress of Advanced Super-Critical Coal (ASC) which aims to increase net electrical efficiency. Meanwhile, in the Integrated Gasification Combined Cycle (IGCC), coal is first gasified to produce synthesis gas and cleaned to remove impurities prior to combustion in a gas turbine. These relatively new technologies together with carbon tax are making power generation from coal expensive. For example, ASC with post combustion CCS would cost £116/MWh.

Nuclear power generation although financially attractive due to cheap fuel cost at £73/MWh is faced with uncertainties over public perception fuelled by recent nuclear incidents. However, biomass conversion technologies are not particularly inexpensive, either. Large generation plant (>50 MW) would cost £121/MWh. Fuel cost contributes a large fraction of total cost at 53.72%. This can be attributed to demanding fuel handling requirement, fuel transport, and storage facilities. This includes pre-treatment processes; *e.g.*: grinding and drying and post-combustion clean-up. Rising fossil-fuel prices and carbon tax levied on fossil fuel generators could drive biomass to be cost competitive in the generation market.

1.6 Biomass

Biomass is a precursor of coal formation, described as organic matter of recent biological origin. Incorporating biomass into the energy generation mix provides several advantages. The global potential of biomass is very broad, estimated at around 33-1135 EJ/year within 50 years timeframe, with agricultural and forestry residues accounting for most of these wastes (Hoogwijk et al., 2003). Daioglou *et al.* (Daioglou et al., 2016) put this figure at 120 EJ/year, and theoretically it could increase up to 140-170 EJ/year. Two-thirds of these comes from the high residue yield plantations in Asia and North America regions. It provides energy security and sustainable development as biomass energy generation does not contribute to natural carbon source; *i.e.*: CO_2 neutral. This is based on a premise that carbon dioxide absorbed by a plant during its lifetime is released to the atmosphere during energy conversion. This could reduce the global carbon footprint in an effort to mitigate global warming.

Biomass has traditionally been used in low energy applications such as domestic cooking and heating in a rural community. Biomass such as wood, charcoal and animal manure is combusted indoor with low conversion efficiency, leading to soot emission which imposes a respiratory health risk. Globally, agricultural residues have been used as feed in biomass-fired CHP plants across Scandinavia, Latin America, and India. For instance, Brazil as the major sugarcane producer has been burning sugarcane bagasse in its co-generation plants, with surplus electricity exported to the utility grid. Sweden has set the best example with its commitment towards renewable energy generation. Currently, 66.4% or 246 TWh of total domestic energy in Sweden is supplied by a mix of renewable sources. The total share of bioenergy generation has surpassed oil at 35.2%, with forestry residues as the primary source of fuel (The Swedish Bioenergy Association, 2016).

1.7 Biomass Conversion Technologies

Biomass conversion technologies exploit the stored chemical energy within a biomass structure into another form of useful energy. *Figure 1-4* highlights the major routes for energy conversion from biomass, which includes biochemical and thermochemical technologies. Choice of conversion technology is heavily influenced by feedstock availability, desired end user, environmental standard, and total cost (Saidur et al., 2011). Biochemical conversion is ideal for 'wet' biomass with more than 50% water content, *e.g.*: sewage sludge. Some of the techniques include anaerobic digestion, fermentation, and esterification.

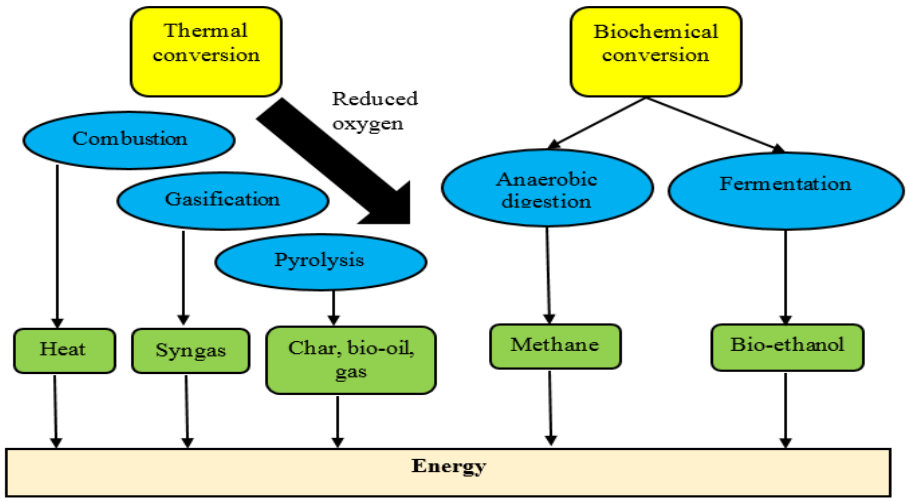

Figure 1-4: Biomass conversion technologies. Adapted from (Basu, 2010a)

Thermal conversion technologies include combustion, gasification, and pyrolysis. Direct combustion or incineration is considered a mature technology, while gasification and pyrolysis are still less proven at industrial scale. The main difference between thermal conversion technologies is the oxygen supplied during the process. Combustion under stoichiometric condition generates heat that can be used in a steam or gas turbine. Partial oxidation of fuel or gasification is designed to optimise the production of syngas, *e.g.*: CO, H_2, and CH_4. These high calorific value (CV) gases can be used directly in internal combustion engines or synthesised into liquid fuels under Fischer-Tropsch process.

Meanwhile, pyrolysis is thermal decomposition of biomass in an inert environment. Unlike combustion process, pyrolysis has garnered attention due to the prospect of valuable product recovery, ranging from char and bio oil~~,~~ to gas. For example, lignocellulosic phenol in bio oil could be a substitute for petroleum-based phenol. The release of moisture and volatiles during pyrolysis leaves behind carbon-rich char of high calorific value. In short, the pyrolysis process has the ability to yield a range of value-added products relative to the initial feedstock.

Until recently, the pyrolysis process has been conducted in an externally-heated reactor where the mode of heat transfer is by conduction, convection, and radiation (Chen et al., 2008). This process is often subjected to several limiting factors which influence product yield and distribution. The current study is looking to exploit microwave radiation to conduct the pyrolysis process, with the aim to produce higher yield and better quality products than conventional pyrolysis.

1.8 Aim and Objectives of the Present Work

To the best of this author's knowledge, no comparative study has been done so far on the thermal behaviour of empty fruit bunch and rice husk pellets under microwave heating and comparing it with conventional heating. This study aims to investigate the effect of the heating process and temperature on the yield and characteristics of char, bio oil and syngas. The experiments were carried out using a fixed-bed pyrolysis reactor and a modified laboratory microwave oven at varying sample temperature, by keeping other parameters constant. Characterisation of biomass feedstock before and after pyrolysis process was also performed. This covers various analyses such as proximate analysis, ultimate analysis, dielectric properties, heating value, FT-IR, GC-MS, surface area analysis and surface image analysis.

Moreover, the detailed behaviour of the electromagnetic field and the effect on dielectric heating of biomass in a multi-mode microwave oven is not fully understood. A multi-physics software package was used to model the microwave heating process. This fundamentally based study is also designed to investigate the effect of waveguide location and biomass bed height on microwave heating efficiency. This is compared with transient heat conduction in conventional heating. Finally, this original study seeks to analyse the

savings associated with the microwave pyrolysis process for the selected Malaysian materials and assesses the potential for industrial scale up.

1.9 Novelty

Comparative study on the characterisation of liquids obtained from conventional and microwave pyrolysis can be considered as novelty of the present work. To the best of author's knowledge, no such study has been done on pyrolysis bio oil. It has successfully demonstrated the effect of microwave technology in eliminating the long-chain hydrocarbons and increasing the presence of mono-aromatics in bio oil.

1.10 Thesis Layout

Chapter 1 explores the underlying issues that rationalise pyrolysis as a route to energy recovery. Chapter 2 looks into the literature and previous work done in this area, including the review of numerical simulation of microwave and conventional heating. Meanwhile, chapter 3 provides a detailed description of experimental setups and methodologies used for biomass and pyrolysis product characterisation. Chapter 4 discusses the properties of biomass materials used in this study and the influence of temperature and heating method on pyrolysis product distributions. This section also sets procedures to determine the efficiency of a pyrolysis system. This is followed by numerical simulation of microwave and transient heating in Chapter 5. Meanwhile, Chapter 6 looks into the challenges and opportunities associated with the scale-up of microwave processing of biomass for biofuels production. Finally, conclusions derived from this study along with some suggestions for future work are highlighted in Chapter 7.

2 Literature Review

This chapter provides a critical review of the work that has been done in this area. It starts with providing an overview of biomass composition, pyrolysis mechanism and the properties of pyrolysis products. The difference between conventional and microwave pyrolysis is also discussed. A summary of previous work done in the area of microwave processing of biomass is presented, followed by a section on numerical simulation of microwave and transient heating.

2.1 Introduction to Biomass

Different interpretation exists with regards to biomass classification. Biomass can be grouped into two major categories; virgin and waste biomass. This is highlighted in *Table 2-1*. In essence, virgin biomass is extracted from primary sources and is grown for specific purpose, *i.e.*: energy crops. Meanwhile, waste biomass is a secondary source of biomass-derived products such as municipal solid waste, agricultural residues, and cooking oil. They represent a prospect for valuable energy recovery, turning waste into useful products.

Table 2-1: Biomass major groups. Adapted with permission from (Basu, 2010b)

Biomass type	Sub-class	Examples
Virgin	Terrestrial biomass	Grasses, energy crops, cultivated crops
	Aquatic biomass	Algae, water plant
Waste	Municipal waste	Municipal solid waste (MSW), sewage sludge, landfill gas
	Agricultural solid waste	Livestock manure, agricultural crop residue
	Forestry residues	Bark, leaves, floor residues
	Industrial wastes	Demolition wood, sawdust, waste cooking oil

2.1.1 Lignocellulosic Biomass

The photosynthesis process utilises water and carbon dioxide in the presence of light to produce carbohydrate and oxygen, which are essential for growth as outlined in Eq: 2-1 (Basu, 2010b) . Some parts of plants; *e.g.*: stem, straw, husk are fibrous and are deemed unfit for human consumption. These components are known as lignocellulose. Unlike sugar-rich crops, *e.g.*: corn that is digestible through fermentation, lignocellulosic biomass requires a different treatment.

$$6H_2O + 6CO_2 \rightarrow 6CH_2O + 6O_2 \qquad \text{Eq: 2-1}$$

Lignocellulosic biomass is made up of hemicellulose, cellulose, lignin, and a smaller number of extractives. A schematic of lignocellulosic components of biomass is illustrated in *Figure 2-1*. According to Vassilev *et al.* (Vassilev et al., 2010), their composition varies between biomass depending on biomass type, species, growth process, and growing condition. Hemicellulose $(C_5H_8O_4)_n$ is a short branched polymer made up of five to six sugar monomers. Glucose, xylose, mannose, galactose, and arabinose constitute the hemicellulose. It has an amorphous structure with low degree of polymerisation (~100-200), making it suitable for hydrolysis. It thermally decomposes at low temperature at around 200-260°C, and is mainly responsible for the production of non-condensable gases and less tar.

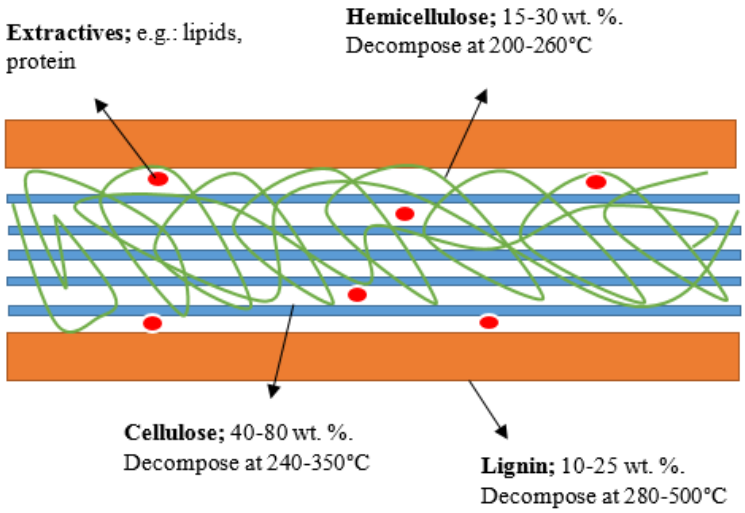

Figure 2-1: Schematic of lignocellulosic components of biomass. Published with permission from (Yin, 2012)

Unlike hemicellulose, cellulose $(C_6H_{10}O_5)_n$ is a long chain polymer made up of glucose monomers. It makes up the major components of lignocellulosic biomass, at around 40 to 80 wt.%. Its crystalline structure with high degree of polymerisation ~10,000, gives it a better thermal degradation than hemicellulose. Cellulose thermally degrades at a temperature around 240-350°C (Yin, 2012) .

Meanwhile, lignin is the primary building block of plant cell wall which provides structural strength and resistance against microbial infection. It is made up of branched polymers of phenyl-propanoid, or 4-propenyl phenol, 4-propenyl-2-methoxy phenol, and 4-propenyl-2.5-dimethoxyl phenol, held together by aromatic benzene rings (Diebold, 1994). The presence of ether bonds and carbon-carbon bonds give it a low degree of oxidation and thus, a higher heating value. Lignin decomposes at a temperature higher than that of cellulose and hemicellulose, at around 280-500°C (Mohan et al., 2006). It is mainly responsible for the formation of char and phenol found in bio oil. However, the presence of lignin in plant cell wall hinders enzymatic hydrolysis of carbohydrates, *i.e.*: cellulose from taking place. This is due to high insolubility of lignin in acid. For this reason, thermal

conversion of lignocellulosic biomass is preferable to biochemical process. The biochemical conversion route would require pre-treatment process to break the lignin wall and loosening the crystalline structure of cellulose and hemicellulose.

An example of pre-treatment is steam explosion, which is aimed to destroy the fibril structure of plant cell wall. During this stage, biomass is subjected to high pressure steam during a short period of time, and depressurised back to atmospheric pressure. This is a complex process where considerable amount of by-products must be removed before subsequent fermentation can take place. Incomplete separation of lignin and cellulose, as well as the presence of by-products during fermentation could inhibit the bio-ethanol formation (Cheng, 2010).

2.2 Biomass Properties

Calorific value is the measure of heat energy released when a specific quantity of fuel undergoes complete combustion. This analysis is often conducted in a bomb calorimeter under constant-volume condition, and expressed as (J/kg). Energy content in biomass is influenced by factors such as moisture content, lignin content, oxygen: carbon ratio and hydrogen: carbon ratio. In general, the heating value of biomass is comparable to low rank coal at around 10-20 MJ/kg due to its high oxygen and ash content (Saidur et al., 2011). Properties of biomass in comparison to bituminous coal are tabulated in *Table 2-2*.

Table 2-2: Biomass properties. Published with permission from (Jenkins et al., 1998)

	Coal[a]	Wheat straw	Rice straw	Switch-grass
Proximate analysis (% dry fuel)				
Fixed carbon	77	17.71	15.86	14.34
Volatile matter	18.49	75.27	65.47	76.69
Ash	4.51	7.02	18.67	8.97
Total	100	100	100	100
Ultimate analysis (% dry fuel)				
Carbon	87.52	44.92	38.24	46.68
Hydrogen	4.26	5.46	5.2	5.82
Oxygen (diff.)	1.55	41.77	36.26	37.38
Nitrogen	1.25	0.44	0.87	0.77
Sulphur	0.75	0.16	0.18	0.19
Chlorine	0.16	0.23	0.58	0.19
Ash	4.51	7.02	18.67	8.97
Total	100	100	100	100
Elemental composition of ash (%)				
SiO_2	37.24	55.32	74.67	65.18
Al_2O_3	23.73	1.88	1.04	4.51
TiO_2	1.12	0.08	0.09	0.24
Fe_2O_3	16.83	0.73	0.85	2.03
CaO	7.53	6.14	3.01	5.6
MgO	2.36	1.06	1.75	3
Na_2O	0.81	1.71	0.96	0.58
K_2O	1.81	25.6	12.3	11.6
SO_3	6.67	4.4	1.24	0.44
P_2O_5	0.1	1.26	1.41	4.5
CO_2/other				
Total	98.2	100	100	100
Undetermined	1.8	1.82	2.68	2.32
Higher heating value (constant volume)				
MJ/kg	35.01	17.94	15.09	18.06

[a] : Low volatile bituminous

Proximate analysis indicates the biomass composition with regards to moisture content, volatiles, fixed carbon, and ash content. It provides an overview on the thermal behaviour of biomass with respect to devolatilisation temperature, ignition temperature, and rate of decomposition. The composition is dependent on temperature, heating rate, nature of biomass, and the presence inorganic species (McKendry, 2002) (Jameel et al., 2010).

Biomass contains relatively higher moisture and volatiles, and lower fixed carbon compared to coal. Devolatilisation of biomass yields more oxygen functional groups, *e.g.*: hydroxyl, carbonyl (-COOH, -OH) which are reactive at low temperature and gives biomass its low heating value (Vassilev et al., 2010). This results in a greater reduction in mass (up to 90 wt.%) of initial biomass compared to less than 10 wt.% in coal at this stage (Jenkins et al., 1998). For instance, volatile matter constitutes around 75 wt.% of biomass composition compared to less than 20 wt.% in coal. Fixed carbon in biomass ranges between 14-20 wt.% relative to 77 wt.% found in coal.

The combustion of fixed carbon leaves behind residual ash. These ashes can be grouped into two categories; inherent ash and entrained ash. The former is naturally occurring and intimately distributed throughout the fuel while the latter is normally entrained during biomass processing steps. Alkali metals, alkaline-earth metals, and salts are commonly found in biomass. These include potassium, sodium, magnesium, silica, and phosphorus. The presence of alkali metals that are inherently volatile, most notably K and Na could be problematic. The reaction between alkali metal and silica produce alkali silicates which have low ash melting point, T<700°C.

The melting ash leads to fouling, slagging, and rapid sintering problems in most biomass-fired power plants (Jenkins et al., 1998). These reduce the heat transfer efficiency, leading to unplanned downtime and increased Operational and Maintenance (O&M) cost. Referring to *Table 2-2*, these ashes exist in oxide form; SiO_2, Al_2O_3, CaO, and MgO to name a few. SiO_2 made up the majority rice straw ash, at around 75%. Although it could be problematic in combustion process, the presence of alkali metals during pyrolysis could lower the devolatilisation temperature and increase the devolatilisation rate (Fahmi et al., 2007).

The composition of organic elements in biomass is determined from ultimate analysis. Elements such as carbon (C), hydrogen (H), and oxygen (O) constitute the major composition of biomass, along with a smaller fraction of nitrogen (N) and sulphur (S). This helps in the determination of biomass heating values and environmental impact associated with the release of sulphur, nitrogen, and chlorine during the combustion process (Saidur et al., 2011). In general, biomass has higher H and O content, but relatively lower C, N, and S compared to coal. It is a highly oxygenated compound with around 30-40 wt.% oxygen, compared to just below 2 wt.% in coal. Its high H: C and O: C ratio explains its low heating value. This is due to lower energy contained in C-O and C-H bonds, than in C-C bonds (McKendry, 2002). However, Van Loo and Koppejan (Van Loo & Koppejan, 2008) argued that C and H contribute positively to heating value, since both are oxidised during combustion to form CO_2 and H_2O, respectively. Biomass is ideal for co-combustion with coal, despite its relatively lower heating value. Lower S and N content means reduced pollutant from high temperature combustion.

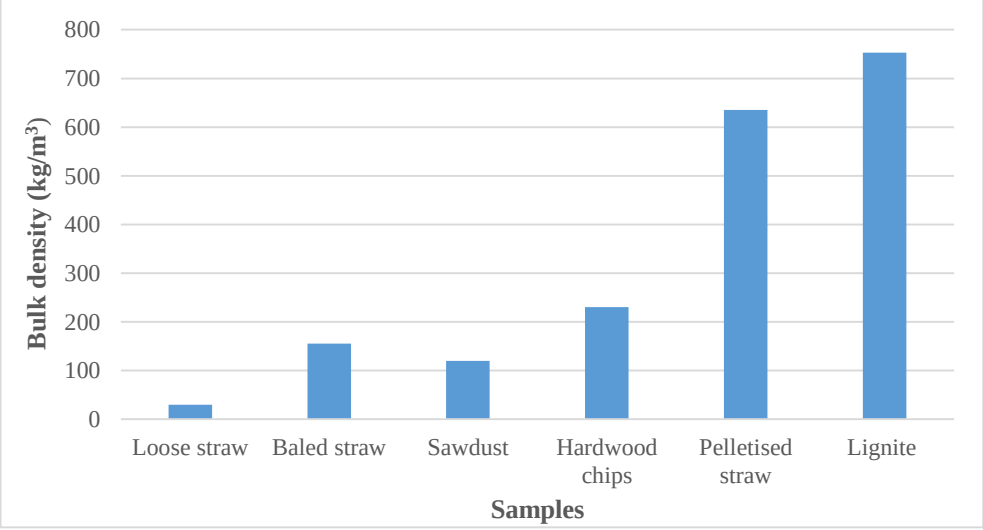

Figure 2-2: Bulk density of biomass relative to coal (Clarke & Preto, 2011)

Bulk density is the weight of a known volume of biomass, expressed as (kg/m^3). Bulk density of biomass is presented in *Figure 2-2*. In general, biomass has low density and low energy content relative to coal. Hence, a bigger volume of biomass is needed to achieve the equivalent energy produced by coal. These factors are making it less attractive for large-scale energy generation and pose challenges in terms of feeding system, transportation, storage, and the choice of conversion technologies (Van Loo & Koppejan, 2008). For biomass to be cost-competitive, a densification process is suggested to increase its energy density. Pelletisation, briquetting, and baling are among common densification steps. For example, pelletisation of loose straw increases its density from 20 kg/m^3 to 635 kg/m^3.

2.3 Pyrolysis

2.3.1 Mechanism

The breaking of molecular bonds within biomass structure under endothermic reactions releases hot vapours or aerosols. Rapid quenching of vapours produces bio oil or tar, while non-condensable vapours form permanent gases. These gases are mainly made up of hydrogen, carbon dioxide, carbon monoxide, methane, and a smaller fraction of light hydrocarbons, *e.g.*: ethylene and ethane (Basu, 2010c). It is widely acknowledged that pyrolysis proceeds in two stages; primary pyrolysis and secondary pyrolysis depending on local temperature as illustrated in *Figure 2-3*. This corresponds to the decomposition temperature of hemicellulose, cellulose, and lignin which governed the heat and mass transfer processes. Devolatilisation rate is influenced by several factors such as heating rate, reaction temperature, moisture content, and the presence of catalyst.

The process begins with biomass drying at a temperature around 100°C. Free or loosely bound water is driven off, allowing heat to penetrate further into biomass. Further increase in temperature initiates chemical reactions, leading to the breakdown of organic functional groups within biomass. Broadly speaking, pyrolysis can be grouped into four reactions; random bond scission, depolymerisation, carbonisation, and side reactions (Babu, 2008). The scission of oxygen functional groups; *i.e.*: OH, C=O at low temperature leads to the formation of free radicals, carbonyl and carboxyl group. This is indicated by a greater evolution of CO, CO_2, and water vapour at low temperature.

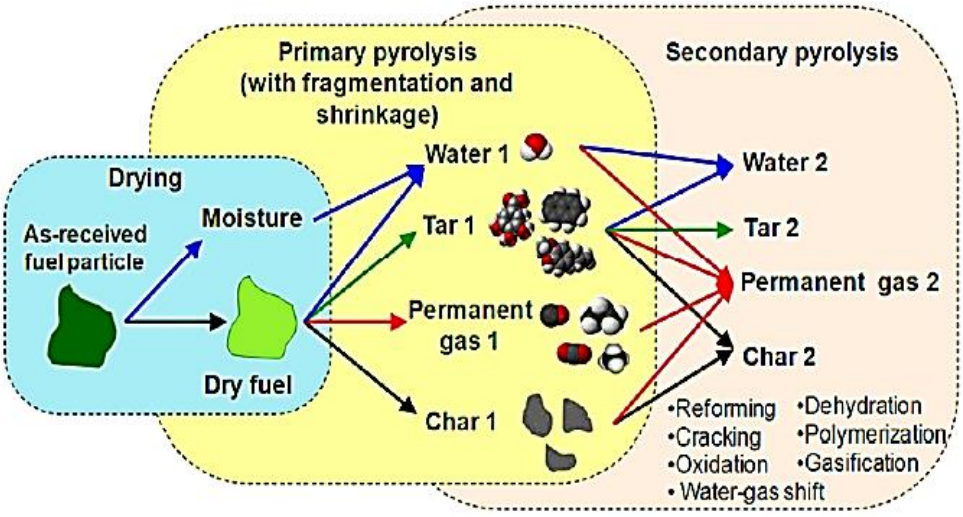

Figure 2-3: Pyrolysis stages. Published with permission from (Neves et al., 2011)

Main pyrolysis begins at a temperature around 350°C, indicated by the release of aerosols. Depolymerisation reaction removes the monomer units from biomass, which participate in the formation of free radicals and chain reactions. This influences the gas composition. For example, the breaking of C- H alkyl results in the formation of CH_4 at low temperature, between 300-500°C. Dehydrogenation of C-H bond at T>450°C contributes to increased H_2 production. This is due to the breakdown of stable aromatic

rings which require higher dissociation energy. For instance, bond dissociation energy required to remove H from CH_3 is 435.2 kJ/mol.

Hot volatiles and char from primary pyrolysis are vulnerable to the risk of exothermic secondary reactions. These reactions could occur in the vapour phase or between vapour-solid phases. These include the thermal cracking of volatiles, re-polymerisation of lighter organic compounds in bio oil, char gasification, and shift reaction. Long vapour residence time in a hot reactor could induce thermal cracking of heavy hydrocarbons into lighter hydrocarbons and permanent gases. Apart from high temperature, the presence of char has a catalytic effect, which causes tar cracking into gases. Fast removal of char from a pyrolysis reactor although recommended, is inefficient. Increased H_2 and CO at higher temperature also imply the extent of secondary cracking of hydrocarbon gases into lighter, permanent gases (Dai et al., 2000).

These volatiles escape through pore openings that enlarge with an increase in temperature. This is observed by an increase in char porosity. Carbonisation is the polymerisation of radicals, achieved through elimination of side chains to form stable chemical structures. These concurrent reactions include aromatisation, and cyclisation of alkyl chains through dehydrogenation. Volatiles released during pyrolysis contributes to the formation of carbonaceous char, of high CV~ 20-30 MJ/kg (Babu, 2008)

2.3.2 Cellulose Decomposition

Several reaction pathways have been proposed to achieve better understanding of cellulose decomposition. The first reaction model was the Broido model as illustrated in *Figure 2-4*. In this model, cellulose is initially converted into ‘active’ cellulose at elevated temperature. The active cellulose then reacts via two parallel pathways; forming volatile

tars and solid intermediate (A). The latter undergo consecutive reactions to form char B and C, with accompanying volatiles.

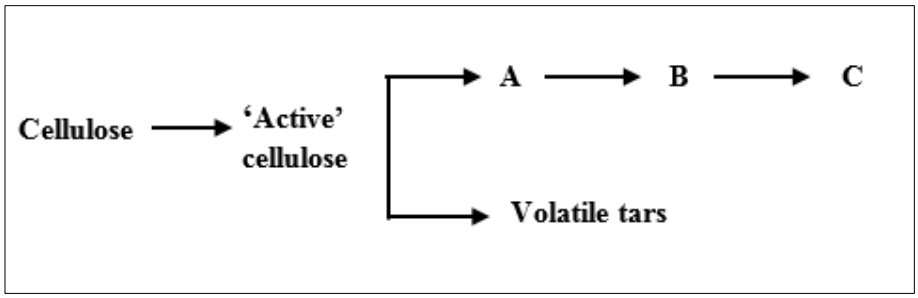

Figure 2-4: Broido model of cellulose decomposition (Varhegyi & Jakab, 1994)

This is later simplified by Shafizadeh by omitting the reactions leading to the formation of char B and C. The Broido-Shafizadeh model proposed that cellulose decomposes into a combination of (char + gases) and condensable volatiles via two competing reactions, as shown in *Figure 2-5*. Several temperature-dependent reactions occur during cellulose decomposition. These reactions are dehydration, depolymerisation, and fragmentation. Initially, a low degree of polymerisation takes place to convert 'inactive' cellulose into active cellulose. This initiation step requires a high activation energy (E_A) of 242.7kJ/mol, yet only a 3-6% mass loss is observed during this period (White et al., 2011)

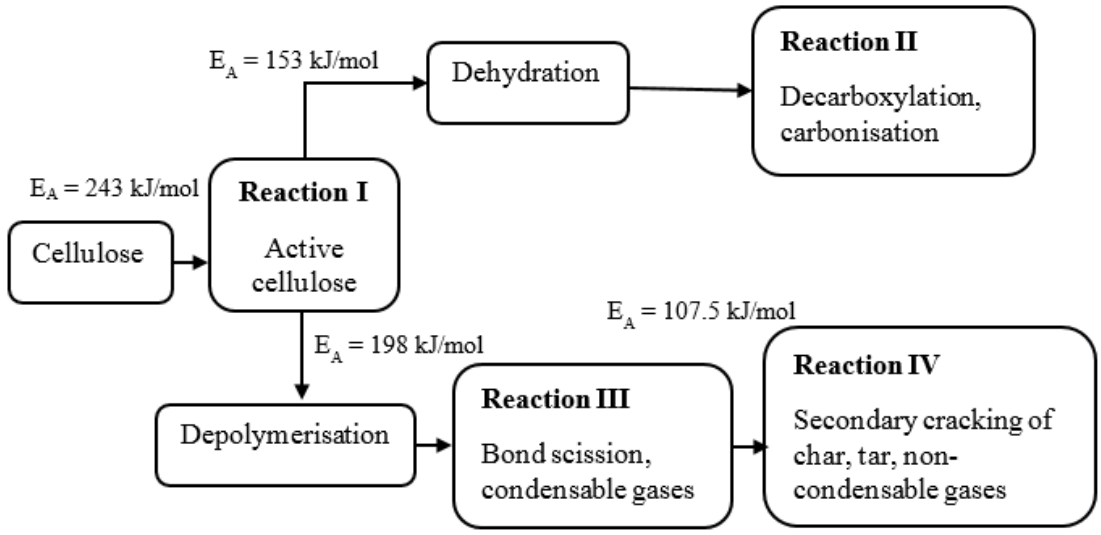

Figure 2-5: Broido-Shafizadeh model of cellulose decomposition. Published with permission from (Basu, 2010c)

This is followed by two competing reactions; dehydration and depolymerisation. Cellulose dehydration is followed by Reaction II. Decarboxylation and carbonisation reactions are responsible for the formation of free radicals, water soluble acids, anhydrides, water vapour, CO_2, CO, and char. This reaction proceeds at a much lower temperature around 200-280°C and slow heating rate.

Meanwhile, cellulose depolymerisation is favoured at high temperature around 280-340°C and fast heating rate. The breakage of glycosidic bonds (Reaction III) yield condensable volatiles. This reaction possesses higher activation energy (E_A) at 198 kJ/mol than dehydration at 153 kJ/mol. It is also responsible for the production of anhydrosugar; *e.g.*: levoglucosan, oligosaccharides, hydroxyl-acetaldehydes, acids, and alcohol. Under very fast heating rate; *e.g.*: flash pyrolysis where T>500°C, direct conversion of cellulose to condensable volatiles and permanent gases through fragmentation may occur. This is achieved via fission, disproportionation, dehydration, and decarboxylation reactions with no char formation (White et al., 2011).

Secondary reactions (Reaction IV) are also included in this model, which proceed at a much lower E_A = 107.5 kJ/mol. This means the thermally unstable 'intermediates' are vulnerable to react further to non-condensable gases, char, and tar as mentioned previously in **Section 2.3.1**. Thus, it is important to quickly extract the condensable vapours from the hot reactor. This can be achieved by increasing the flow rate of purge gas and having a small reactor.

2.3.3 Bio Oil Properties

Bio oil is a homogeneous mixture of aqueous and organic phase, and is usually dark-brownish in colour. It is a product of rapid and simultaneous depolymerisation and fragmentation of lignocellulosic components during thermal decomposition of biomass. It mainly consists of water-soluble compounds such as acids, ketones, phenols, furfurals, and aromatic hydrocarbons (Bridgwater, 2012). Biomass dehydration results in bio oil with high water content, at around 15-30 wt.%., with low energy density. This poses several problems in downstream applications.

High water content reduces the vaporisation rate of oil droplets and increases ignition delay time in a combustion engine. It risks lowering the combustion temperature and induces flame instability problems. The presence of char residues or alkaline metals, *i.e.*: potassium in bio oil, could catalyse the ageing of bio oil during storage. It can be described as re-polymerisation of lighter organic compounds to form heavier tar, indicated by phase separation of bio oil into aqueous phase and lignin-rich phase. This reaction produces more water as by-product. High water content (>30 wt.%) also has been found to induce a phase separation problem (Lehto et al., 2014).

Bio oil is highly oxygenated. Analysis shows that it consists around 35-40 wt.% oxygen, with low H: C ratio. The latter could induce instability problem during mixing with conventional oil. The presence of weak acids, *e.g.*: acetic acid in bio oil poses challenge during storage and risk of corrosion in the boiler. Typical pH range of untreated bio oil is found to be between 2.5 to 3. Unlike crude oil, distillation of bio oil is practically impossible since it is made up of water-soluble compounds that are inherently volatile. Fractional distillation or heating above 100°C could cause losses of valuable organic compounds such as xylene. Moreover, continuous heating at high temperature induces thermal cracking of tar into char, at around 45 wt.% of original bio oil. Heating value of bio oil is found to be half of conventional hydrocarbon oil at around 20 MJ/kg.

2.3.4 Tar Composition

Tar can be grouped into five different classes; depending on its molecular weight and solubility in water as shown in *Table 2-3***.** Very heavy tar compounds are represented by Tar Class 1. This is followed by heterocyclic aromatic compounds, with -O and -N attached to the aromatic rings. Phenol C_6H_6O and pyridine C_5H_5N are representative of tar class 2. Mono-aromatic hydrocarbons such as benzene, toluene, and styrene with single ring can be classified as tar class 3. Meanwhile, light PAH compounds with 2-3 benzene rings such as indene, naphthalene and fluorine are representative of tar class 4. Compounds with more than three benzene rings such as pyrene and chrysene can be classified as heavy PAH compounds.

Temperature exerts a strong influence on tar formation as depicted in *Figure 2-6*. The presence of mixed oxygenates, *e.g.*: levoglucosan, acetic acid, furfural and catechol are observed during low temperature pyrolysis, T~400°C. Lignin decomposition at high temperature, T>500°C contributes to increased formation of phenols and mono-aromatic

hydrocarbons. However, a further increase in temperature up to 900°C results in the formation of heavy PAH compounds. This is believed to be caused by two reactions; the condensation of light aromatic compounds into heavier tar and the cracking of very heavy tar (tar class 1) into tar class 4 and 5.

Table 2-3: List of tar compounds. Published with permission from (Li & Suzuki, 2009)

Tar class	Class name	Property	Representative compounds
1	GC-undetectable	Very heavy tars, cannot be detected by GC	Determined by subtracting the GC-detectable tar fraction from the total gravimetric tar
2	Heterocyclic aromatics	Tars containing hetero atoms; highly water soluble compounds	Pyridine, phenol, cresols, quinoline, isoquinoline, dibenzophenol
3	Light aromatic (1 ring)	Usually light hydrocarbons with single ring; do not pose a problem regarding condensability and solubility	Toluene, ethylbenzene, xylenes, styrene
4	Light PAH compounds (2–3 rings)	2 and 3 rings compounds; condense at low temperature even at very low concentration	Indene, naphthalene, methylnaphthalene, biphenyl, acenaphthalene, fluorene, phenanthrene, anthracene
5	Heavy PAH compounds (4–7 rings)	Larger than 3-ring; these components condense at high-temperatures at low concentrations	Fluoranthene, pyrene, chrysene

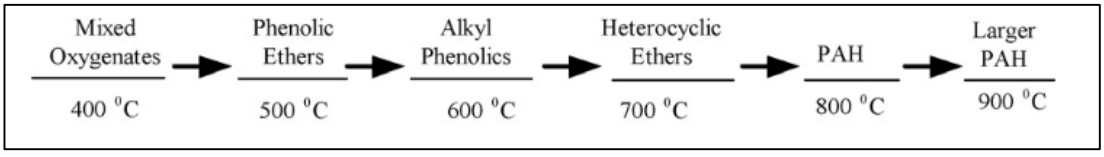

Figure 2-6: Tar formation scheme. Published with permission from (Li & Suzuki, 2009)

2.3.5 Pyrolysis Types

As pointed out above; heating rate, operating temperature, hot vapour residence time, and feedstock properties are among factors that influence pyrolysis product yield. The latter incudes moisture content, particle size, and the presence of catalyst which influence the rate of devolatilisation and heat transfer efficiency. Depending on temperature and heating rate, pyrolysis can be grouped into slow pyrolysis, fast pyrolysis, and flash pyrolysis as shown in *Table 2-4*. Heating rate varies in the range of 0.1-1000 °C/s, with no clear boundary between slow and fast pyrolysis. However, it is accepted that heating rate >5°C/s is set as a common threshold for fast pyrolysis (Neves et al., 2011)

Slow pyrolysis is conducted at moderate temperature (~600°C) and residence time ~4s to produce char, oil, and gas. Meanwhile, fast and flash pyrolysis are optimised for maximum bio oil yield. Flash pyrolysis is characterised by very high heating rate >1000°C/s and short vapour residence time of less than 1s, capable of producing ~75% oil yield. Pulverised biomass with high surface area is usually employed in flash pyrolysis to ensure rapid heating.

Table 2-4: Types of pyrolysis. Adapted from (Jahirul et al., 2012)

Pyrolysis type	Heating rate	Temperature (°C)	Residence time	Major products
Slow pyrolysis	Low	~600	Long, 4s	Char, oil, gas
Fast pyrolysis	High	~400-650, 650-900	Short, 1s	Oil ~ 60-75%
Flash pyrolysis	High	450-1000	Very short, <1s	Oil ~ 75%

2.4 Microwave Heating

Unlike mechanical waves which require media, *e.g.*: solid, liquid, and gas for energy transfer, electromagnetic waves radiation could travel through free space; *i.e.*: vacuum. Microwave is a type of radiation within the electromagnetic spectrum, with wavelength ranging from 1mm to 1m, as illustrated in *Figure 2-7*. It is widely used in

heating applications and chemical synthesis. It has a frequency range between 300 MHz to 300 GHz, although 0.915-2.45 GHz is used as standard in industrial and domestic microwave oven applications. This is done to avoid interference with ultra-high frequency used in radar and telecommunication applications (Fernandez et al., 2011).

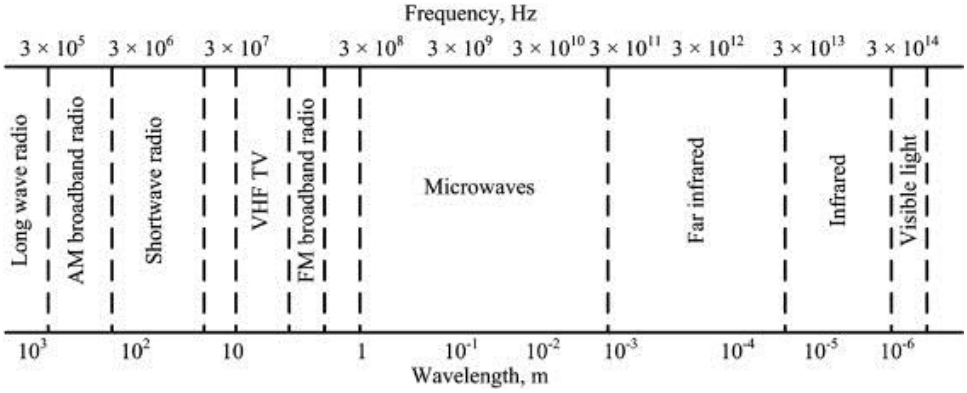

Figure 2-7: Electromagnetic spectrum. Published with permission from (Motasemi & Afzal, 2013)

Microwaves are a type of transverse waves; where electric field (E) and magnetic field (H) are oscillating at a right angle or perpendicular to each other. This is illustrated in *Figure 2-8*. Microwave heating is the result of microwave energy absorption by dielectric materials. In general, materials can be grouped into three different categories; *i.e.*: conductor, insulator, and absorber based on their dielectric behaviour within an electromagnetic field.

Oven cavity is an example of perfect electrical conductor, where microwaves are impenetrable and reflected throughout. On the other hand, insulator is a transparent material which permits microwaves to travel through it without incurring any dielectric loss. Materials with high penetration depth are commonly used as microwave insulators. These include quartz and Teflon, with penetration depth of 160 m and 92 m, respectively.

Meanwhile, materials that absorb microwave energy such as wood, water, graphite are commonly known as microwave absorber or dielectric materials.

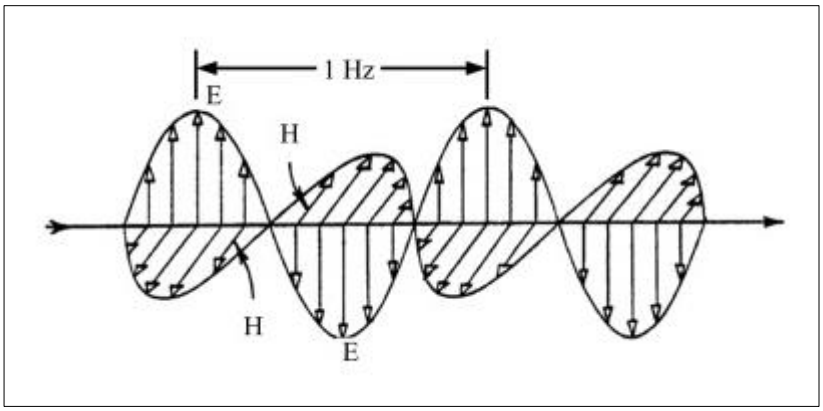

Figure 2-8: Electric (E) and magnetic (H) field components in microwave. Published with permission from (Motasemi & Afzal, 2013)

These materials have a higher tendency to be polarised by an oscillating electric field. The likelihood of molecules to follow the alternating field results in the heat generation through molecular friction and dielectric loss. This is otherwise known as dielectric polarisation. Ionic liquids such as water and acid have a higher chance of being polarised, compared to non-polar substances such as beeswax. One important aspect of dielectric polarisation is response time (RT) of dipoles relative to microwave frequency. It is preferable for RT to match or slightly lag behind the changing electric field, for molecular friction to occur. This condition is met at microwave frequency of 2.45 GHz, which allows the dipoles to align in the field, but not to follow alternating field precisely (Yin, 2012). Heat generated during this process is known as dielectric heating or commonly known as microwave heating.

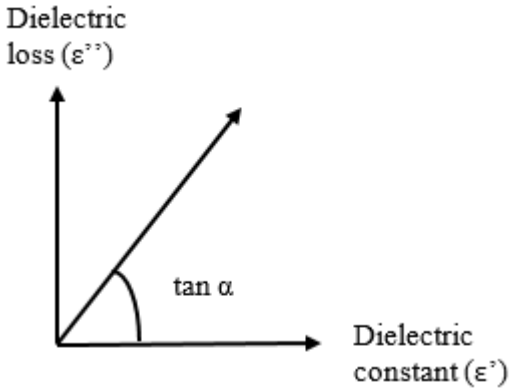

Figure 2-9: Complex permittivity of dielectric material

The ability of dielectric material to absorb microwave radiation and converting it into heat is characterised by complex permittivity (ε). This refers to the real and imaginary parts in the complex plane, such that ε = ε'-jε'', as illustrated in *Figure 2-9*. Dielectric constant (ε') is the measure of material to conduct and store electrical energy in an electric field. Meanwhile, dielectric loss (ε'') is a term referring to the ability of material to dissipate this energy into heat. Loss factor (α) defines the ability of material to convert electromagnetic radiation into heat at a specified frequency and temperature.

2.4.1 Microwave Modes

In general, microwave ovens can be classified into single-mode and multi-mode cavities. An example of a multi-mode cavity is domestic microwave oven. Multiple radiation is reflected within the enclosed metallic cavity, creating a field with simultaneous resonant modes. This generates multiple hot and cold spots within the cavity, which influences the heating uniformity of the sample load. Heat distribution can be improved by introducing a mode stirrer and rotating table into the oven. For instance, the presence of a mode stirrer disturbs the standing wave pattern inside the oven cavity. This continuously moves the location of hot and cold spots throughout the cavity.

Meanwhile, a rotating table is an example of travelling load. Uniform heating is achieved as the load travels across the location of maximum and minimum electromagnetic field. In contrast, only a single mode of radiation is generated in single mode cavity. This creates a well-defined electromagnetic field, with known region of high and low energy intensity. This allows a sample to be placed in a particular hot spot for maximum energy conversion. The nature of focused radiation in a single mode cavity is particularly useful during high temperature processing of low-loss materials; *e.g.*: ceramic (Acierno et al., 2004)

2.4.2 Conventional Heating versus Microwave Heating

Differences in heating methods are illustrated in *Figure 2-10*. Pre-heated air, radiant furnace, and fluidised bed are typical examples of external heat sources for particle drying in conventional heating. This process however is often slow and inefficient. A non-linear temperature gradient is observed in this type of heating. The particle surface records a higher temperature than the core, as heat propagates from outer regions inwards. Heat transfer efficiency is often determined by thermal properties such as thermal conductivity, density, specific heat and also convection heat transfer coefficient (Motasemi & Afzal, 2013).

In contrast, the conversion of electromagnetic energy into heat energy results in volumetric heating throughout the particle during microwave heating. Particle core records a higher temperature than the surface. The internal heat generation causes moisture evaporation and initiates the subsequent chemical reactions.

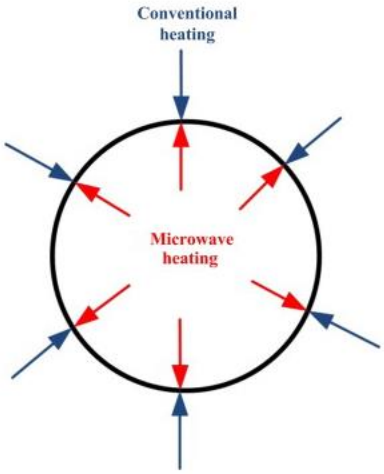

Figure 2-10: Difference in heating process. Published with permission from (Motasemi & Afzal, 2013)

Microwave heating has proven to be beneficial in the context of pyrolysis. This can be explained by the interaction of hot volatiles as they progress from core towards the particle surface. In the case of conventional heating, these volatiles have to travel through the hotter region of the particle, leading to thermal cracking into gases. However, these volatiles progress through a colder region of the particle during microwave heating; reducing risk of secondary reactions (Miura et al., 2004).

2.5 Previous Work on Microwave Pyrolysis of Biomass

Microwave pyrolysis has gained interest in recent years. It is seen as an alternative which could lift the strict requirements associated with conventional pyrolysis. These include particle size, moisture, poor heat transfer, and high furnace temperature which favour secondary reactions. It utilises a similar setup to conventional pyrolysis. An inert environment is maintained by a continuous flow of non-reactive gas; *e.g.*: N_2, and bio oil recovery is achieved through rapid quenching of volatiles. The only difference lies in their heating processes.

Investigation into microwave pyrolysis has covered various biomass materials such as rice straw (Huang et al., 2008), coffee hulls (Domínguez et al., 2007), waste automotive oil (Lam et al., 2012), oil palm biomass (Salema & Ani, 2011), sewage sludge (Domínguez et al., 2005) (Tian et al., 2011), wheat straw (Krieger-Brockett, 1994)(Zhao et al., 2012), waste paper (Popescu et al., 2008), corn stover (Wan et al., 2009) (Lei et al., 2009) and microalgae (Du et al., 2011)(Beneroso et al., 2013). This strongly suggests that microwave pyrolysis can be applied to a wider range of biomass regardless of feedstock size and water content. Microwave pyrolysis eliminates cost associated with biomass pre-treatment such as drying and grinding.

Among parameters studied in the microwave pyrolysis of biomass include particle size, microwave power, reaction temperature, and addition of catalyst and microwave absorber. The effect of particle size is found to be insignificant during microwave pyrolysis than in conventional pyrolysis, as demonstrated by (Lei et al., 2009). Ground stover particles with d=0.5-4 mm are found to be similarly pyrolysed. Miura *et al.* (Miura et al., 2004) have successfully demonstrated the microwave pyrolysis of wood blocks with diameter ranging between 0.06 to 0.3 m. A cross section of a wood block was examined after three minutes into the pyrolysis process, as shown in *Figure 2-11*. It was revealed that carbonisation starts from the centre of the wood, which confirmed the nature of volumetric heating.

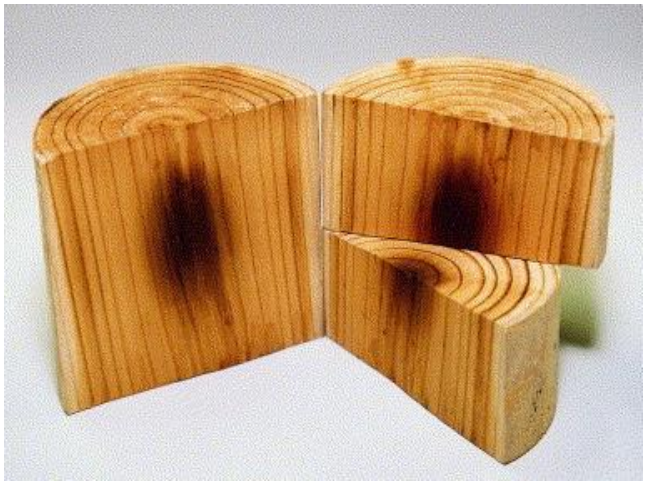

Figure 2-11: Cross section of wood block, ϕ= 80 mm. Published with permission from (Miura et al., 2004)

In addition to that, microwave heating is found to enhance or speed up the chemical reactions during pyrolysis. These reactions proceed at a much lower temperature during microwave pyrolysis, compared to conventional pyrolysis. This has been demonstrated by Budarin *et al.* (Budarin et al., 2009) with low temperature activation of wheat straw, where bio oil is produced at a claimed temperature below 180°C, compared to 350°C during conventional processing. Rapid microwave heating also means reduced reaction time. This is achieved in a matter of just several minutes, compared to ~40 minutes in a standard fixed-bed pyrolysis reactor. The latter would require the reactor to be heated up until it has reached desired temperature before biomass introduction. Better efficiency has resulted in total energy saving from microwave pyrolysis, as indicated by (Lam et al., 2012; Zhao et al., 2011).

The effect of microwave power has been investigated by (Hu et al., 2012; Tian et al., 2011; Du et al., 2010; Yu et al., 2007). 300 W is found to be the minimum power to initiate pyrolysis process, with low bio oil yield obtained at P ≤ 480 W. An increase in microwave power has resulted in increased production of gas and bio oil at the expense of

reduced char yield. This is due to the sample being subjected to a higher heating rate. During microwave pyrolysis of *Chlorella vulgaris,* sample temperature rose from 200 to 800°C, when microwave power was increased from 750 to 2250 W. Maximum gas yield of 52.37 wt.% is also recorded at maximum wattage.

The effect of reaction temperature on product yield and distribution was investigated. Slow devolatilisation at low temperature (T< 400°C) resulted in low oil and gas yield. An increase in temperature caused more condensable volatiles to be released, until it reaches certain temperature. At this stage, maximum oil yield is achieved. Beyond this temperature, a decrease in bio oil and char yield is observed, while gas yield attained peak value. This trend is consistent with findings from (Ren et al., 2012; Zhao et al., 2012; Lei et al., 2011; Domínguez et al., 2007). Microwave pyrolysis is claimed to produce higher bio oil and gas yield due to rapid devolatilisation than conventional pyrolysis. However, it has also been pointed out that lower bio oil yield was obtained from microwave pyrolysis (Salema & Ani, 2011; Domínguez et al., 2007). The presence of hotspots during microwave heating causes higher local temperature than bulk temperature. This causes secondary cracking of tar into non-condensable gases.

Liquid yield is affected by reaction temperature, reaction time, and the presence of microwave absorber. Bio oil obtained from microwave pyrolysis is claimed to have a higher oil fraction, with aromatic hydrocarbons that are comparable to crude oil. It also reported to have a higher concentration of phenol and phenolic material, which can be credited to lignin decomposition at high temperature. This is usually achieved during catalytic microwave pyrolysis of biomass, as demonstrated by (Bu et al., 2011). Maximum phenol

(38.9%) and phenolic material (66.9%) were achieved by blending activated carbon with biomass, in 3:1 ratio, at 316°C.

Moreover, the behaviour of inorganic species in biomass material under microwave radiation has been studied by (Omar et al., 2011; Wan et al., 2009). It was found that most metal oxides, *e.g.*: FeO_3 and alkali metals are readily heated, and could positively affect the microwave absorption. For instance, potassium enhances carbon conversion into CO via dry gasification reaction. However, silicates such as SiO_2 are difficult compounds to heat up, although they retain heat for a longer period of time. This might influence the microwave absorption for rice biomass with high silica content.

The biggest challenge associated with microwave pyrolysis is reliable temperature monitoring and repeatability. The formation of multiple hot and cold spots in a multi-mode microwave oven could yield uneven temperature profile. When using a thermocouple as a temperature probe, its tip could act as an antenna which focuses microwave energy, giving higher local temperature than that of bulk. Nevertheless, thermocouples are employed due to their quick reaction time. Grounded thermocouples could provide electrical isolation from microwave radiation, limiting electromagnetic interference. This can be mitigated by having a temperature-feedback loop which controls the microwave radiation based on temperature reading.

2.6 Review on Numerical Simulation

2.6.1 Microwave Heating

An accurate mathematical model is necessary in order to predict the behaviour of a material under microwave radiation. Modelling microwave heating requires the coupling of non-linear electromagnetic field with Fourier's conduction heat transfer. Most of these work originated from food processing industry, which mainly involve drying, thawing, and the effect of application of microwave energy on chemical changes and the final product quality. Researchers in the past have discovered some variables that influence heating uniformity of sample. These include geometry (Araszkiewicz et al., 2007; Zhang & Datta, 2005; Chamchong & Datta, 1999), load size (Salema & Afzal, 2015; Vilayannur et al., 1998), and dielectric properties (Chamchong & Datta, 1999; Peyre et al., 1997).

One of the main issues when dealing with microwave heating using multi-mode applicator is a non-uniform temperature distribution. Significant improvement in heating uniformity can be achieved by incorporating mode stirrer or rotating table into the cavity. Some researchers have also demonstrated microwave combination heating, where they integrate infrared and/or hot air with microwave heating (Datta & Rakesh, 2013; Datta & Ni, 2002). Meanwhile, the influence of mode stirrer or rotating table on field distribution has been studied by (Kurniawan et al., 2015; Geedipalli et al., 2007; Plaza-González et al., 2004). By considering discrete angles of the stirrer or turntable, the effect of rotation on heating pattern can be realised. This is based on the assumption that the heating rate of material is slow compared to the movement of mode stirrer. Hence, the position of stirrer is considered fixed at a given time. Another attempt has been made to simulate the turntable rotation by MATLAB-COMSOL multi-physics interface. A custom MATLAB code is

written to simulate rotation of the turntable at several discrete positions, where the average EM field is computed. These data is then imported to COMSOL for the subsequent heat transfer computation (Pitchai et al., 2015).

To the best of author's knowledge, very little to no information can be found on the effect of waveguide location or the direction where the microwaves enter the cavity on the electric field distribution. Domestic microwave ovens have different built or configurations which might affect the electric field distribution, heating pattern and power density.

Microwave heating is the result of a dynamic process as illustrated in *Figure 2-12.* Photonic energy is lost as microwaves travel through a dielectric medium. The electromagnetic losses become the source for internal heat generation. Change in the thermal and dielectric properties is observed as biomass undergoes phase change. Consequently, this influences the strength of electromagnetic field. Temperature distribution inside the biomass can be predicted by coupling the wave equation and Fourier's heat transfer equation.

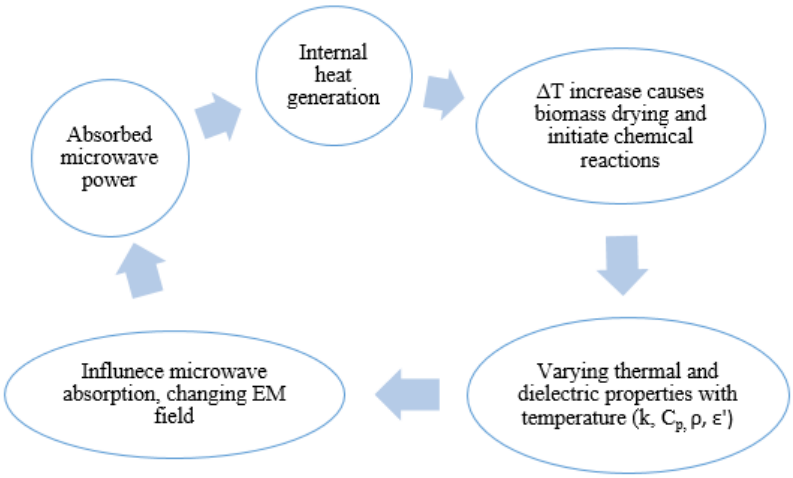

Figure 2-12: Coupling of electromagnetic field and temperature distribution

2.6.2 Transient Heating

Both internal and external heat transfer are the two controlling factors in the heat transfer phenomena. The former is mainly governed by particle size while the latter is influenced by local temperature, heating rate, and heat transfer coefficient. The transient heat conduction is characterised by a set of dimensionless parameters such as Biot (Bi) number and Fourier (Fo) number. Bi number defines the thermal resistance of a body when exposed to surrounding heat. Meanwhile, Fo number predicts the time response of a body to achieve equilibrium with bulk temperature (T∞). Low Bi and Fo number is often associated with a small particle size, where d<1mm. This indicates that the particle size is insignificant and the heat transfer process is governed by external factors. A uniform temperature distribution can be achieved, when T=T∞.

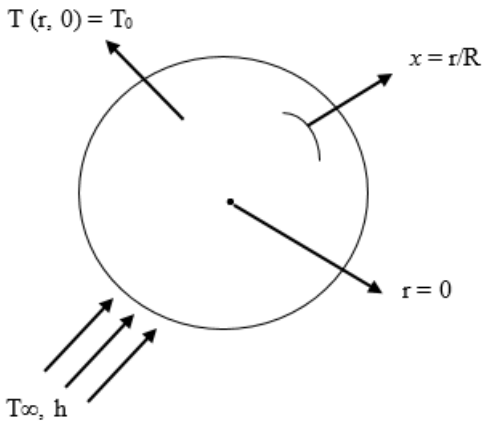

Figure 2-13: Radial conduction in a cylindrical biomass particle

This model assumes an infinitely long cylinder where conduction takes place in a radial direction (dr) in a one-dimensional system (1D), as depicted in *Figure 2-13.* It is assumed that conduction is the only mode of heat transfer, neglecting the effects of porosity and internal heat convection.

2.7 Summary

This chapter explores the potential of Malaysian lignocellulosic biomass materials for energy recovery via thermochemical conversion processing. It addresses the majority of available waste biomass with primary composition of cellulose, hemicellulose and lignin. The latter is the most difficult component to break down, due to its stable chemical structure. For this reason, thermal treatment is preferred for energy recovery from lignocellulosic biomass, compared to biochemical treatment. Low energy density combined with the presence of inherently volatile inorganic species could affect the choice of conversion technologies. Pyrolysis is thermal decomposition of biomass in an inert environment to produce solid charcoal, bio oil and gas. This process occurs in a sequence of steps which corresponds to moisture evolution, lignocellulose degradation, followed by secondary reactions to form stable products. Moisture and volatiles released during pyrolysis raise the energy density of the biomass residue. Dielectric polarisation of ionic molecules; *e.g.*: water under microwave radiation, has contributed to rapid dielectric heating in domestic cooking application. There is now a growing interest to exploit microwave radiation as primary heat source in the pyrolysis process. Microwave pyrolysis utilises moisture within biomass for efficient internal heating, whereas this factor could be limiting in the context of conventional pyrolysis. Moreover, this innovative process is claimed to give higher volatiles yield than conventional pyrolysis, with better product quality. Furthermore, core volumetric heating in microwave pyrolysis could prevent secondary cracking of condensable volatiles into permanent gases, maximising oil yield. Microwave pyrolysis is seen as an attractive alternative to conventional pyrolysis, with better energy efficiency and simpler setup.

3 Materials and Methods

This chapter begins with description of the biomass materials used in this study. It also provides a detailed description of experimental setups and methodologies used during pyrolysis experiments. Equipment used and the standard procedures adopted during sample characterisation are also highlighted. Confidence limit used for justification of error analysis is briefly described at the end of this chapter.

3.1 Biomass Feedstock

Empty Fruit Bunch (EFB) and rice husk pellets used in this study are sourced from Malaysia. They are obtained as by-products after the milling process. Oil palm or *Elaeis Guineensis* is a perennial crop with 25-year lifespan, which is cultivated for the production of edible oil. Mechanical threshing of fresh fruit bunch (FFB) in a rotating drum leaves behind solid residue, *i.e.*: EFB as shown in *Figure 3-1*. The fruitlets then undergo mechanical screw pressing to extract the crude palm oil. This process leaves behind useful wastes such as palm oil mill effluent (POME), pressed cake, and palm kernel nuts. The latter would undergo subsequent processing to produce palm kernel oil. It is estimated that EFB accounts for 22.44% of the total residues from oil palm biomass, at 4.426 tonne/hectare/year (Chang, 2014). Global palm oil production in 2015 stands at a total of 60.80 Million Tonne (MT), a 7.84% increase from 2012 level (United States Department of Agriculture, 2016). Malaysia is one of the biggest palm oil producers in the world, with total plantation area of 5.642 Million Hectare in 2015 (Malaysian Palm Oil Berhad, 2015).

Figure 3-1: Empty fruit bunch (QM Consultants, 2016)

Meanwhile, rice or *Oryza Sativa* is staple food for approximately half of the world population, with cultivated land covering Asia, Americas and Europe. The global rice production is projected at 480.7 MT in 2016/17, with total cultivated area of 161.1 Million Hectare. Rice husk is an outer layer of rice grain, which is separated during milling process, as depicted in *Figure 3-2.* It accounts for 20% of the total rice weight. This puts the global potential of rice husk at 143.38 MT (Childs, 2016).

Figure 3-2: Rice husk (Stylus, 2016)

Traditional practice in dealing with these wastes includes open burning or being used as boiler fuel in the mill itself. Burning these wastes in an open field triggers air pollution and toxic emission from dioxin. In the case of palm oil waste, uncontrolled release of POME would emit greenhouse gas, *i.e.*: methane into the atmosphere and cause groundwater contamination from leachate. The cultivation of greater amounts of palm oil and rice is not without biodiversity and sustainability issues. Steady increase in annual output of palm oil and rice worldwide raises the question for better utilisation of wastes from these sectors.

3.2 Conventional Pyrolysis

3.2.1 Overview

A series of conventional pyrolysis experiments (CP) were carried out using a cylindrical fixed-bed reactor, with a total volume of 41 L. The pyrolysis chamber was externally heated using 15.8 kW radiant heater. 200 g pellets were fed into the central heating zone through two ball valves, once it has reached the desired operating temperature. An inert environment was maintained by a continuous flow of nitrogen (99.98% purity) at 4 LPM. The flow is controlled by FL-2014 rota meter, with ±5% accuracy. The total reaction time was 30 minutes.

The experimental setup is shown in *Figure 3-3*. The temperature was input into the control unit as shown in *Figure 3-4*. The temperature was measured by K-type thermocouple (Al-Cr) fitted below the chamber, which provides a feedback loop to the control unit to maintain the process temperature. It was capable of measuring a wide temperature range between -200 to 1250°C, with ± 0.75% accuracy.

In order to measure the energy consumption during conventional pyrolysis, two current sensors rated at 71 A were fitted to two lives wires supplying the upper and bottom heaters. They were connected to a transmitter and display unit. The OWL + USB interface enabled live data recording on a personal computer (PC).

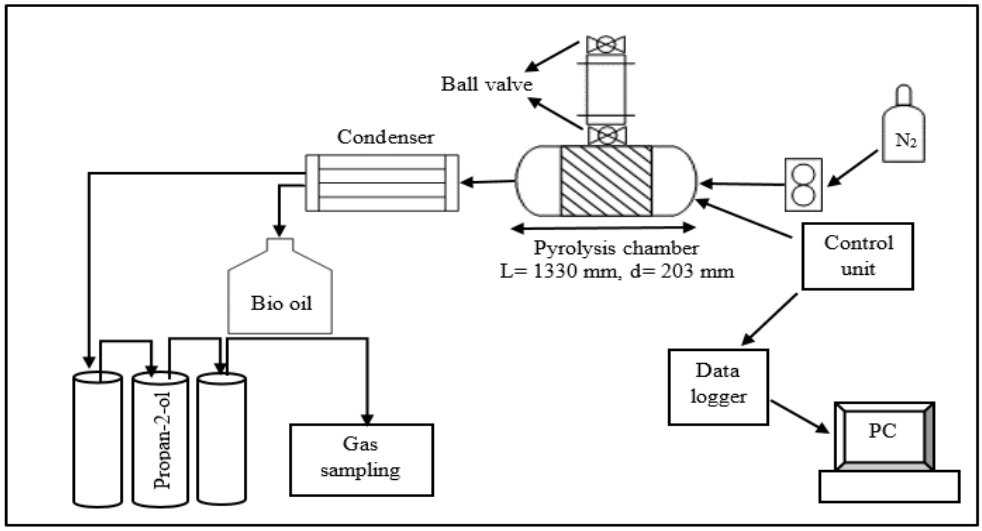

Figure 3-3: Conventional pyrolysis setup

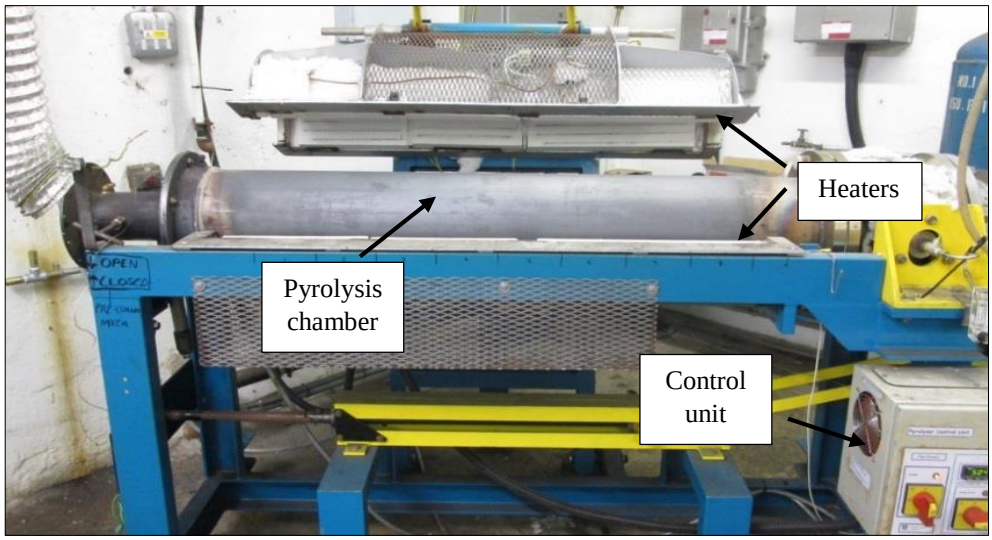

Figure 3-4: Front view of pyrolyser

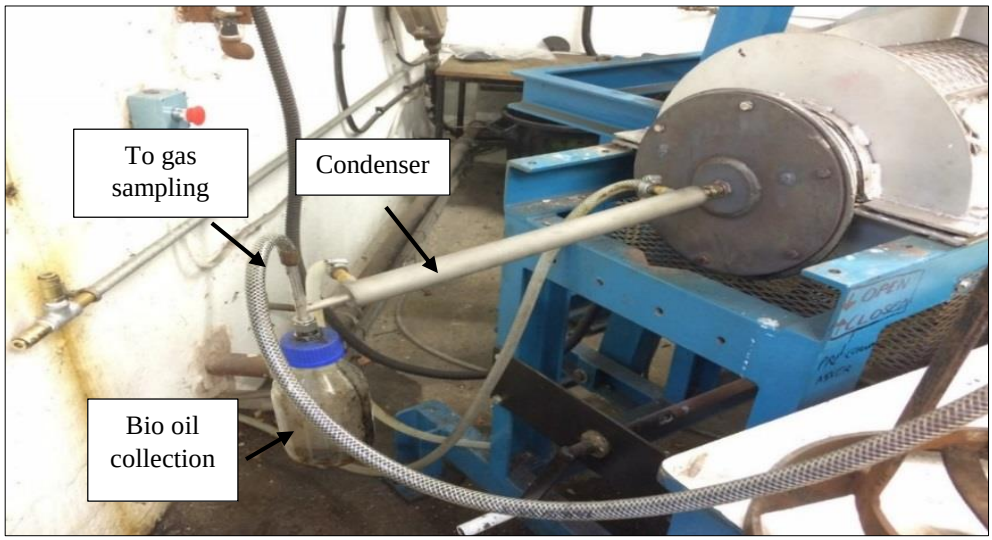

Figure 3-5: Product recovery setup

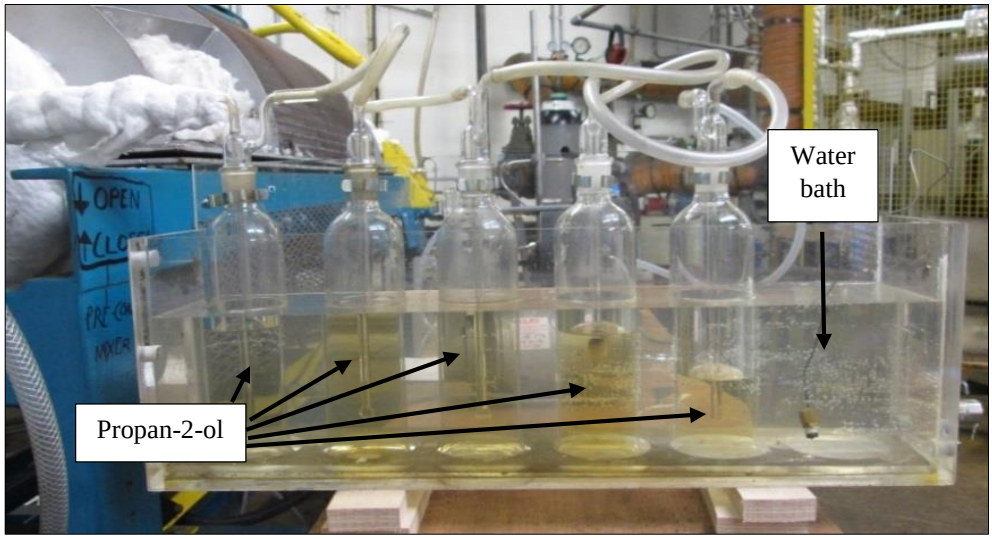

Figure 3-6: Tar clean-up

The exiting hot volatiles were quenched by water condenser in *Figure 3-5* for bio oil recovery. Non-condensable volatiles passed through a series of impinge bottles filled with propan-2-ol for tar clean up as shown in *Figure 3-6*. These bottles were kept in water bath at 4°C. This ensures only dry, clean gas was collected for offline gas analysis. Pyrolysis gas was sampled into 1L Supel-Inert foil gas sampling bag. It was recommended for the storage of low molecular weight gases such as H_2, CH_4, CO, and CO_2. Gas sampling was taken at an interval of 6, 8, 10 and 12 minutes from the moment the samples were

introduced into the reactor. Char and bio oil were weighed at the end of experiment for yield computation. Gas was calculated by difference.

3.2.2 Methodologies

1. Bio oil collection bottle was initially weighed. 200 g of biomass was prepared. Nitrogen flow rate was set at 4 LPM. Extractor and water supply to condenser were turned on.
2. The pyrolyser was heated to a set operating temperature, i.e.: 500 and 800 °C. Once it has reached the set temperature, biomass was fed through ball valves. Initial time (t_0) was recorded.
3. Gas sampling was taken at an interval of 6, 8, 10 and 12 minutes after t_0. The reason behind this is to let the biomass pellets heating up to equilibrium temperature ($T\infty$). A vigorous smoke was seen flowing out of the condenser at t>3 minutes and dies down after 15 minutes. Hence, gas sampled within this interval is believed to be representative of pyrolysis gas composition at a chosen reaction temperature. The reactor was left to run for 30 minutes after t_0 to ensure complete pyrolysis.
4. After 30 minutes, power supply to both heaters was turned off. Once the pyrolyser had reached ambient temperature, char and bio oil were weighed for mass balance analysis.
5. The nitrogen, water supply and extractor were turned off.

3.3 Microwave Pyrolysis

3.3.1 Overview

A series of microwave pyrolysis (MP) experiments were conducted using the BP-125 laboratory microwave oven (Microwave Research & Applications, USA). It was a multi-mode microwave oven rated at 1000 W with 2.45 GHz operating frequency. The experimental setup is shown in *Figure 3-7*. It was equipped with programmable process controller for temperature and heating rate (CAL9500P), with RS232 communication for data monitoring as shown in *Figure 3-8*.

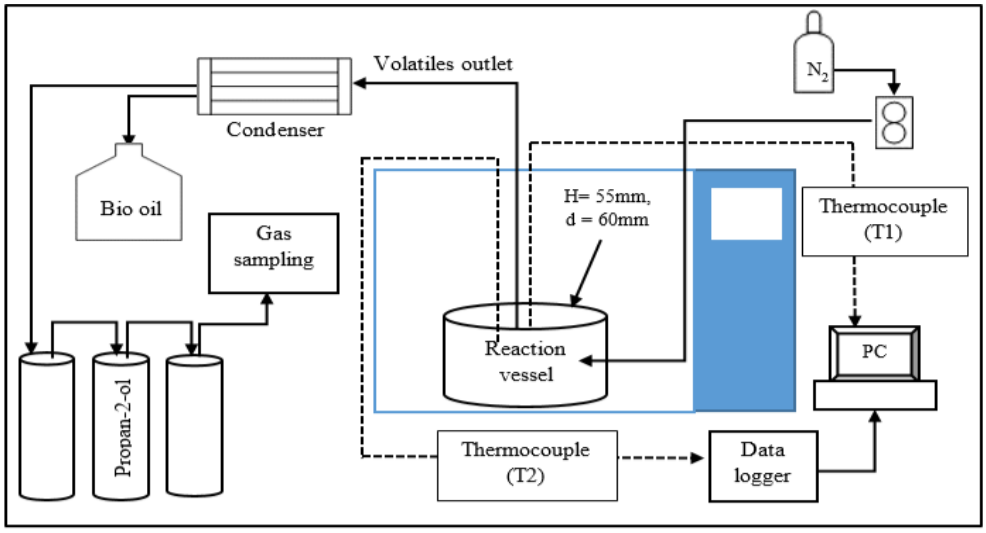

Figure 3-7: Microwave pyrolysis setup

Figure 3-8: Front view of the BP-125 microwave oven

Similar to conventional pyrolysis, it has an ON/OFF power control to maintain the process temperature. It was modified to accommodate N_2 inlet, volatiles outlet and two ϕ= 3mm K-type thermocouples (Al-Cr) as shown in *Figure 3-9*. The thermocouple was covered in a stainless steel sheath with an ungrounded junction type rated at 1250°C. The thermocouples were grounded to oven cavity with bulkhead compression fittings. Standard size thermocouple connectors with zinc ferrite core were used between probes and connection wires to suppress the electromagnetic interference

The reaction took place in a 100 mL porcelain crucible, enclosed within a refractory furnace. The furnace is made up of Fibrefrax Duraboard capable to withstand high temperature up to 1500°C. 40 g of biomass pellets were used in the experiment without any addition of microwave receptors. The reaction took place for another 20 minutes after reaching the set temperature, with N_2 flow (99.98% purity) set at 2 LPM. The data

acquisition system shown in *Figure 3-10* measured process temperature and power input every 1 sec, which were logged into a personal computer (PC) for energy monitoring.

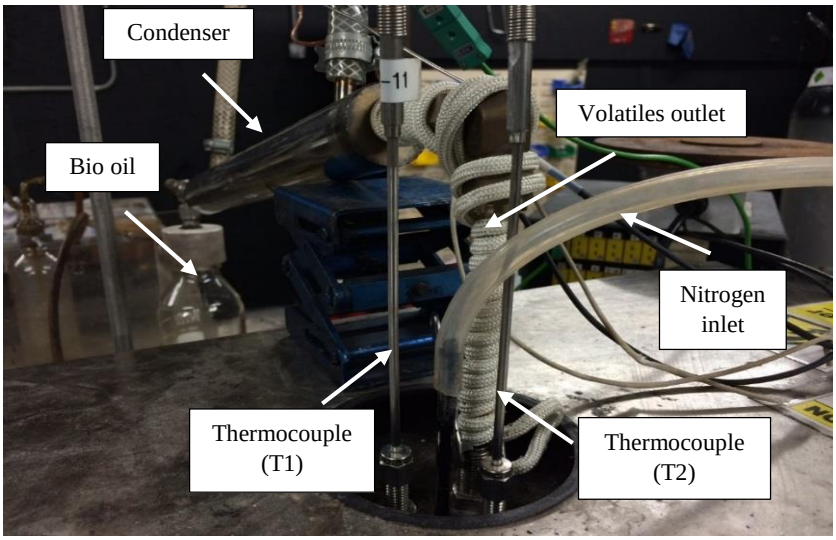

Figure 3-9: Volatiles extraction and temperature measurement setup

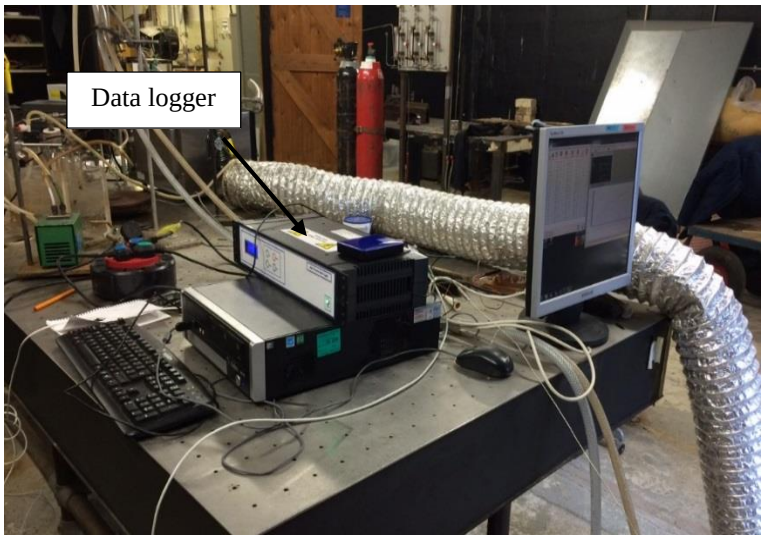

Figure 3-10: Data acquisition setup

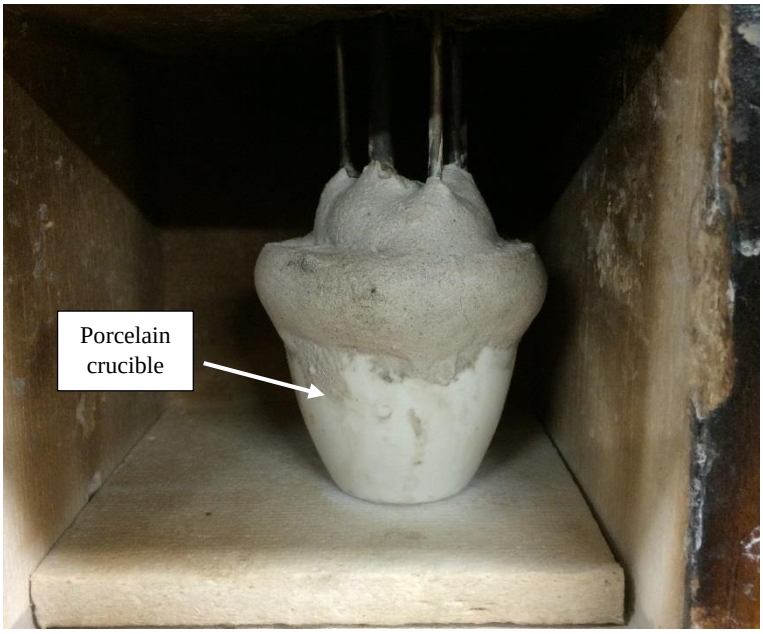

Figure 3-11: Reaction vessel in a refractory furnace

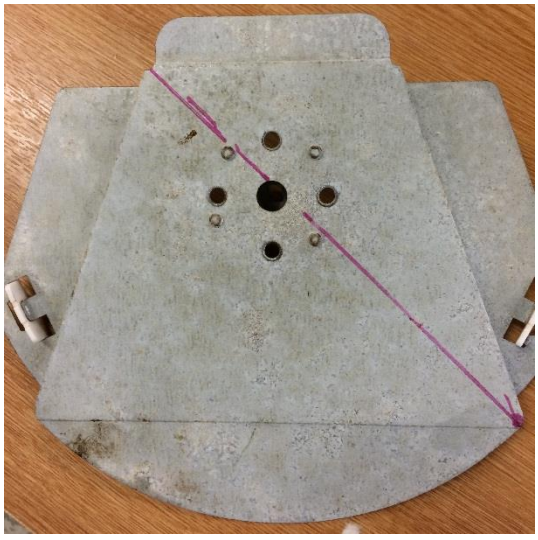

Figure 3-12: Mode stirrer

The crucible in *Figure 3-11* was sealed with fire cement to prevent volatiles leakage which could affect overall pyrolysis yield. A 125 W electric rope heater was wrapped around the quartz tube carrying hot volatiles to prevent premature condensation. Meanwhile, the volatiles extraction setup *i.e.*: condenser and tar clean-up was similar to conventional pyrolysis. Microwaves entered the cavity through a bottom-feed waveguide,

where the radiation was broadcasted by a metallic mode stirrer shown in *Figure 3-12*. The mode stirrer, moving at 29 rpm shifted the stationary waves and attenuated the occurrence of hot and cold spots inside the cavity. By doing this, a more uniform heating distribution can be achieved.

The aim of the present study was to investigate the influence of end temperature during conventional and microwave pyrolysis of biomass. In particular, this investigation focused on the influence of different heating methods on the distribution of pyrolysis products. The pyrolysis experiments were conducted at final temperatures of 500 and 800°C. Each test was repeated three times to ensure data consistency and repeatability.

3.3.2 Methodologies

1. 40 g of biomass was loaded into a porcelain crucible. Thermocouples were embedded into the sample bed, with quartz tubes carrying nitrogen and volatiles. The setup was then sealed with fire cement. Initial weight of the bio oil collection bottle was recorded.
2. Electric rope heater was wrapped around the quartz tube carrying volatiles. An extractor and water supply to the condenser were turned on.
3. Desired reaction temperature, i.e.: 500 and 800 °C was set on the oven controller. Microwave power was turned on. Unlike conventional pyrolysis, pyrolysis gas was sampled immediately after the reactor has reached the set temperature for a continuous period of 10 minutes.
4. From the time it had reached the set temperature, the biomass samples were left to pyrolyse for another 20 minutes.

5. Microwave oven, extractor, water supply and nitrogen were turned off. The char was left to cool until it reached ambient temperature. Char and bio oil were collected at the end of experiment for mass balance analysis.

3.3.3 Calculation of Pyrolysis Product Yield

The mass of char and bio oil are weighed at the end of the experiment. Gas emitted during pyrolysis is counted as the difference between initial weight of biomass and the sum of pyrolysed char and bio oil, as depicted in *Eq: 3-1*. Meanwhile, yield of pyrolysis product is computed following Eq: 3-2, where M_i is the weight of pyrolysis product (g) and M is the initial weight of biomass (g).

$$Gas = Initial\ weight\ of\ Biomass - \sum Char\ + Bio\ oil \quad \text{Eq: 3-1}$$

$$Yield, Y_i\ (\%) = \frac{M_i}{M} \times 100 \quad \text{Eq: 3-2}$$

3.3.4 Comparison between Fixed and Variable Power Configuration

There are two types of power configuration settings used in the microwave oven. Variable power settings are commonly found in domestic microwave oven. This gives a pulsed radiation or ON/OFF duty cycle, which limits the transfer of microwave power into heating the samples, as shown in *Figure 3-13*. This is similar to what often found in a multi-mode microwave reactor. Power output is taken as an average over radiation time. Unlike fixed power control, total radiation time is not equal to the amount of time the samples are kept in the chamber. Microwave power efficiency is also influenced by sample movement due to power pulling and frequency pulling (Leonelli & Veronesi, 2015)

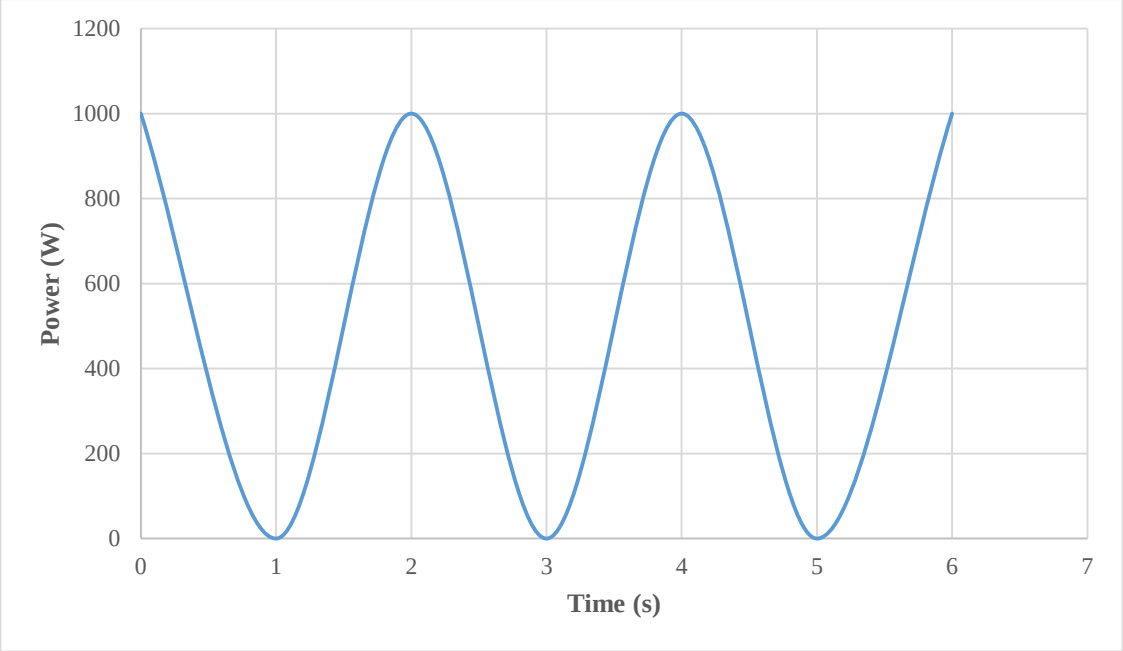

Figure 3-13: Variable power configuration

On the other hand, microwave oven with fixed power configuration emit a constant power level over the course of radiation. An example of these is shown in *Figure 3-14*. This type of power setting is commonly found in a single-mode microwave reactor or dedicated reactor for chemical synthesis, where the nature of focused radiation and high heating rate is inherent. However, it comes with disadvantage. Some microwave power is lost and ended up not being absorbed by the samples. A water sink or cooling gas were usually employed to absorb the radiation in order to minimise damage to the magnetron.

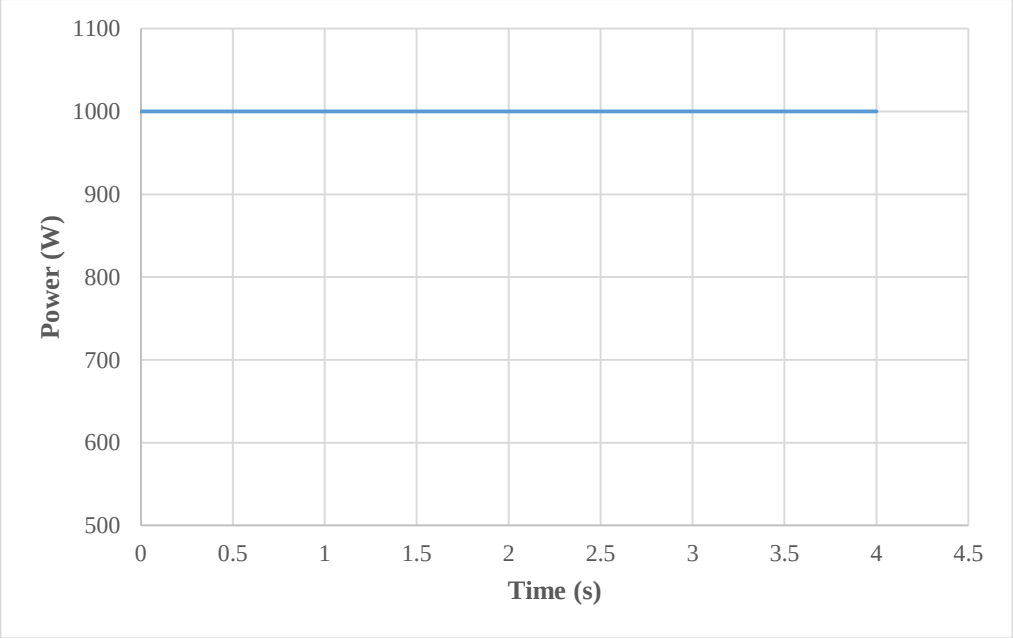

Figure 3-14: Constant power level in a fixed power configuration

3.4 Description of Temperature Measurement System

Two K-type (Al-Cr) thermocouples were placed within 5 cm apart in the MP experiment to minimise the risk of electromagnetic interference. They were properly grounded to the oven cavity to reduce the risk of arcing. In this study, T1 is the thermocouple wired to the microwave oven controller, while T2 is an independent thermocouple connected to the data logger. The temperature profiles against time are presented in *Figure 3-15* and *Figure 3-16* for 500 and 800°C pyrolysis, respectively.

It can be seen that T1 and T2 registered different temperatures during microwave heating process, although they essentially recorded a similar temperature at t=0 min. Uneven profiles were observed at around t=10 minutes, due to the cyclic load of microwave power to maintain the sample at set temperature. This is best represented by T2 in *Figure 3-15*, while the temperature recorded by T1 varies between +20% of set temperature.

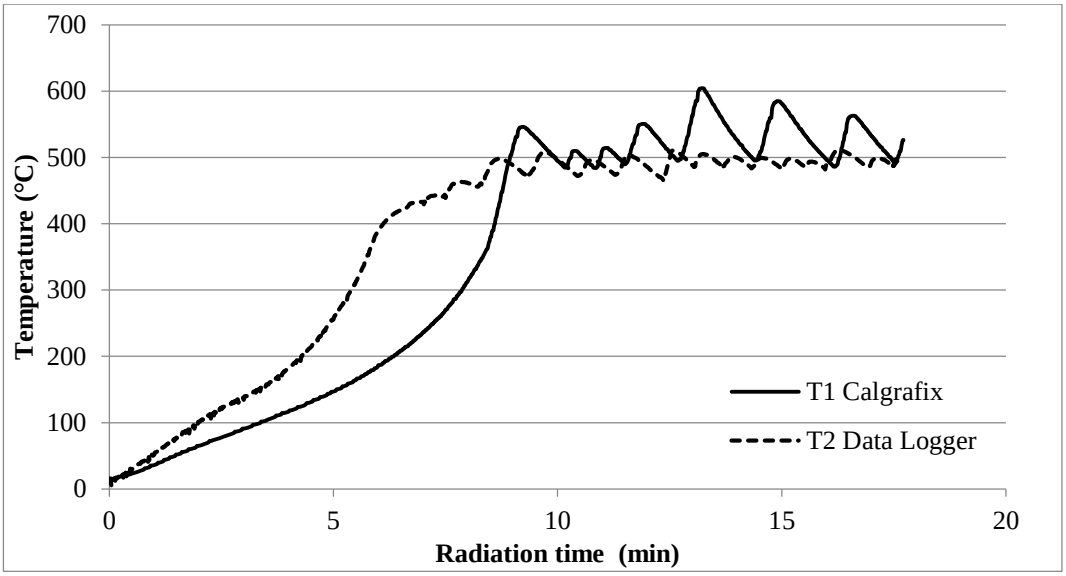

Figure 3-15: Temperature profiles during MP EFB at 500°C

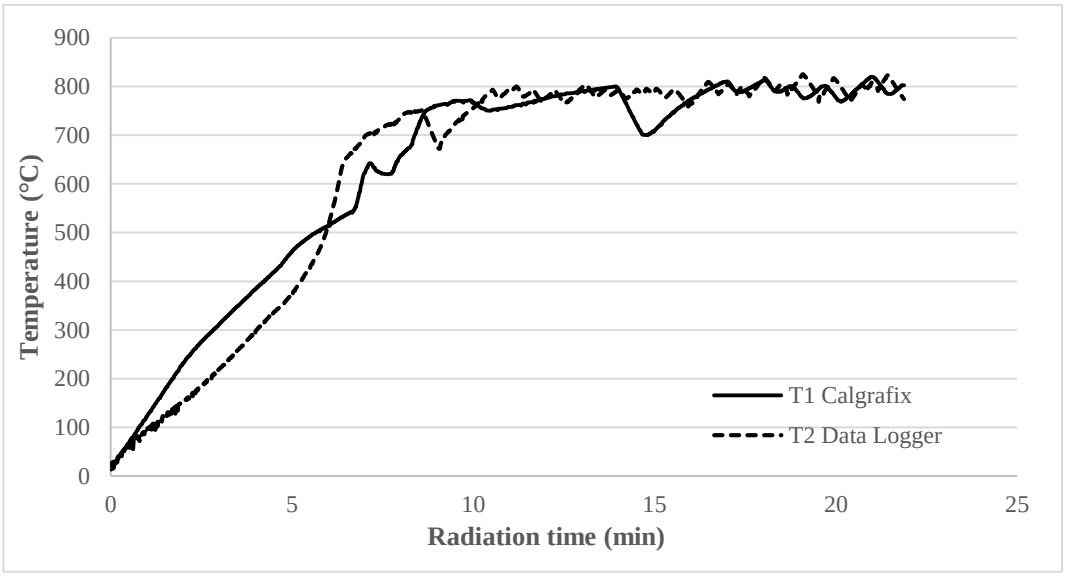

Figure 3-16: Temperature profile during MP EFB at 800°C

3.4.1 Microwave Thermocouple Effect

In order to determine the effects microwave has on the thermocouple, a simple test was conducted using 40 g of biomass pellets. 180°C was chosen as set temperature. The microwave energy was supplied for about 3 minutes in order for heating to take place. Microwave power was turned off beyond this point and the thermocouples were left to cool

naturally for about 20 minutes. The temperature profiles are presented in *Figure 3-17*. It can be seen that there is a great discrepancy between the temperature reading from T1 and T2.

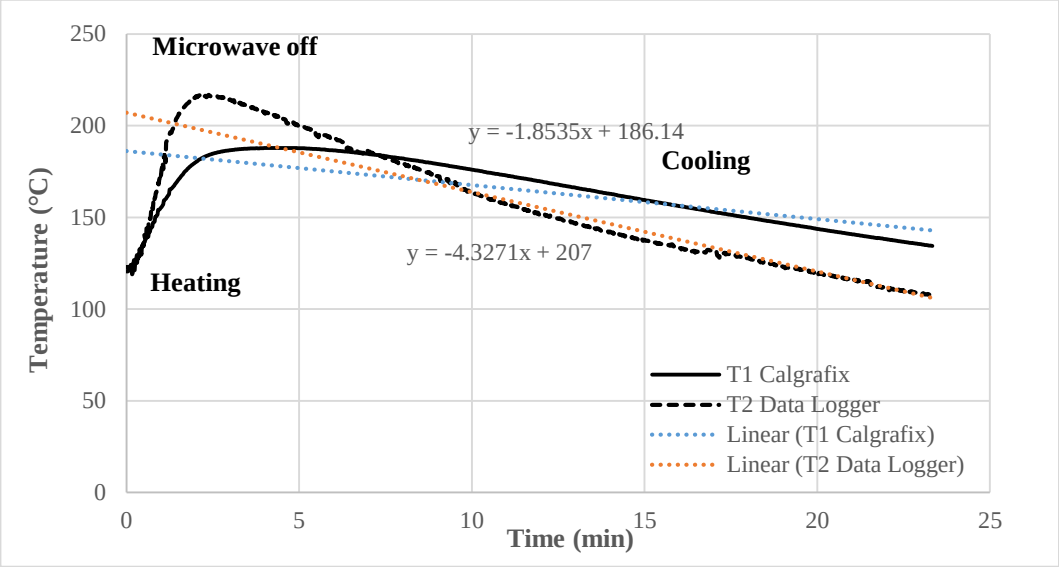

Figure 3-17: Thermocouple reading during microwave heating and natural cooling

During microwave heating, both graphs resemble parabolic curves until the microwave was switched off. Although the microwave oven control was set to 180°C, T2 recorded a jump in temperature or overshoot. The maximum temperature measured by T2 just before the microwave was switched off was about 20% higher than the initial set temperature. The thermocouples then lost heat to the surrounding during cooling period. The rate of cooling follows a linear relationship.

Thermocouple response time (τ) is defined as the time required for a sensor to reach 63.2% of a step change in temperature under a specified set of conditions. It was computed from the line graph in *Figure 3-18*, where the time constant was multiplied by 1.5 for an ungrounded type thermocouple (Engineering, 2017). The K-type thermocouple with metal sheath covering used in this study has a response time (τ) of 21s. This indicates a slower response time or lag to any instantaneous change in temperature.

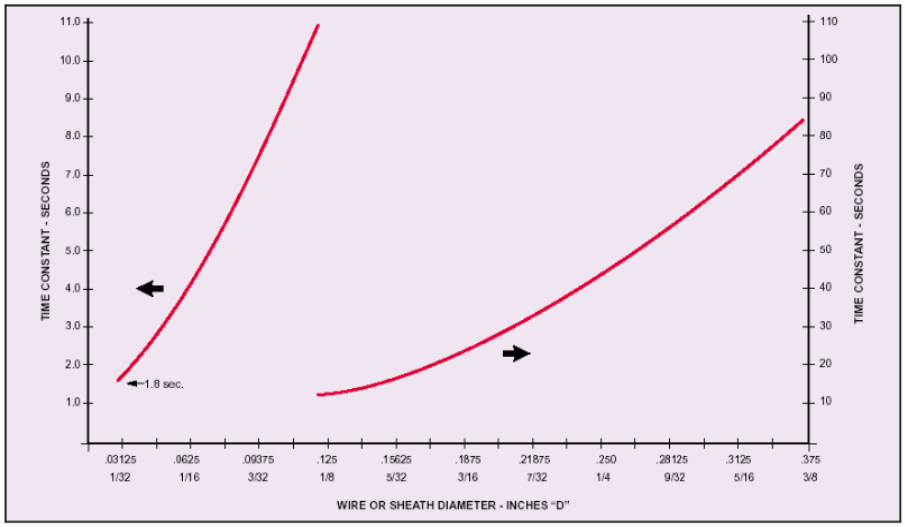

Figure 3-18: Time constant (τ) of thermocouple made with ungrounded junction type (Engineering, 2017)

Although the thermocouple tip was embedded into the sample bed, the temperature measured was likely to be the temperature of hot volatiles. The response time was heavily influenced by the thermocouple junction type and sheath diameter, where an exposed junction with smaller sheath diameter would have a faster response time. Further investigation on the microwave thermocouple effect is conducted in **Section 5.2.4.**

3.5 Solid Analysis

3.5.1 Ultimate Analysis

Ultimate analysis was performed to determine the concentration of organic compounds, CHNS/O. Equipment used in this study was Thermo Scientific Flash 2000 Organic Elemental Analyser as shown in *Figure 3-19*. It has a detection limit of 100 ppm. It used a PTFE multi-separation column, (l= 2m, ϕ= 6mm x 5mm) that worked on thermal conductivity detector (TCD) for elemental determination. The instrument was first calibrated using standard material, BBOT[1]. 2-3 mg of solid sample was placed into a tin

[1] 2,5 bis (5-ter-butyl-benzoxazol-2-yl) thiophene

capsule, with Vanadium Pentoxide for sulphur determination. The analysis was conducted according to ASTM D3176, where oxygen concentration was computed by difference.

Figure 3-19: Thermo Scientific Flash 2000 Organic Elemental Analyser

3.5.2 Trace Analysis

Due to cost of the appropriate instrument, biomass samples were sent to an external company for the determination of trace elements in solid. They were tested for the presence of sodium (Na), potassium (K), magnesium (Mg), calcium (Ca), iron (Fe), zinc (Zn), copper (Cu), lead (Pb), aluminium (Al), silica (Si), and phosphorus (P). 500 mg of biomass was initially dissolved in 10 mL HNO_3 pure reagent. The samples were left in an Anton-Paar Multiwave Go at 160ºC for 25 minutes to achieve complete dissolution of the solid matrix. The analytes were then analysed in Thermo Fisher iCAP 7600 ICP-OE spectrometer.

3.5.3 Proximate Analysis

Proximate analysis was carried out to determine the amount of moisture, volatiles, fixed carbon and ash. The analysis was performed using Perkin Elmer TGA 4000 shown in *Figure 3-20*. A sample weighing around 17-18 mg was thermally degraded from 30 to 100°C at 20°C/min under constant purge of N_2 at 20 mL/min. It was further heated from 100 to 900°C at 25°C/min to ensure complete removal of volatiles. At this point, the purge gas was switched from N_2 to O_2 at 40 mL/min for combustion to take place. The sample was held at this temperature for 7 minutes. Finally, the sample was heated from 900 to 950°C at 10°C/min to oxidise the remaining fixed carbon. The residue left indicated an incombustible ash. Mass loss increment (ΔY) was computed from the point where mass loss had reached a plateau. This corresponds to the moisture, volatiles, and fixed carbon while ash was computed by difference. The analysis was conducted according to ASTM D3172.

Figure 3-20: Thermogravimetry analyser

3.5.4 Calorific Value

Equipment used in the calorific value determination was Parr 6200 isoperibol bomb calorimeter shown in *Figure 3-21*. It involves the total recovery of latent heat of water vapour following complete combustion. The analysis was conducted according to ASTM D5865, using samples weighing between 0.9-1.1 g. The sample was placed inside a combustion vessel filled with 99.98 % pure O_2 at 30 bar. 10 cm ignition wire was placed just above the sample to initiate combustion. The combustion vessel was then immersed in 2000±5 g of water before the reaction took place. Gross calorific value (GCV) of biomass was determined following *Eq: 3-3*.

Figure 3-21: Parr 6200 calorimeter

$$GCV = \frac{W.\Delta T - e_1 - e_2 - e_3}{m} \quad \text{Eq: 3-3}$$

$$W = (H.m + e_1 + e_2 + e_3)/\Delta T \quad \text{Eq: 3-4}$$

Where W is the energy equivalent (J/°C), ΔT is the net temperature rise (°C), e_1 and e_2 are correction for heat of formation of HNO_3 and H_2SO_4, respectively (J). Meanwhile, e_3 is the correction for heat of combustion of fuse wire (J) and m is the sample mass (kg). Fuse correction factor was given at 9.63 J/cm.

During combustion with pure oxygen at high pressure, nitrogen and sulphur molecules reacted with water vapour to form HNO_3 and H_2SO_4, respectively. However, biomass used in this study contained traces amounts of N and S as mentioned in **Section 4.1**. Hence, the calorific value determination only accounts for the wire correction factor (e_3). Standardisation procedure was carried out initially following *Eq: 3-4* to determine the energy equivalent (W) of the calorimeter. 1 g of benzoic acid with a known heat of combustion, *i.e.*: H = 26.434 MJ/kg was chosen for this procedure. This yielded an energy equivalent of 10.12 kJ/°C which was then used in the previous GCV calculation.

3.5.5 Scanning Electron Microscopy

Scanning Electron Microscopy (SEM) analysis was carried out to observe the surface morphology of char after the pyrolysis process. Equipment used was Philips XL 30S FEG, as shown in *Figure 3-22*. It was coupled with Inca X-Sight, a type of Energy Dispersive Spectroscopy (EDS) for elemental analysis. A cross section of char was adhered to a carbon stick, and onto aluminium stub for analysis. It used secondary electron (SE) detector, which was set at 15 kV. The analysis was conducted following the methodologies outlined in ASTM 1508-12a.

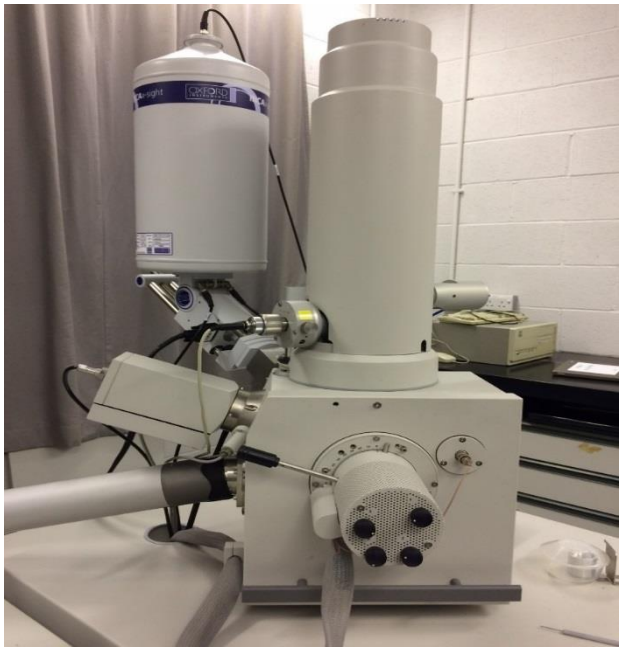

Figure 3-22: Philips XL30S FEG

3.5.6 B.E.T Surface Area

The surface area of char was determined using Micromeritics 3Flex Surface Characterisation Analyser shown in *Figure 3-23*. It measures the physical adsorption/desorption of N_2 isotherm at 77.4 K, at a relative pressure of $P/P_{0.}$ The specific surface area is then determined using Brunauer-Emmett-Teller (BET) equation described below. About 0.25g char, as-received was initially degassed in a vacuum oven at 250°C for 3 hours to remove any residual volatiles. The final weight of dried sample after vacuum degassing was recorded.

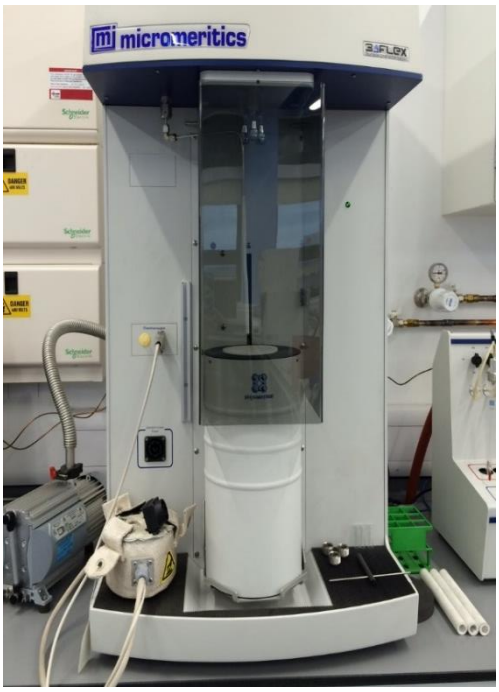

Figure 3-23: Surface characterisation analyser

$$\frac{1}{v\left[\left(P_0/P\right)-1\right]} = \frac{c-1}{v_m c}\left(\frac{p}{p_0}\right) + \frac{1}{v_m c} \qquad \text{Eq: 3-5}$$

Where v is the adsorbed gas quantity (L), v_m is the monolayer adsorbed gas quantity (L), and c is the BET constant. Meanwhile, P and P_0 are the partial and saturation vapour pressure of N_2 (Pa) at the temperature of adsorption, respectively.

3.5.7 Dielectric Properties

The ability of material to absorb microwave energy and converting it into heat energy is related to its dielectric properties. This is studied using an open ended micro-strip stub connected to a 2.45 GHz Vector Network Analyser (VNA) shown in *Figure 3-24*. The fabricated circuit consists of copper micro-strip (w=9.18 mm) and a Teflon sample holder (ϕ= 20mm, h= 20mm) built on a Duroid disc.

An initial calibration is performed on the VNA followed by circuit calibration. When dielectric material is placed on the sample holder, this causes an increase in fringing capacitance and a down shift in resonance frequency or S-parameter. This is due to the dielectric loading at the end of micro-strip line. The result is then replicated using an ANSYS High Frequency Structure Simulator (HFSS) tool through an iterative process. The dielectric material is assumed to be homogeneous and is assigned arbitrary values, *i.e.*: ϵ' and tan α. The iteration process is carried out until the simulated value shows close agreement with the measured value.

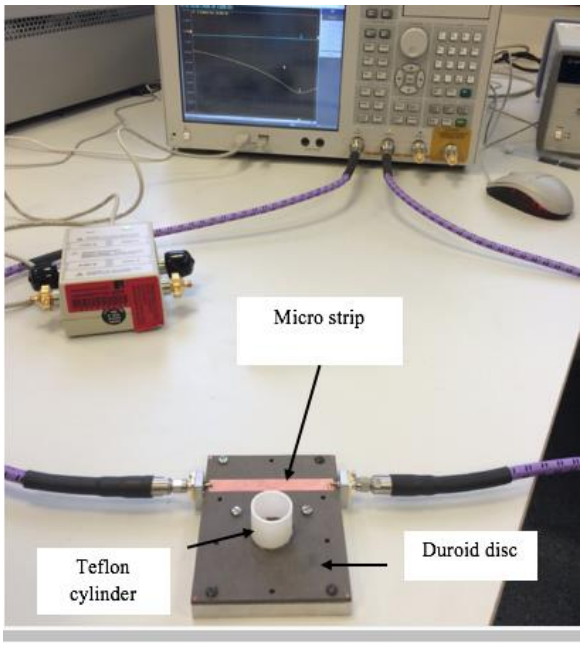

Figure 3-24: Vector Network Analyser connected to an open ended micro-strip stub

3.6 Liquid Analysis

3.6.1 Ultimate Analysis

The analysis was performed using similar equipment to that in **Section 3.5.1**. Bio oil was first homogenised before an aliquot was extracted for CHNS/O determination. 5 mg of oil sample was used, with an addition of Chromosorb W mesh 30/60 for nitrogen determination. The procedure followed ASTM D5291-16 which is the Standard Test Method for Instrumental Determination of CHNS in Petroleum Products and Lubricants. Meanwhile, the gross calorific value (GCV) of bio oil was determined using a correlation based on ultimate analysis (wt.%) as proposed by (Sheng & Azevedo, 2005). This is shown in *Eq: 3-6*.

$$GCV\ (MJ/kg) = -1.3675 + 0.3137\,C + 0.7009\,H + 0.0318O \qquad \text{Eq: 3-6}$$

3.6.2 FTIR Analysis

Fourier Transform Infrared Spectroscopy (FTIR) analysis was conducted using a Perkin Elmer Frontier spectrometer coupled with an Attenuated Total Reflectance (ATR) accessory shown in *Figure 3-25*. It enables the determination of various functional groups and possible compounds in pyrolysis bio oils. The equipment was first checked against background noise, which was factored into the subsequent analysis.

A light beam in the mid infrared region (4000-600 cm^{-1}) was transmitted into the sample. When beam frequency matched the natural frequency of a particular chemical bond, the resonance gave rise to a molecular motion (*i.e.*: molecular stretching/bonding). This molecular motion was translated into peak intensity or transmittance (%T) at a different wave number (cm^{-1}). The analysis was conducted according to ASTM E1252.

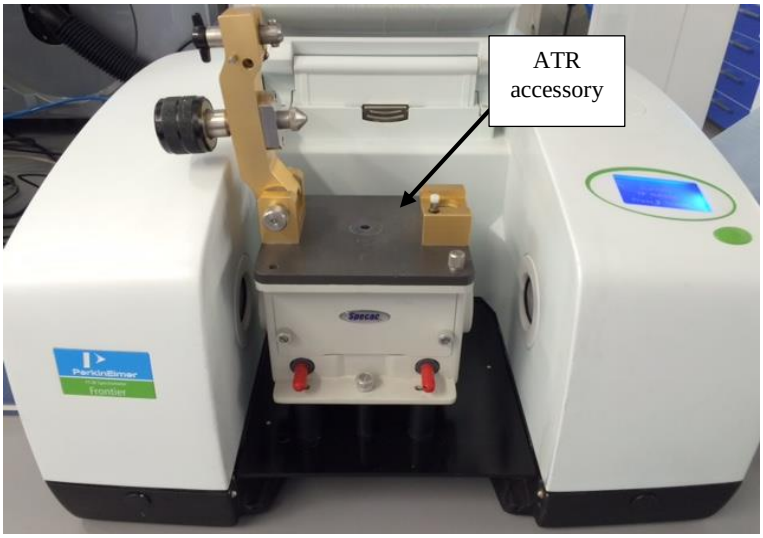

Figure 3-25: Perkin Elmer Frontier spectrometer

3.6.3 GC-MS Analysis

Pyrolysis oils were also analysed for Volatile Organic Compounds (VOC) and Semi-Volatile Organic Compounds (SVOC). The equipment used for this purpose was Shimadzu GCMS-QP2010 shown in *Figure 3-26*, with RESTEK Rxi-5Sil MS capillary column and He as the carrier gas. The sample was first homogenised and extracted using solvent prior to analysis. For VOC determination, an aliquot was sealed in a vial with water and sodium chloride and subjected to heating and agitation. A sample of headspace is then analysed, with detection limit of 0.04 mg/kg.

Meanwhile for SVOC determination, an aliquot is extracted with dichloromethane and agitated through sonication before being injected to the GC. It has a detection limit of 0.5 mg/kg. The procedure followed ASTM D5769 which is the Standard Test Method for Determination of Benzene, Toluene, and Total Aromatics in Finished Gasoline by Gas Chromatography/-Mass Spectrometry.

Figure 3-26: Shimadzu GCMS-QP2010

It is also worth noting that not all tar fractions can be analysed from the capillary column. One of the limitations of GC/MS analysis lies in its inability to analyse heavy tar fractions. This is partly due to the limit imposed by the maximum column temperature, which in this case is 350 °C. This means, heavy tar fractions with boiling points outside the column operating range would not appear on the chromatogram.

3.7 Gas Analysis

Gas bags were immediately analysed to prevent dilution. The analysis was carried out using Thermo Scientific Trace 1310 Gas Chromatograph equipped with Thermal Conductivity Detector (GC-TCD), as shown in *Figure 3-27*. It used a molecular sieve 5A packed column for permanent gases (*l*= 2m, *id*= 2mm), with 10 µL injection volume. Helium (He) was used as carrier gas at 30 mL/min. The oven and detector temperature were kept at 50 and 200°C, respectively. The GC was initially calibrated for pyrolysis gas with the following concentration; H_2 (30%), CO_2 (20%), CH_4 (8%), CO (20%) and O_2 (2%). N_2 was computed by difference. Meanwhile, the gross calorific value (GCV) of pyrolysis gas was determined based on composition (vol.% dry) according to *Eq: 3-7* (Li et al., 2004).

Figure 3-27: Thermo Scientific Trace 1310 Gas Chromatograph

$$GCV\ (MJ/m^3) = [(12.63\ \times CO) + (12.75\ \times H_2) + (39.82 \times CH_4)]/100 \qquad \text{Eq: 3-7}$$

3.8 Error Analysis

The measurement presented herein considers a 95% confidence limit. Confidence limit is defined as:

$$\bar{X}\ \pm\ t_{1-\frac{\alpha}{2},N-1}\ \frac{s}{\sqrt{N}} \qquad \text{Eq: 3-8}$$

Where $\bar{X}$ is the sample mean, s is the sample standard deviation, N is the sample size, α is the significance level, and $N-1$ is the degree of freedom. In this case α is chosen as 0.05, which means there is a P (0.05) probability that the measured data would fall outside the normal distribution. A quick look into the t-table revealed a t-value of 4.303 for N=3, with 2 degrees of freedom would indicate the 95% confidence limits. This value is consistently used in tables throughout the next chapter and shown graphically as error bars where appropriate.

3.9 Summary

This chapter explores various approaches to biomass and pyrolysis product characterisation. Biomass materials were initially tested for calorific value, trace elements in solid, CHNS/O composition, and proximate analysis. These were followed by a series of conventional and microwave pyrolysis experiments at 500 and 800°C. The former was carried out using a fixed-bed pyrolysis reactor, where heat was supplied by 15.8 kW radiant heater. Meanwhile, microwave pyrolysis tests were carried out using 1 kW multi-mode microwave oven. Both experimental setups were connected to a water-cooled condenser and tar cleaning for bio oil and dry gas collection. Power consumption was measured by a data logger, which provides real time data recording. In order to discern the influence of temperature, pyrolysis products were subjected to various analysis. Pyrolysed chars were tested for heating value, ultimate and proximate analysis, dielectric properties, surface image analysis and B.E.T analysis. Bio oils were tested for chemical compounds via GC-MS and FTIR analysis. Finally, pyrolysis gas composition was determined using GC-TCD equipment. The measurement presented herein considers a 95% confidence limit.

4 Results and Discussion of Conventional and Microwave Pyrolysis

This chapter begins by providing a detailed description of the biomass materials used in this study. The influence of temperature and heating mechanism on pyrolysis product distribution are clearly presented and discussed. This section also looks into the efficiency of pyrolysis system and microwave thermocouple effects. Finally, energy yield analysis is conducted to determine the potential for process optimisation.

4.1 Characterisation of Biomass Feedstock in This Study

The empty fruit bunch (EFB) and rice husk pellets used in this study are shown in *Figure 4-1*. From physical observation, EFB pellets have a more fibrous structure, while rice husk pellets are sturdier. EFB pellets are 8 mm in diameter, with length ranging from 13 to 55 mm. Meanwhile, rice husk pellets are 9 mm in diameter with length between 10 to 50 mm. Pyrolysis experiments were conducted using biomass pellets as-received. However, in order to perform sample characterisation in **Section 3.5**, biomass pellets and chars were initially ground using RETSCH PM100 ball mill and sieved to obtain particle size of ≤125 μm.

Table 4-1 highlighted the chemical properties of biomass used in this study. In general, both biomass materials have a moisture content below 6 wt.%. The total combustibles made up around 91 wt.% and 81 wt.% of EFB and rice husk composition, respectively. The high amount of volatiles at around 69 wt.% on average suggests the potential of energy recovery via pyrolysis process. Meanwhile, incombustible ash made up almost 14 wt.% of rice husk. The results correlate well with the findings from ultimate analysis.

Figure 4-1: Biomass pellets used in this study. A) EFB pellets and B) Rice husk pellets

Table 4-1: Properties of biomass feedstock

Properties	**EFB**	**Rice husk**
Proximate analysis (wt.%)		
Moisture content	5.67 ± 0.20	5.15 ± 0.08
Volatile matter	72.89 ± 0.45	64.27 ± 0.24
Fixed carbon	18.13 ± 0.05	16.74 ± 0.05
Ash	3.31 ± 0.37	13.84 ± 0.07
Ultimate analysis (wt.%)		
C	45.04 ± 0.67	38.45 ± 1.28
H	6.82 ± 0.20	6.07 ± 0.22
N	1.55 ± 0.02	0.90 ± 0.03
S	0.07	0.03
*O**	46.52	54.55
H/C	1.82	1.89
O/C	0.77	1.06
Empirical formula	$CH_{1.82}O_{0.77}$	$CH_{1.89}O_{1.06}$
Calorific value (MJ/kg)	18.61 ± 0.02	15.84 ± 0.05

*Computed by difference

These volatiles were mainly composed of C=O, C-O bonds with low degree of oxidation. Ultimate analysis revealed low carbon content at just 46 wt.% and 39 wt.% in the EFB and rice husk, respectively. Nitrogen was recorded at below 2 wt.% with negligible amount of S (<0.1 wt.%) in both materials. Biomass in this study recorded calorific value between 15-19 MJ/kg, which is comparable to low grade coal, *i.e.*: lignite. The lower CV of rice husk at 15.84 MJ/kg can be attributed to its high ash and O content at around

55 wt.%. Biomass composition in this study sits well within the range found by (Omar et al., 2011) and (Lim et al., 2012).

4.1.1 Analysis of Trace Elements Present in Biomass

Major elements found during trace analysis of biomass are presented in *Figure 4-2*. These include alkali metals, alkaline-earth metals, and transition metals and salts such K, Ca, Mg, Fe, P, and Si. These elements are essential for plant growth. It can be seen that silica (Si) made up the majority of rice husk trace elements at 58,800 μg/g. Si and K are also found to be dominant in EFB at 14,900 μg/g and 14,476 μg/g, respectively. Other metals such as Ca, Fe, and Mg are found in lower concentration in both materials.

Meanwhile, minor elements are presented in *Table 4-2*. These include Pb, Zn, Cu, Al, Mn and Na. The presence of heavy metals in the biomass was considered negligible. For instance, less than 2 μg/g of toxic Pb was recorded in both materials. In the context of biomass combustion, this could affect the bottom-ash disposal and flue gas emission issues. The significant presence of alkali and alkaline-earth metals plays a catalytic role during biomass pyrolysis. Alkali metals, especially K acts a catalyst by lowering the activation energy and degradation temperature of cellulose (Nowakowski et al., 2007). Meanwhile, alkaline-earth species, *i.e.*: Mg and Ca have a less significant influence compared to alkali metals. Study by Long *et al.* (Long et al., 2012) has shown that around 53-76% of alkali metals were evolved during pyrolysis, in contrast to 27-40% of alkaline-earth metals.

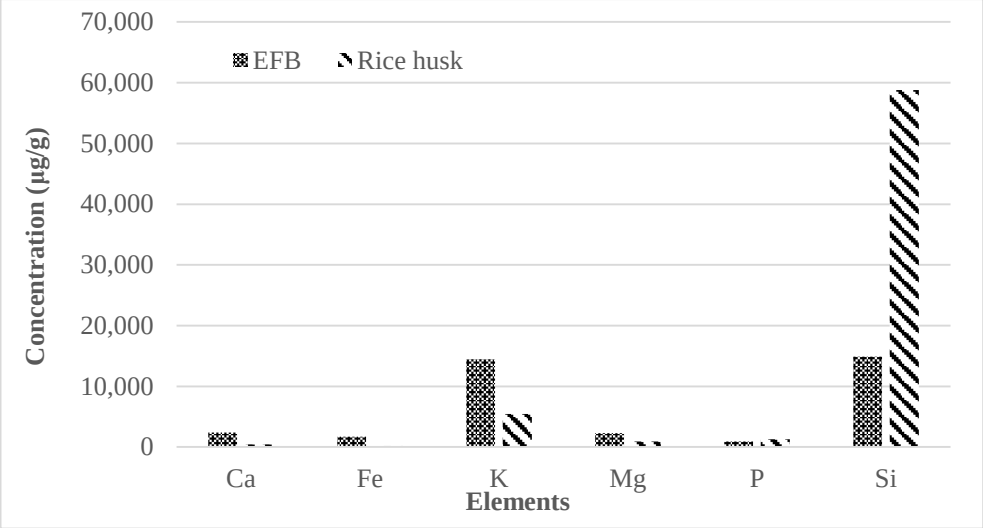

Figure 4-2: Major elements of biomass feedstock

Table 4-2: Minor elements of biomass feedstock

Biomass	Concentration (µg/g)					
	Na	Al	Cu	Pb	Zn	Mn
EFB	74.76	559.91	37.09	1.05	47.17	55.41
Rice husk	36.80	47.13	1.64	1.39	22.98	0.02

This is due to the intrinsic properties of valence bonds in Ca and Mg compared to the mono-valence bond found in Na and K. A small but significant amount of K was released at low temperature (180-500°C) and the amount progressively increased beyond 500°C (Olsson et al., 1997).

4.1.2 Derivative Thermogravimetry Analysis

The thermal behaviour of biomass can be seen from the DTG curves shown in *Figure 4-3*. It provides information with respect to an initial degradation temperature, decomposition rate, and peak temperature. These were influenced by the intrinsic properties of biomass, heating rate, and temperature (Shafizadeh, 1982). The peaks observed in the DTG curves correspond to the moisture evolution stage (~100°C), and hemicellulose and cellulose decomposition. The first stage accounts for around 6% loss in moisture at 0.30 mg/min. In the case of EFB, hemicellulose decomposition started at around

200°C and peaked at a rate of -1.73 mg/min at 314°C. Maximum decomposition rate of -2.86 mg/min is observed during cellulose decomposition at 349°C. The thermally-stable lignin is considered to decompose over a wide temperature range between 250-500°C (Antal Jr et al., 1998; Raveendran et al., 1996).

Meanwhile, a greater decomposition rate of -2.29 mg/min is observed during hemicellulose decomposition of rice husk, which peaked at 329°C. Its cellulose decomposition is much lower than that of EFB at just -2.46 mg/min. No further weight loss is observed beyond 830°C. Another thing to note is the possible effect of alkali metals species, notably K and Na during thermal decomposition. EFB has a total of 14,551 μg/g alkali metals in contrast to 5,492 μg/g found in the rice husk. Alkali metals tend to shift the peak degradation temperature of cellulose and hemicellulose towards the lower temperature region. In this case, the cellulose pyrolysis of EFB occurred at 358°C, about 15°C lower than rice husk (Fahmi et al., 2007; Nowakowski et al., 2007; H Yang et al., 2006).

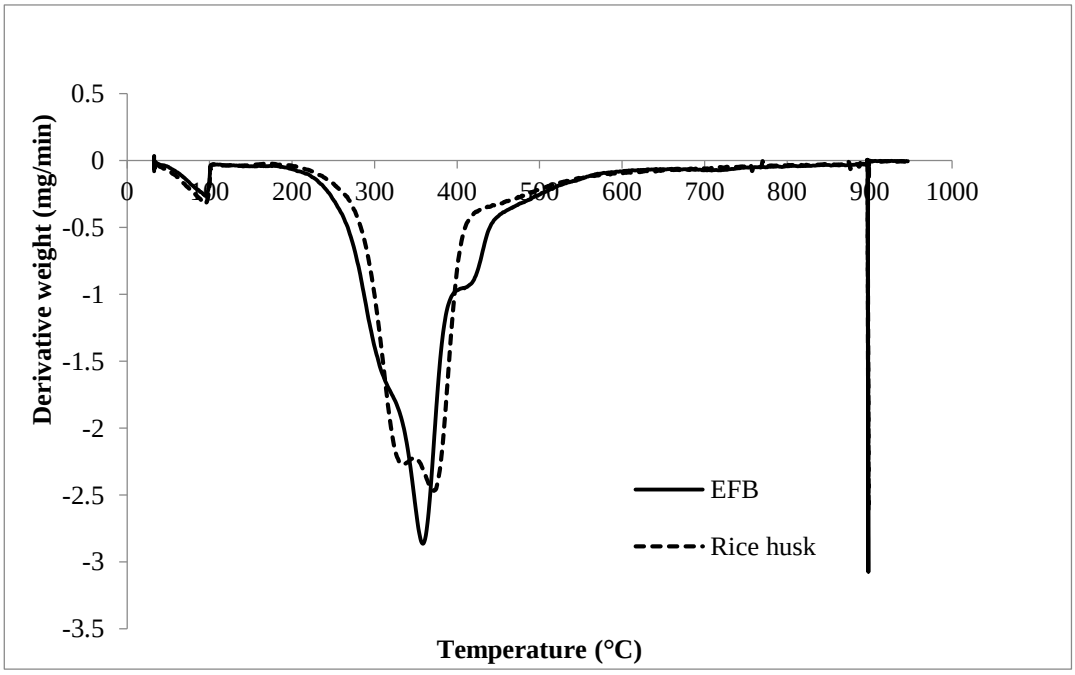

Figure 4-3: DTG curves

4.2 The Effect of Temperature and Heating Process on Pyrolysis Product Yield

Product yield from the pyrolysis of EFB and rice husk are summarised in *Figure 4-4* and *Figure 4-5*, respectively. In general, gas production increased with an increase in temperature, at the expense of char and bio oil, regardless of heating methods. A similar trend has been observed by (Bu et al., 2012; Domínguez et al., 2007; Haiping Yang et al., 2006; Onay & Kockar, 2003; Demirbaş, 2001). For instance, gas yield increases from 48.90 to 69.38 wt.% as the reaction temperature is increased from 500 to 800°C during conventional pyrolysis of EFB (CP EFB). Similarly, this resulted in a decrease of both char and bio oil by 8.80 and 11.70 %, respectively. This can be explained by greater primary decomposition and an enhanced secondary reaction at high temperature. Both favour the conversion of tar and char into lighter hydrocarbons or syngas.

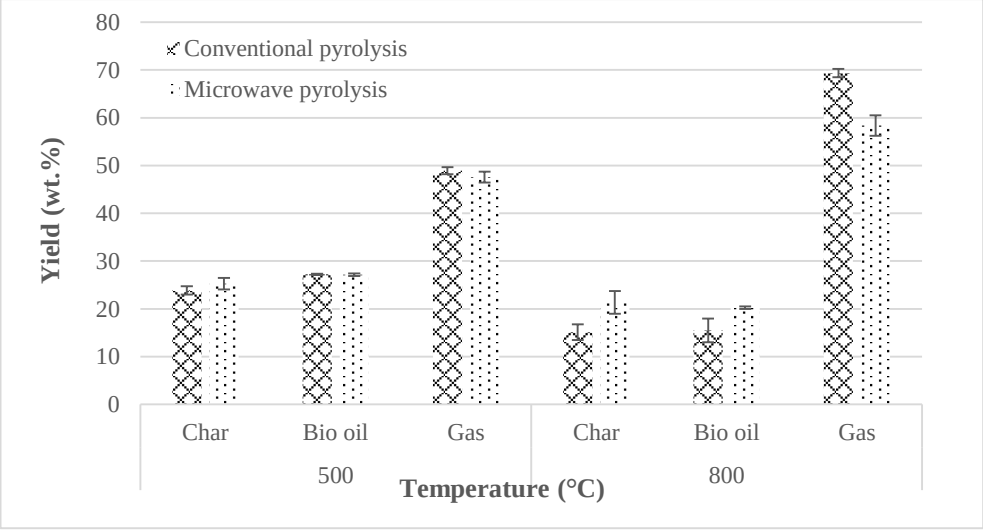

Figure 4-4: Product yield from EFB pyrolysis

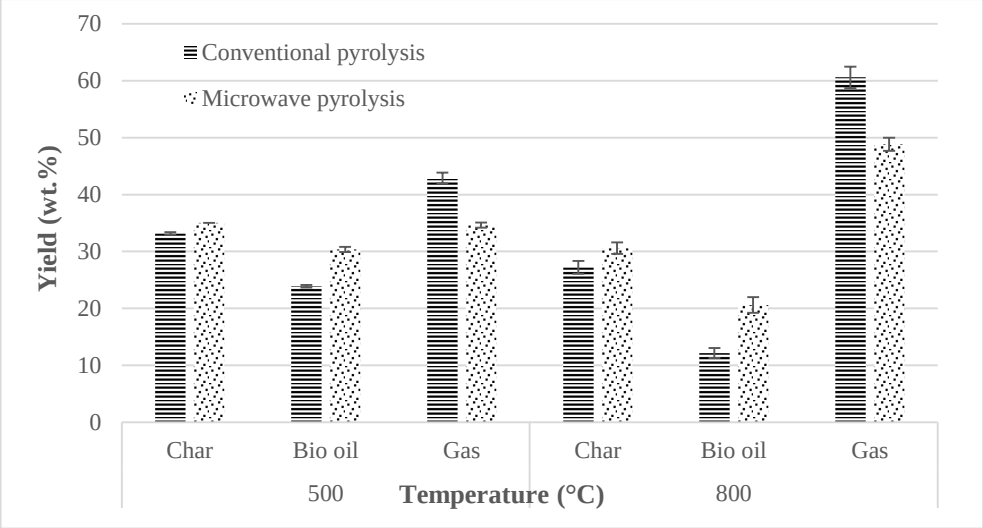

Figure 4-5: Product yield from rice husk pyrolysis

Meanwhile, microwave pyrolysis is found to yield a higher amount of bio oil and char than conventional pyrolysis. For example, MP of rice husk pellets at 800°C recorded around 8.5 % higher bio oil yield than CP at similar temperature. Similarly, the yield of char obtained from MP is about 1-7 % higher than CP. The higher char yield in MP can be attributed to the nature of pulsed radiation often found in a multi-mode microwave oven. The cyclic power could possibly reduce the amount of microwave energy going into heating the biomass (Salema & Ani, 2012). This is made worse by the fact that the microwaves were fed from the bottom of the oven cavity, which will be discussed in **Section 5.2.3**.

Greater bio oil yield observed in MP can be explained by microwave-specific effects induced by rapid heating. In this case, MP recorded a heating rate of 50 °C/min, compared to around 35 °C/min during CP. Dipole rotation that proceeds at a rate of 2.45×10^9 per second causes volumetric heating and increases the sample bulk temperature. This leads to overheating due to the formation of hot spots and elimination of wall effects unlike samples heated under electric furnace. The latter results in the formation of high

quality products due to lack of further degradation as the volatiles travelling along the colder region of biomass.

Meanwhile, non-thermal effect is mainly concern with the interaction of MW radiation with the reactant molecules. This aspect is harder to quantify due to slower conversion of microwave energy to kinetic energy when compared to kinetic to thermal energy. It has been found that microwaves can increase molecular mobility and affect reaction kinetics by lowering the activation energy (E_a) and increasing the Arrhenius pre-exponential factor (Namazi et al., 2016). The latter implies an increasing rate of collision and thus, a higher reaction rate. This means chemical reactions can be sped up at a much lower activation temperature compared to conventional heating as demonstrated by (Zhou et al., 2016; Budarin et al., 2009). It was found that chemical activation via MP increases reaction rate by 15% than conventional heating at similar temperature due to targeted activation or material selectivity that occur under MW radiation.

A higher gas yield is observed during conventional pyrolysis for all temperatures and samples. Gas yield recorded in CP is about 1-12 % higher than MP. This can be attributed to the prolonged hot vapour residence time in CP before reaching the condenser. The reactor in CP has a total length of 1330 mm, while these volatiles were immediately quenched in the case of MP. This induces the thermal cracking of tar and char gasification into non-condensable gases. A similar situation has been observed by Natarajan and Ganapathy Sundaram (Natarajan & Ganapathy, 2009). Moreover, alkali metals left inside char could promote the steam-reforming of vapours to produce H_2. Quick char removal and increasing the sweep gas flow rate could minimise the extent of secondary reactions.

The chars produced from the conventional and microwave pyrolysis of rice husk pellets are about 9-12% greater than EFB pyrolysis. Higher char yield can be attributed to its high ash content and slightly larger particle size than EFB pellets, as mentioned previously in **Section 4.1**. The latter indicates poor heat transfer caused by the large temperature gradient between the core and surface of the pellet. Meanwhile, low carbon conversion is observed during pyrolysis due to the strong presence of SiO_2, which retains its inert structure despite high temperature. This compound forms a strong molecular bond with carbon, which is not easily broken at the pyrolysis temperature in this study (Bharadwaj et al., 2004).

The strong presence of alkali metal salts is known to increase overall char yield (Williams & Horne, 1994). However, the higher amount of alkali metals found in EFB could induce char gasification. Hence, the lower char but higher gas yield recorded from EFB pyrolysis. CP of EFB recorded a higher bio oil yield than rice husk at both temperatures. However, a reversal in the trend is observed during microwave pyrolysis. Bio oil recorded during microwave pyrolysis of rice husk is about 0.35-3% higher than those recorded during MP of EFB.

4.3 Char Analysis

4.3.1 Ultimate and Proximate Analysis

The ultimate and proximate analysis of EFB and rice husk chars are summarised in *Table 4-3* and *Table 4-4*, respectively. In general, a decrease in moisture and volatiles are observed with an increase in reaction temperature. The evolution of volatiles has contributed to char formation of higher fixed carbon and ash proportions relative to parent material. Proximate analysis revealed a significant amount of residual volatiles left inside the pyrolysed chars; between 5-15 wt.% and 3-9 wt.% for EFB and rice husk, respectively.

Table 4-3: Chemical properties of EFB chars relative to raw biomass

Pyrolysis method	**None**	**Conventional Pyrolysis**		**Microwave Pyrolysis**	
Samples	**EFB**	**EFB500**	**EFB800**	**EFB500**	**EFB800**
Proximate analysis (wt.%)					
Moisture content	5.67	2.07 ± 0.12	2.11 ± 0.18	2.11 ± 0.03	2.31 ± 0.01
Volatile matter	72.89	10.05 ± 0.16	5.87 ± 0.03	14.49 ± 0.02	7.07 ± 0.03
Fixed carbon	18.13	72.84 ± 0.05	76.71 ± 0.06	70.70 ± 0.06	76.63 ± 0.05
Ash	3.31	15.04 ± 0.09	15.31 ± 0.02	12.70 ± 0.10	13.99 ± 0.07
Ultimate analysis (wt.%)					
C	45.04	69.28 ± 0.70	71.70 ± 1.13	68.08 ± 0.02	69.73 ± 0.05
H	6.82	1.87 ± 0.03	0.63 ± 0.03	2.30 ± 0.06	0.71 ± 0.06
N	1.55	1.07 ± 0.05	0.72 ± 0.01	0.93 ± 0.01	0.88 ± 0.01
S	0.07	<100ppm	<100ppm	<100ppm	<100ppm
O*	46.52	27.78	26.95	28.69	28.68
H/C	1.82	0.32	0.11	0.41	0.12
O/C	0.77	0.30	0.28	0.32	0.31
Empirical formula	$CH_{1.82}O_{0.77}$	$CH_{0.32}O_{0.30}$	$CH_{0.11}O_{0.28}$	$CH_{0.41}O_{0.32}$	$CH_{0.12}O_{0.31}$

*Computed by difference

Table 4-4: Chemical properties of rice husk chars relative to raw biomass

Pyrolysis method	**None**	**Conventional Pyrolysis**		**Microwave Pyrolysis**	
Samples	**RH**	**RH500**	**RH800**	**RH500**	**RH800**
Proximate analysis (wt.%)					
Moisture content	5.15	1.37 ± 0.08	0.91 ± 0.06	2.06 ± 0.03	1.43 ± 0.02
Volatile matter	64.27	8.53 ± 0.01	3.96 ± 0.01	8.77 ± 0.05	4.09
Fixed carbon	16.74	54.01 ± 0.07	55.82 ± 0.37	51.28 ± 0.26	55.11 ± 0.11
Ash	13.84	36.09 ± 0.03	39.31 ± 0.05	37.89 ± 0.12	39.37 ± 0.02
Ultimate analysis (wt.%)					
C	38.45	55.09 ± 0.18	58.14 ± 0.84	52.17 ± 0.09	52.92 ± 0.07
H	6.07	1.62 ± 0.02	0.51 ± 0.03	1.63 ± 0.08	0.61 ± 0.07
N	0.90	0.68 ± 0.06	0.42 ± 0.02	0.60 ± 0.02	0.53 ± 0.01
S	0.03	<100ppm	<100ppm	<100ppm	<100ppm
O*	54.55	42.61	40.93	45.60	45.94
H/C	1.89	0.35	0.11	0.37	0.14
O/C	1.06	0.58	0.53	0.66	0.65
Empirical formula	$CH_{1.89}O_{1.06}$	$CH_{0.35}O_{0.58}$	$CH_{0.11}O_{0.53}$	$CH_{0.37}O_{0.66}$	$CH_{0.14}O_{0.65}$

*Computed by difference

However, the chars produced from MP have higher moisture and volatiles with lower fixed carbon compared to CP chars. For instance, MP EFB at 500°C recorded around 14.5 wt.% volatiles, while similar pellets pyrolysed under conventional heating contained about 10 wt.% volatiles. This indicates that the materials are partially pyrolysed, which can be attributed to particle size and insufficient reaction time (Domínguez et al., 2007). An increase in reaction temperature from 500 to 800°C has resulted in 3-9 % increase in fixed carbon for all samples due to greater devolatilisation.

Likewise, bond scission and the breakdown of aromatic rings released H, O, and a smaller amount of N and S in the form of gas and bio oil. The resultant char contains higher C and lower H and O than raw pellets. In general, conventional pyrolysis is more efficient at removing these volatiles than MP. For example, about 25% decrease in O content is

recorded when rice husk pellets were pyrolysed under conventional heating, compared to just 17% observed during microwave hearing.

Similarly, the carbon content of EFB pellets increased by 37% during CP at 800°C, compared to just 34% during CP of rice husk. Much of these C and O are retained in the char, which imply carbon conversion inefficiency of rice husk. Low H (<1 wt.%) is recorded in all char samples at 800°C. This is believed to correlate with maximum H_2 evolution observed during high temperature pyrolysis, due to the breakdown of aromatic rings. Thus, it is safe to assume that the elements released over the course of pyrolysis participated in the syngas and bio oil formation (Haiping Yang et al., 2006; Demirbas, 2004). Likewise, N and S content in the char decreases as these elements were released during pyrolysis.

A decrease in H/C and O/C ratio is observed when the biomass experienced thermal decomposition, where the effect is greater in CP with an increase in reaction temperature. H/C ratio decreases from 1.82 to 0.11 and from 1.89 to 0.11 during CP of EFB and rice husk pellets at 800ºC, respectively. Meanwhile, O/C ratio decreased by half during CP RH500°C from 1.06 to 0.53. Further increase in pyrolysis temperature has resulted in about 63% decrease in O/C ratio from the initial biomass.

4.3.2 Calorific Value

The gross calorific value (GCV) of pyrolysed chars relative to their parent materials are presented in *Figure 4-6***.** Pyrolysis produces char of higher CV than raw biomass, which is in agreement with the results from ultimate and proximate analysis. The highest CV recorded is 27 MJ/kg for EFB and about 21 MJ/kg for rice husk, both obtained during CP at 800°C. This corresponds to 45% and 32% increase in CV from raw EFB and rice husk

pellets, respectively. A slight variation is observed between the char produced from conventional and microwave pyrolysis at similar temperature. Lower CV is recorded from MP chars. For instance, MP RH at 500°C produced char containing 19.42 MJ/kg of energy, about 1.33% lower than its CP counterpart. The energy content of EFB and rice husk chars in this study was found to be slightly higher than [18] and [24] at 25.16 MJ/kg and 19.66 MJ/kg, respectively.

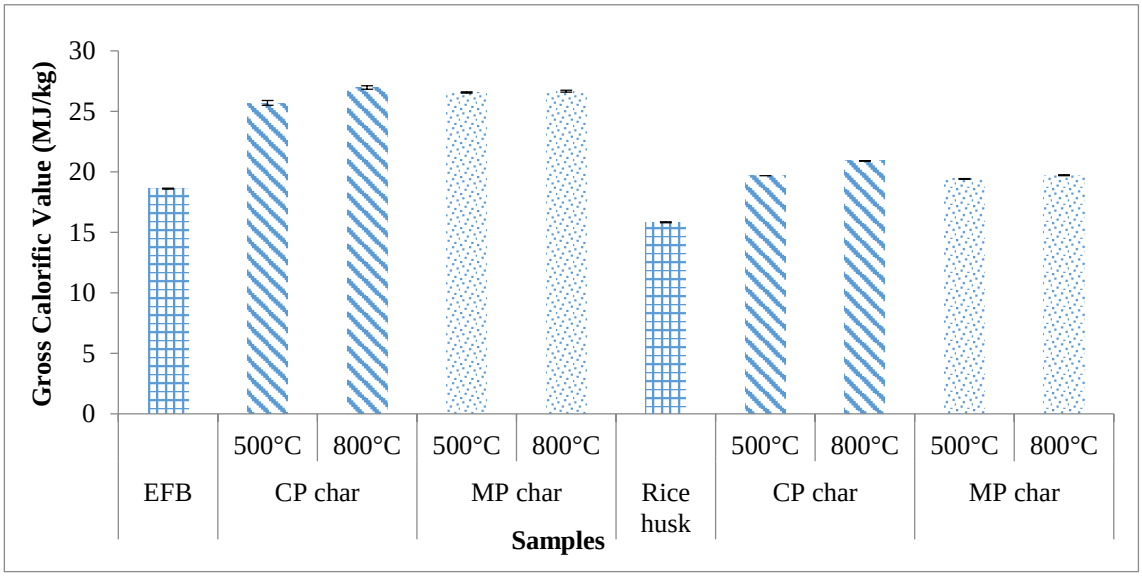

Figure 4-6: Calorific value of chars relative to raw biomass

4.3.3 Scanning Electron Microscopy

Pores with irregular-shaped outlets were formed during pyrolysis to release volatiles. From observation, EFB and rice husk chars exhibit similar surface morphology. However, *Figure 4-7 (L)* revealed an amorphous structure in some parts of rice husk char. *Figure 4-7 (R)* also shows the presence of small globules dotted on the char surface.

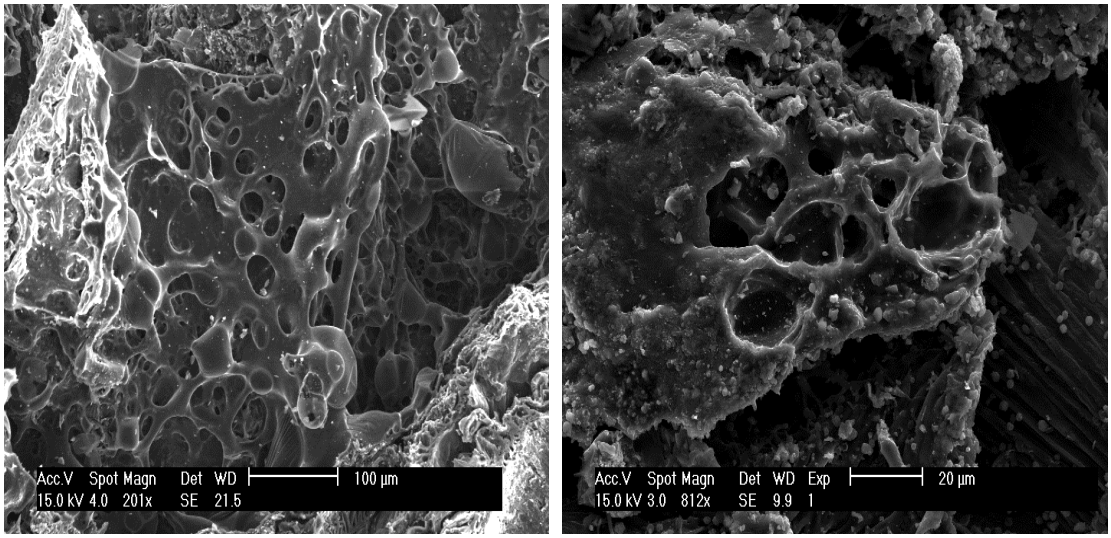

Figure 4-7: (L) MP RH char at 800°C and (R) Small globules on CP RH at 800°C

The difference in pore structure from conventional and microwave pyrolysis of rice husk at 500°C is highlighted in *Figure 4-8*. From the top figure, it was clear that these pores were not fully developed at low temperature. There is evidence of clogged pores in the case of CP RH char, where this phenomenon is not observed in the MP RH char. It is believed that dry tar is deposited on the wall of CP char, which can be attributed to its heating nature and direction of volatiles flow.

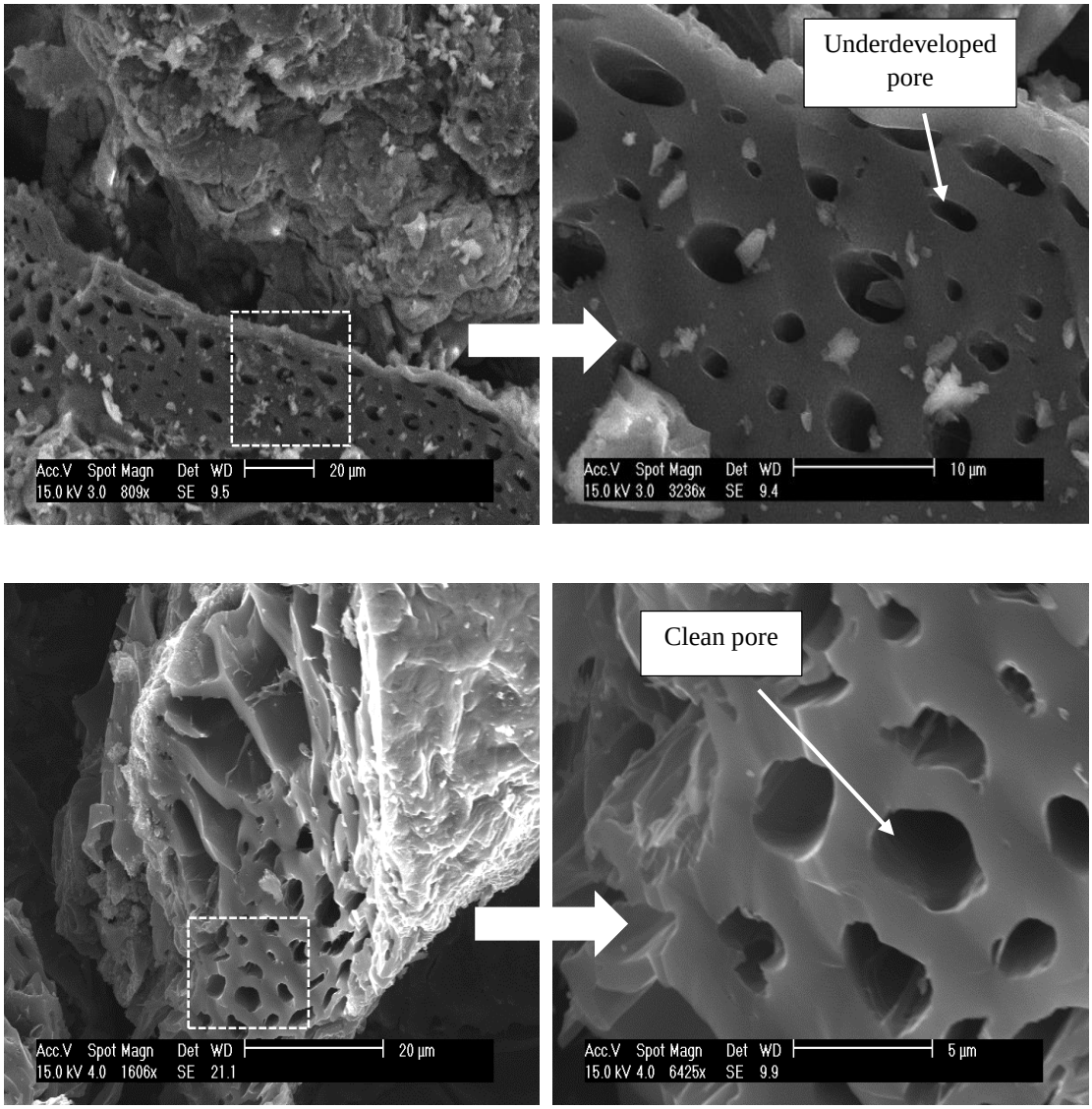

Figure 4-8: SEM images of rice husk char obtained from top: conventional pyrolysis, bottom: microwave pyrolysis at 500°C

As these volatiles escaped through the hotter region of biomass, they were exposed to the risk of secondary cracking into char. A similar phenomenon has also been observed by (Miura et al., 2004). On the contrary, microwave heating reduces the risk of secondary reaction as these volatiles flow through the colder region of the biomass. Clean pores are also observed during MP EFB at 500°C, as shown in *Figure 4-9*.

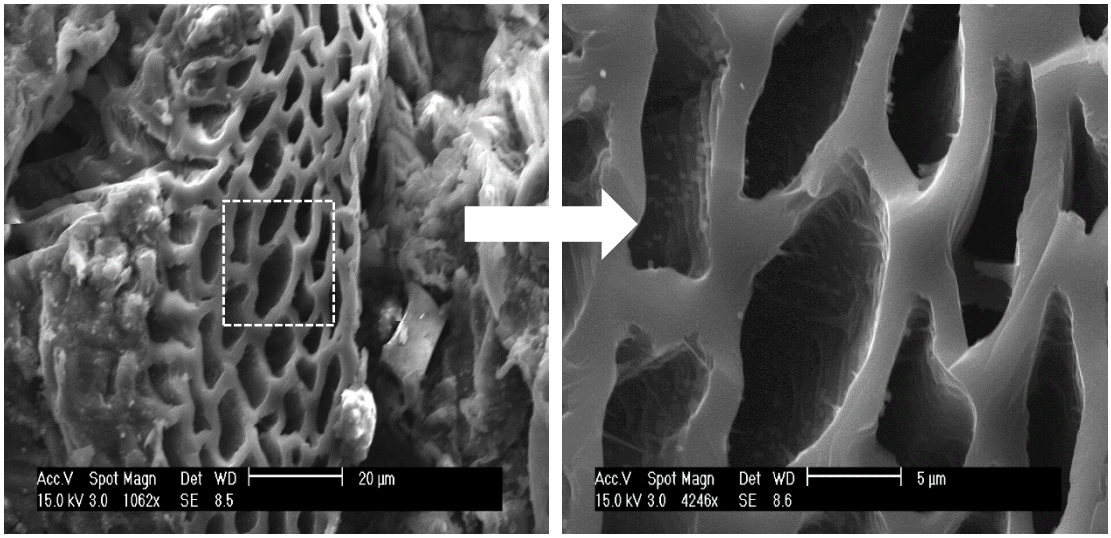

Figure 4-9: SEM images of MP EFB char at 500°C

However, increasing reaction temperature to 800° has resulted in the wall fracture or cracks in MP RH char as shown in *Figure 4-10 (L).* This might be caused by thermal peaks associated with microwave heating. The conversion of biomass into char advances with an increase in reaction temperature. In the case of microwave heating, the char produced has a greater relative permittivity (ε_r) than raw biomass. They are better at absorbing microwave energy, which causes a higher local temperature.

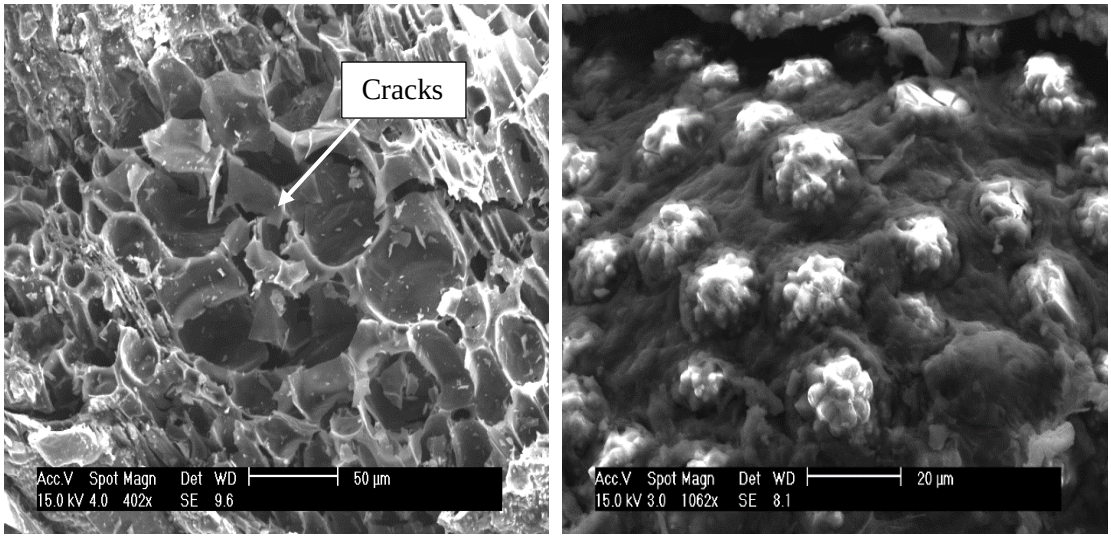

Figure 4-10: (L) MP RH char at 800°C, and (R) MP EFB char at 800°C

The presence of small globules is observed on the wall of EFB and RH chars as indicated in *Figure 4-10 (R)* and *Figure 4-11*, respectively. Energy Dispersive Spectroscopy (EDS) analysis indicates the presence of inorganic species, most notably SiO_2 and K_2O. These compounds could possibly melt and clog the pores due to their low melting point. This possibly reduces the specific surface area with increasing reaction temperature. This matches finding by (Yu et al., 2010), who discovered stepwise inorganic matter accumulation on the char surface from SEM analysis.

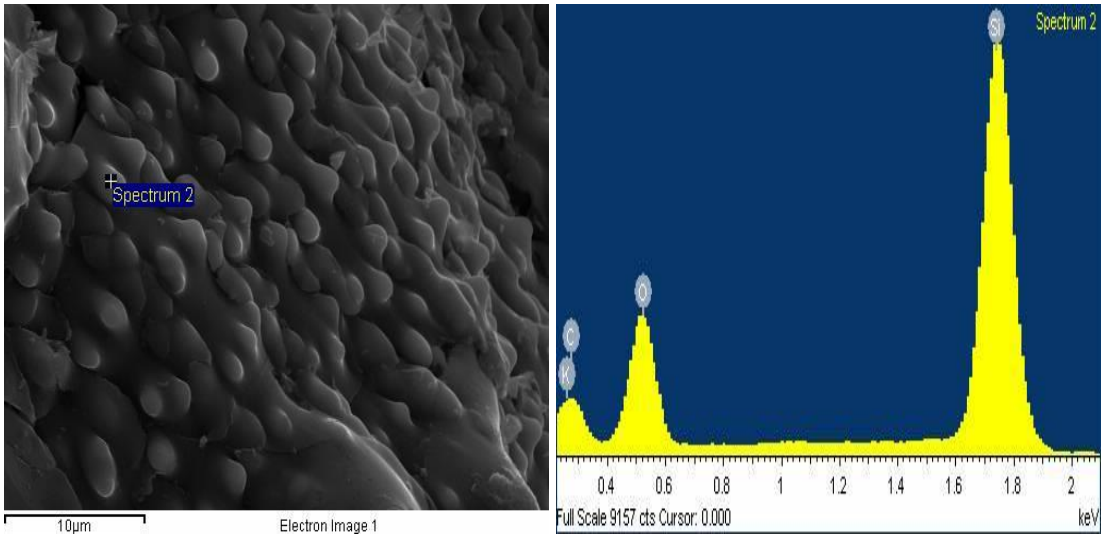

Figure 4-11: Energy Dispersive Spectroscopy (EDS) spectrum of MP RH char at 800°C

4.3.4 B.E.T Specific Surface Area

The specific surface area of rice husk chars is highlighted in *Figure 4-12*. These chars can be categorised as mesoporous carbon with pore diameter between 2-50 nm. In general, these chars have a surface area of more than 100 m^2/g. The highest surface area of 410 m^2/g is obtained during MP at 500°C. This is followed by char from CP at similar temperature, at around 383 m^2/g. However, a declining trend in surface area is observed when the pyrolysis temperature is increased from 500 to 800°C.

Microwave pyrolysis at 800°C produced char with the lowest surface area at 238 m^2/g. This can be attributed to wall rupture and pore shrinkage at high temperature and long holding time. The latter is more pronounced in MP due to longer holding time of 38 minutes, compared to 30 minutes during CP. This leads to the destruction of the micro-pore structure and the sintering effect that blocks the pores. This is highlighted previously in the **Section 4.3.3**. A similar phenomenon is observed by (Wang et al., 2009; Lua & Guo, 1998) where the surface area of char starts to decrease at a temperature around 750°C.

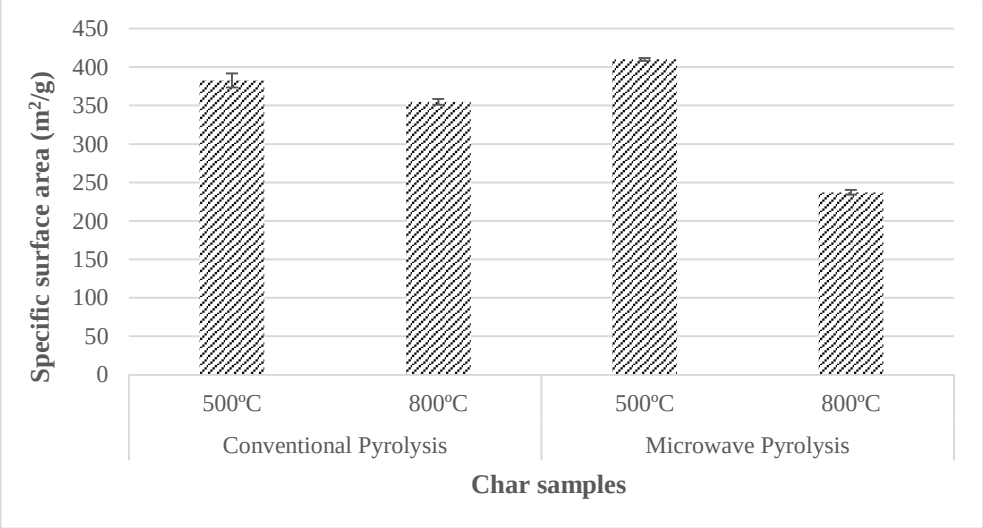

Figure 4-12: Specific surface area of pyrolysed rice husk char

4.3.5 Relative Permittivity

Table 4-5 shows the relative permittivity of microwave pyrolysed chars and their parent materials. This consists of dielectric constant (ε') and the imaginary part or dielectric loss (ε''). These values are known to be influenced by several factors such as microwave frequency, moisture, mineral and carbon content (Tripathi et al., 2015). Both biomass materials used in this study have low relative permittivity; at 1.5-0.03*j for EFB and 1.6-0.06*j for rice husk.

Table 4-5: Dielectric properties of biomass samples at f=2.45 GHz and T=298K

Samples	Dielectric constant (ε ')	Dielectric loss factor (ε '')	Tan α
EFB	1.50	0.03	0.02
MP EFB char at 500°C	3.00	0.26	0.09
MP EFB char at 800°C	5.60	0.45	0.08
Rice husk	1.60	0.06	0.04
MP RH char at 500°C	2.98	0.18	0.06
MP RH char at 800°C	6.10	0.43	0.07

In this respect, rice husk has a better capability for absorbing microwave energy and turning it into heat energy than EFB. Relative permittivity is observed to increase with an

increase in pyrolysis temperature. For instance, dielectric constant increases from 1.5 to 3.0 as the EFB is pyrolysed under microwave radiation at 500°C. This value increases further to 5.6 at 800°C. A similar trend is observed during microwave pyrolysis of rice husk, where ε' increases from 1.6 to 6.10 during MP at 800°C.

Moisture and volatiles released during pyrolysis give rise to the production of carbon-rich char, which is better at absorbing microwave power. More microwave energy is converted into heat at high temperature, as indicated by an increasing dielectric loss (ε''). This gives tan α values between 0.06-0.09, which is comparable to the dielectric properties of coal (Menéndez et al., 2010). This indicates that the moisture and char on their own are sufficient to sustain the pyrolysis process, without any addition of microwave absorber.

4.4 Bio Oil Analysis

4.4.1 Ultimate Analysis

Bio oil obtained in this study comprises of an aqueous and organic phase. The heavier tar is found at the bottom of the container, while the lighter aqueous phase sits on the top. *Table 4-6* and *Table 4-7* show the ultimate analysis of EFB oils and rice husk oils, respectively. Similar to char, the carbon content appeared to increase with increasing reaction temperature, which is consistent for all bio oil samples. Increasing pyrolysis temperature also results in a greater reduction in terms of O and H content. However, bio oil exhibits significantly higher hydrogen at around 6-9 wt.% compared to less than 2 wt.% found in the pyrolysed chars.

Between the technologies, microwave pyrolysis is found to yield a higher amount of C and less O, which contribute to its higher CV than CP oils. For instance, about 8% increase in C is observed when EFB pellets are pyrolysed under microwave heating at

800ºC, compared to 62.80 wt.% recorded during conventional pyrolysis. On a similar note, it recorded 15% decrease in oxygen from 26.34 wt.% during MP.

Meanwhile, CP and MP of rice husk produced a bio oil of lesser quality than EFB. This is indicated by lower C and greater oxygenated compounds. It also has less H at around 6.66-7.70 wt.%, compared to 7.60-9.20 wt.% found in the EFB bio oils. For this reason, bio oil has a higher H/C and O/C ratio than char, with a decreasing trend with an increase in temperature. A higher O/C ratio is recorded in rice husk bio oils at around 0.45-0.59, compared to 0.25-0.33 in EFB bio oils. This explains the lower CV of rice husk oils at around 21-23 MJ/kg, compared to 25-26 MJ/kg recorded from EFB bio oils.

Increasing reaction temperature resulted in a slight increase in the energy content of bio oils. Switching from the CP to MP process contributed to a CV gain for all samples up to 6.08%, as in the case of rice husk. This is due to the substantial reduction in moisture and increased carbon content. The analysis also revealed the presence of oxygenated compounds that are highly polar as can be verified through GC-MS analysis later.

Table 4-6: Chemical properties of EFB bio oils

Pyrolysis method	**Conventional Pyrolysis**		**Microwave Pyrolysis**	
Samples	**EFB500**	**EFB800**	**EFB500**	**EFB800**
Ultimate analysis (wt.%)				
C	61.44 ± 0.24	62.80 ± 0.36	65.33 ± 1.01	68.08 ± 0.49
H	9.20 ± 0.10	9.15 ± 0.15	8.25 ± 0.19	7.57 ± 0.12
N	2.41 ± 0.08	1.71 ± 0.09	2.21 ± 0.01	1.87 ± 0.02
S	<100ppm	<100ppm	<100ppm	<100ppm
*O**	26.95	26.34	24.21	22.48
H/C	1.80	1.75	1.52	1.33
O/C	0.33	0.31	0.28	0.25
Elemental formula	$CH_{1.80}O_{0.33}$	$CH_{1.75}O_{0.31}$	$CH_{1.52}O_{0.28}$	$CH_{1.33}O_{0.25}$
Calorific value (MJ/kg)	25.21	25.58	25.68	26.00

*Computed by difference

Table 4-7: Chemical properties of rice husk bio oils

Pyrolysis method	**Conventional Pyrolysis**		**Microwave Pyrolysis**	
Samples	**RH500**	**RH800**	**RH500**	**RH800**
Ultimate analysis (wt.%)				
C	51.10 ± 0.71	53.49 ± 0.79	56.03 ± 0.45	57.54 ± 0.34
H	7.70 ± 0.28	6.93 ± 0.48	7.56 ± 0.02	6.66 ± 0.03
N	1.33 ± 0.06	1.99 ± 0.35	1.67 ± 0.06	1.54 ± 0.10
S	<100ppm	<100ppm	<100ppm	<100ppm
*O**	39.87	37.59	34.74	34.26
H/C	1.81	1.55	1.62	1.39
O/C	0.59	0.53	0.47	0.45
Elemental formula	$CH_{1.81}O_{0.59}$	$CH_{1.55}O_{0.53}$	$CH_{1.62}O_{0.47}$	$CH_{1.39}O_{0.45}$
Calorific value (MJ/kg)	21.33	21.46	22.61	22.44

*Computed by difference

4.4.2 GC-MS Analysis

In general, bio oil is made up of several classes of compounds such as aliphatic hydrocarbons, aromatic hydrocarbons, phenol and its derivatives, along with a smaller amount of oxygenates. The results from GC-MS analysis are tabulated in *Table 4-8* and *Table 4-9* for EFB and rice husk oils, respectively. The analysis indicates a notable amount of Polycyclic Aromatic Hydrocarbons (PAH) in CP RH oil at 500°C, at a total of 30,000 µg/L. This is contrary to the much lighter compounds, *i.e.*: mono-aromatics found in MP oil. These chemical compounds such as benzene, toluene, and styrene were present in MP oils, with greater concentration at high pyrolysis temperature.

Table 4-8: GC-MS analysis of EFB oils (µg/L)

Pyrolysis method	**Conventional pyrolysis**		**Microwave pyrolysis**	
Chemical compounds	**EFB500**	**EFB800**	**EFB500**	**EFB800**
Mono-aromatics				
Benzene	<600	<600	967	2385
Toluene	<600	<600	3823	4782
Ethyl benzene	<600	<600	488	636
m&p xylene	<600	<600	658	1167
o-xylene	<600	<600	352	618
Styrene	<600	<600	1130	1179
PAHs				
Naphthalene	719	781	308	2685
Phenolic				
Phenol	6324900	1282300	1320856	1618540
2,4-dimethylphenol	64190	<600	31832	59257
2-methylphenol	387860	32410	87534	148450
3/4-methylphenol	424910	138480	137888	260770

For example, total mono-aromatics in MP EFB oils recorded 45% increase from 7418 µg/L when the reaction temperature is increased from 500 to 800ºC. These compounds were not detected in any CP oils, with the exception of CP RH at 500°C. A significant rise in the concentration of mono-aromatics with temperature suggested that microwave heating causes more cracking reactions than a conventional furnace. A similar trend was also observed by (Ferrera-Lorenzo et al., 2014; Domínguez et al., 2005). The formation of aromatic hydrocarbons could be the result of the Diels-Alder reaction; *i.e.*: the cyclisation of alkenes to aromatics and the de-oxygenation of furans and phenol into aromatics (Horne & Williams, 1996).

Table 4-9: GC-MS analysis of rice husk oils (μg/L)

Pyrolysis method	**Conventional pyrolysis**		**Microwave pyrolysis**	
Chemical compounds	**RH500**	**RH800**	**RH500**	**RH800**
Mono-aromatics				
Benzene	1819	<600	820	516
Toluene	1477	<600	1338	1440
Ethyl benzene	<600	<600	136	140
m&p xylene	<600	<600	267	285
o-xylene	<600	<600	139	140
Styrene	643	<600	351	454
PAHs				
Naphthalene	20105	<600	370	1012
Acenaphthylene	5820	2190	<600	<600
Anthracene	1740	4260	<600	<600
Phenanthrene	1930	6650	<600	<600
Phenolic				
Phenol	2324600	446000	505699	642903
2,4-dimethylphenol	102250	11150	37481	47501
2-methylphenol	376100	8040	87150	97816
3/4-methylphenol	712760	37610	214792	249074

Meanwhile, phenol made up the majority of bio oil along with other phenolic compounds such as 2,4-dimethylphenol and 3,4 methylphenol. A stark contrast is observed in the total phenolic count between CP and MP oils. Phenol and its derivatives recorded an increase with rising temperature in MP, but showed a decreasing trend in CP. The former could be the direct result of increased carbon-based absorber at high temperature.

A possible increase in hot spots during microwave heating could induce higher local temperature. It can also be caused by continuous secondary degradation that occurs with increasing temperature. Similar result has been observed by Mushtaq *et al.* (Mushtaq et al., 2015) and Bu *et al.* (Bu et al., 2011), who studied the catalytic effect of carbon on the total phenolic yield. In this respect, higher phenolic yield can be achieved with microwave

pyrolysis. Switching from CP to MP has resulted in up to 44% increase in the total phenolic count during EFB pyrolysis at 800ºC.

Meanwhile, naphthalene is the simplest PAH compound and was present in all oil samples. It recorded an increase with increasing temperature, most notably during MP. However, no other PAH compounds were detected in MP oils. Compounds such as acenaphthylene, anthracene, and phenanthrene were found during CP of rice husk, with increasing trend at higher temperature. These compounds are unfavourable due to their carcinogenic nature. For example, phenanthrene increases up to 6650 μg/L from 1930 μg/L, as the reaction temperature is increased from 500 to 800ºC.

This increase can be explained by primary/secondary tar conversion via a dimerization reaction, taking place between two light PAH compounds at high temperature. This is also caused by the polymerisation of unsaturated C_2-C_4 hydrocarbons that are relatively unstable. Primary pyrolysis vapours are reactive and immediately polymerise into heavier tar compounds upon condensation (Van Paasen et al., 2004; Diebold & Czernik, 1997). Phenol, a representative of secondary tar is converted into tertiary tar at a temperature between 750-850ºC. This explains the decreasing amount of phenol at high temperature in CP oils.

Bio oil has numerous possibilities for use as biofuels or chemical intermediates in industrial applications. However, characteristics such as low pH, high oxygen content, and high viscosity have hindered its use in commercial applications. For this purpose, bio oil needs to go through physical upgrading such as hot vapour filtration and feedstock washing to remove the ash content, or catalytic upgrading such as hydro treating and zeolite cracking. Phenol found in this study can be a substitute for petroleum-based phenol; a

chemical intermediate in the plastic industry. However, its high water solubility might cause pollution and exorbitant wastewater disposal cost (Bridgwater, 2012; Van Paasen et al., 2004)

4.4.3 FT-IR Analysis

FTIR spectra of bio oils indicated the presence of several functional groups such as alkanes, alkenes, aldehydes, phenol, alcohols, and aromatics. These spectra are shown in *Figure 4-13* to *Figure 4-16*. Possible chemical compounds at each spectrum are listed in *Table 4-10*. These spectra were identical for both EFB and rice husk oils, regardless of heating method and temperature. Thus, it can be concluded that biomass-derived pyrolysis oils are comprised of similar functional groups.

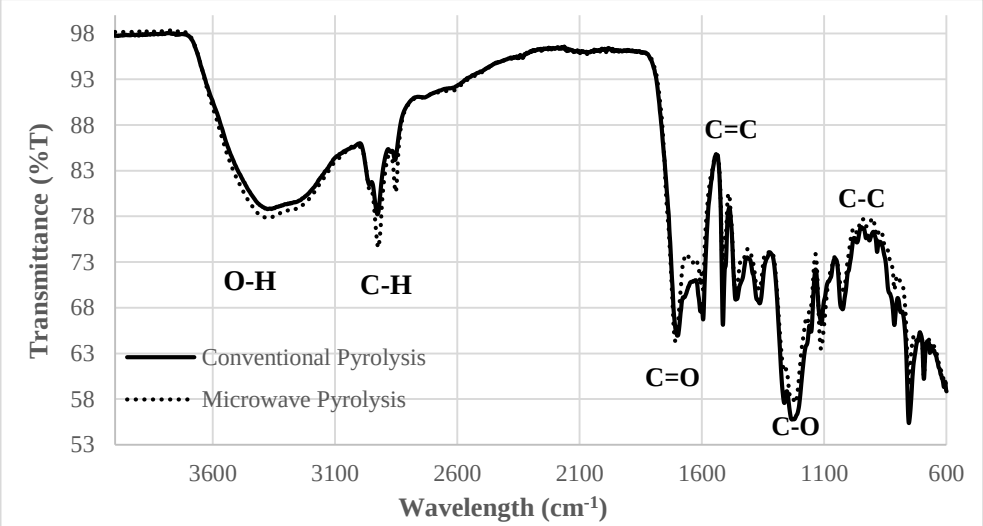

Figure 4-13: FTIR spectra of EFB oils at 500°C

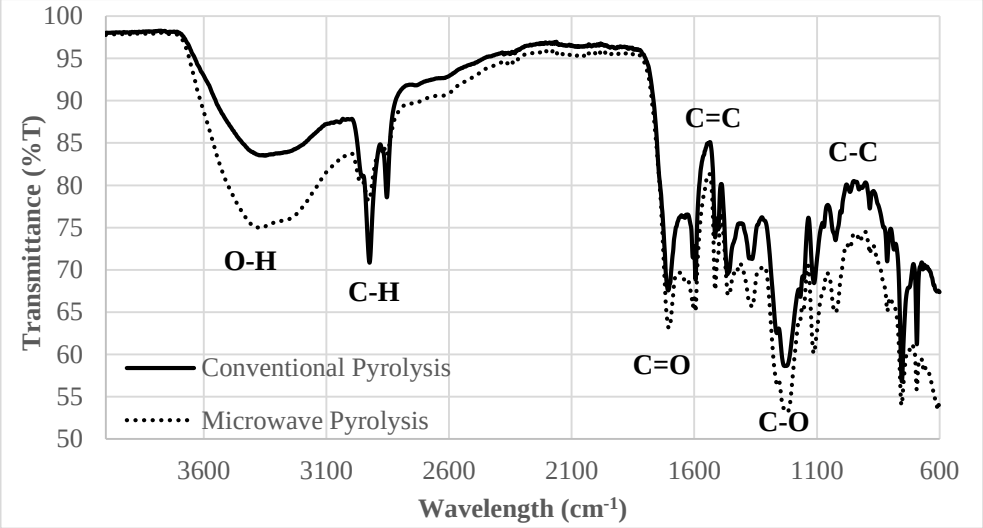

Figure 4-14: FTIR spectra of EFB oils at 800°C

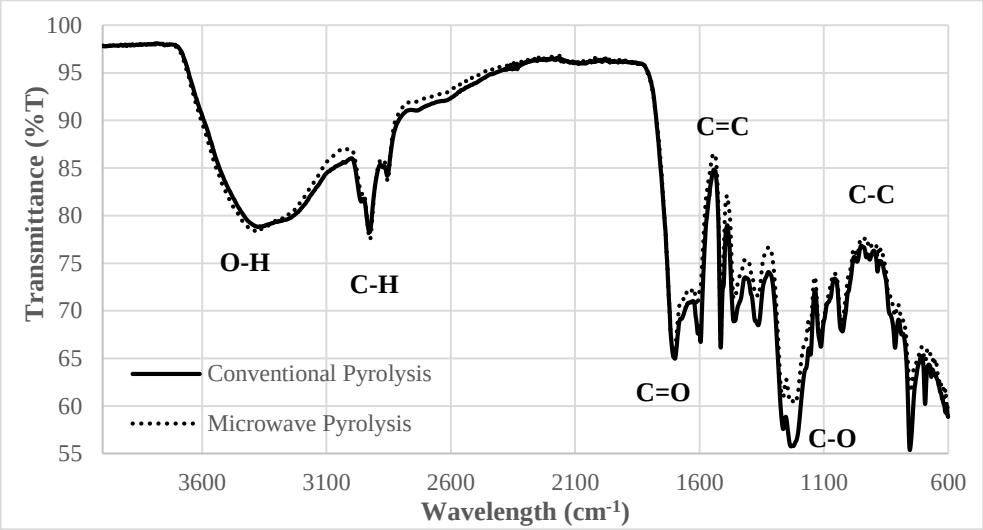

Figure 4-15: FTIR spectra of rice husk oils at 500°C

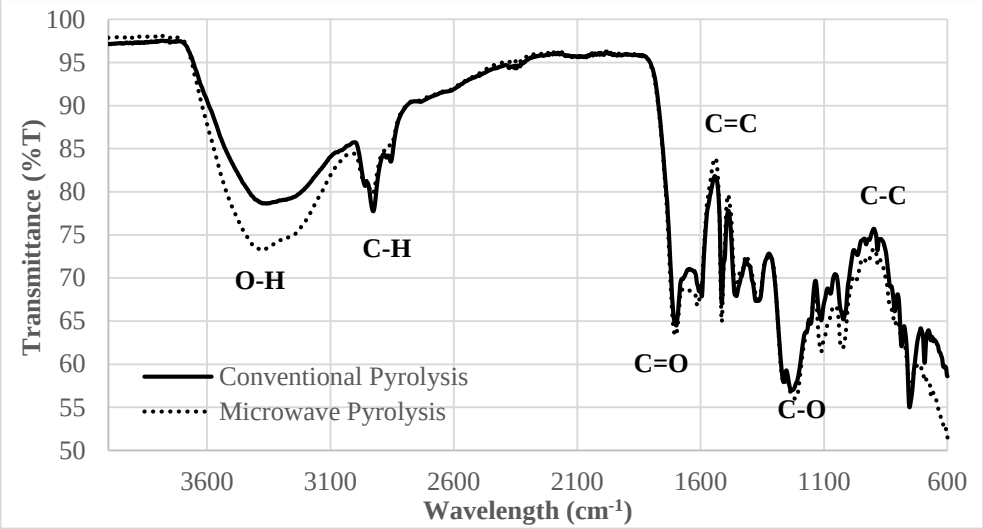

Figure 4-16: FTIR spectra of rice husk oils at 800°C

Table 4-10: Chemical compounds in biomass pyrolysis oils

Frequency range (cm^{-1})	Type of vibration	Possible compounds
3500-3200	O-H stretch	Alcohols, phenol
3000-2850	C-H stretch	Alkanes
1820-1660	C=O stretch	Carbonyls, carboxylic acids, ketones, aldehydes
1600-1450	C=C stretch	Alkenes
1640-1550	N-H bending	Amines
1300-1000	C-O stretch	Alcohols, carboxylic acids, ether
900-690	=C-H out of plane	Aromatic hydrocarbons, alkyl halides

Based on the spectra, alcohols and phenol were characterised by an O-H stretching in the frequency region of 3500-3200cm^{-1}. It can also be affected by the presence of water in bio oil. These were confirmed by the narrow C-O stretching in the region of 1300-1000 cm^{-1}, which suggested the presence of alcohols, carboxylic acids, and ether (Pavia et al., 2009). The difference in peak intensity was observed for 800°C pyrolysis oils, particularly in the region of 3400 cm^{-1} which suggests the presence of O-H bonds. Strong absorption by MP oils could indicate a higher quantity of oxygenates; *e.g.*: phenol present during high temperature pyrolysis.

Meanwhile, strong C-H absorption at around 3000 cm^{-1} could indicate the presence of alkanes. The presence of carboxylic acids and carbonyl groups are characterised by the C=O peak in the region of 1820-1660 cm^{-1}. Several sharp and narrow peaks in the frequency region of 1600-1450 cm^{-1} suggest the presence of alkenes. The molecular vibration in the region below 1000 cm^{-1} could indicate the existence of mono or polycyclic aromatic hydrocarbons. These FTIR spectra did not indicate any presence of triple bond compounds, due to a very broad spectrum in the region of 2000 cm^{-1}.

4.5 Gas Analysis

Figure 4-17 and *Figure 4-18* show the gas evolution during pyrolysis of EFB and rice husk pellets, respectively. It revealed the significant influence of reaction temperature and pyrolysis method on gas distribution. The breakdown of organic compounds in biomass and further temperature-dependent reactions released CO_2, CH_4, CO, and H_2.

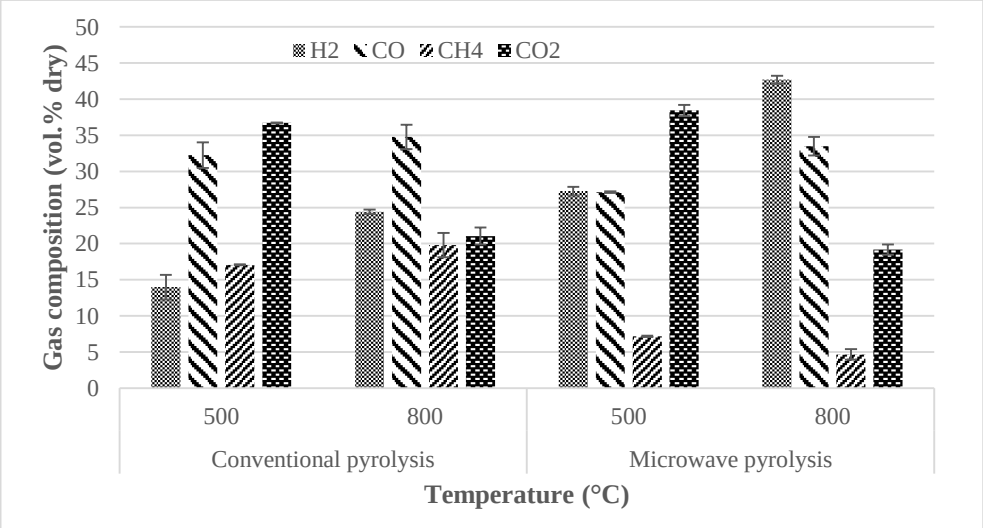

Figure 4-17: Gas evolution during EFB pyrolysis (N_2 free)

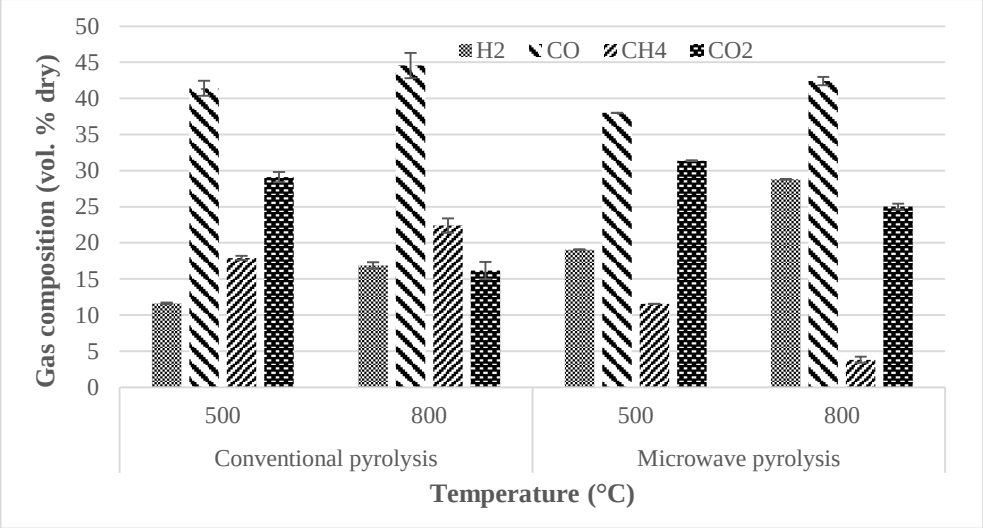

Figure 4-18: Gas evolution during rice husk pyrolysis (N_2 free)

Table 4-11: Energy content of pyrolysis gas

Pyrolysis method	**Conventional Pyrolysis**				**Microwave Pyrolysis**			
Sample	EFB500	EFB800	RH500	RH800	EFB500	EFB800	RH500	RH800
Total H_2 +CO (vol. %)	46.23	59.17	53.01	61.44	54.39	76.19	57.06	71.19
Total CO_2+ CH_4 (vol. %)	53.77	40.83	46.99	38.56	45.61	23.81	42.94	28.81
GCV (MJ/m^3)	13.98	15.59	14.63	16.98	8.06	11.68	10.88	10.41

Table 4-11 shows the total concentration of syngas and greenhouse gases emitted during pyrolysis process. In general, the concentration of syngas (H_2+CO) is observed to increase with rising temperature regardless of heating method, although the effect is more pronounced in MP than CP. For instance, MP EFB at 800ºC has resulted in about 29% increase in the total syngas production compared to CP at similar temperature. At the same time, a declining trend is observed in the total greenhouse gases (CH_4+CO_2) emitted at high temperature. Greater reduction in GHG emission is demonstrated by microwave pyrolysis process, where the value recorded is 42% lower than CP at similar temperature.

With respect to gas composition, an increase in reaction temperature has resulted in a greater production of H_2 and CO. The highest H_2 yield at 43 vol.% is obtained during MP

EFB at 800ºC. Similarly, maximum CO at 45 vol.% is recorded during CP RH at 800ºC. Higher CO from rice husk pyrolysis can be attributed to high oxygen content in the raw biomass, as highlighted in **Section 4.1**. This is due to intense thermal cracking of heavier hydrocarbons into permanent gases at elevated temperature, as shown in *Eq: 4-1*.

Moreover, moisture released during biomass dehydration participated in the water-gas reaction with carbon to produce CO and H_2, as indicated in *Eq: 4-2* (Sutton et al., 2001). Char left inside the hot reactor is further gasified into CO via Boudouard reaction shown in *Eq: 4-3*.

$$Tar \rightarrow CH_4 + H_2O + H_2 + C_mH_n \quad \text{Eq: 4-1}$$

$$C + H_2O \leftrightarrow CO + H_2 \quad \text{Eq: 4-2}$$

$$C + CO_2 \leftrightarrow 2CO \quad \text{Eq: 4-3}$$

$$CO + H_2O \leftrightarrow CO_2 + H_2 \quad \text{Eq: 4-4}$$

$$CH_4 + CO_2 \leftrightarrow 2CO + 2H_2 \quad \text{Eq: 4-5}$$

CO_2 participation in the above reaction explained its reduction at high temperature, which is consistent for all samples. Higher evolution of CO_2 is expected during the initial stage of pyrolysis due to the breakdown of C=O bonds through decarbonylation and decarboxylation (Haiping Yang et al., 2006). It was also related to the water-gas shift reaction in *Eq: 4-4*, favoured at low temperature to produce CO_2 and H_2. However, an increase in temperature shifts the reaction towards the reactants side to produce more CO. CO_2 in this study was found to contradict previous findings. Its value is around 4-7% higher in MP than CP. This was due to slow removal of volatiles in MP, which allows the moisture

to react with CO. The sweep gas (N_2) was set to 4 LPM in CP, compared to just 2 LPM during MP.

Meanwhile, a different trend is observed in CH_4 evolution with temperature. In the case of conventional pyrolysis, a greater CH_4 yield is observed with an increase in reaction temperature. For instance, its yield increases by 26% from 17.9 vol.%, when the temperature is increased from 500 to 800ºC during CP of rice husk. This is expected as the breaking of C=H bonds at an elevated temperature releases more CH_4 and H_2. This is achieved via cracking and reforming of aromatic rings.

An increase in CH_4 can also be attributed to greater hydrogasification reaction in in a H_2-rich environment. However, a lower yield of CH_4 is observed with an increase in reaction temperature during MP. This reduction might be caused by dry-reforming of methane as indicated in *Eq: 4-5* to produce more CO and H_2. For example, MP EFB at 800ºC recorded about 36% lower CH_4 than MP of similar biomass at 500ºC.

The gross calorific value of pyrolysis gas is also listed in *Table 4-11*. N_2 and CO_2 do not contribute to the heating value. Conventional pyrolysis produces gas of higher heating value at around 13-17 MJ/m^3, compared to around 8-12 MJ/m^3 generated from microwave pyrolysis. It can be seen that the lower CH_4 yield in MP negatively affects its heating value. Nevertheless, higher syngas production at an elevated temperature raises the energy value of pyrolysis gas. Greater syngas evolution during EFB pyrolysis contributed to its higher heating value than rice husk.

4.6 Energy Consumption

This section aims to quantify the energy consumption between pyrolysis processes. Power drawn over the course of pyrolysis can be quantified by measuring the current flow at a constant voltage source of 230V. *Figure 4-19* and *Figure 4-20* show the power input during conventional and microwave pyrolysis, respectively. Except for CP, the power profiles in MP only cover radiation time up to 19 minutes. This is due to inability of the data logger to continuously record data beyond this point.

The nominal power drawn during CP is around 14 kW, where most of this power is involved during heating. It took around 40 and 90 minutes for the pyrolysis chamber to reach the temperature of 500 and 800ºC, respectively. It then took about 58% of nominal power to maintain the chamber at a set temperature.

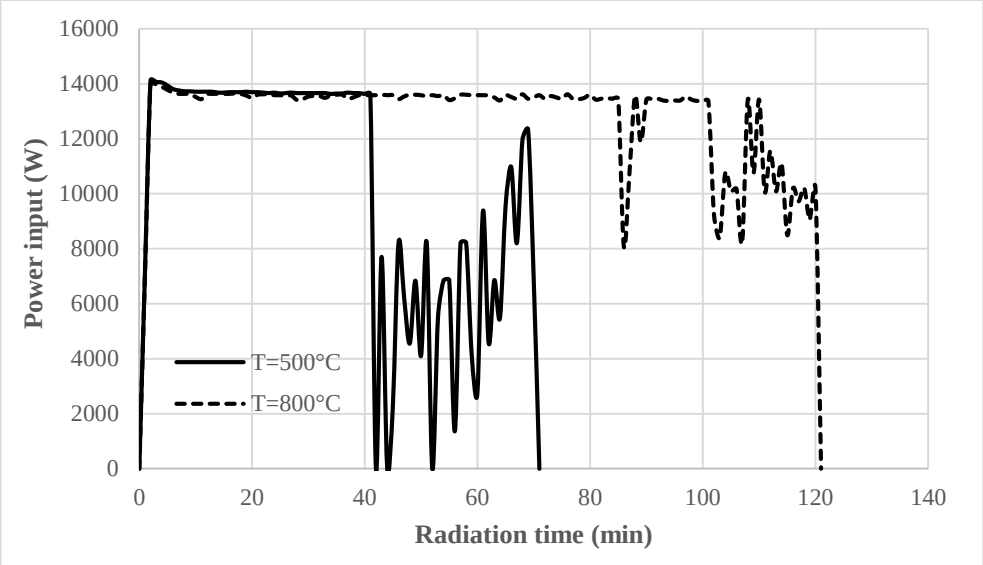

Figure 4-19: Power input during conventional pyrolysis

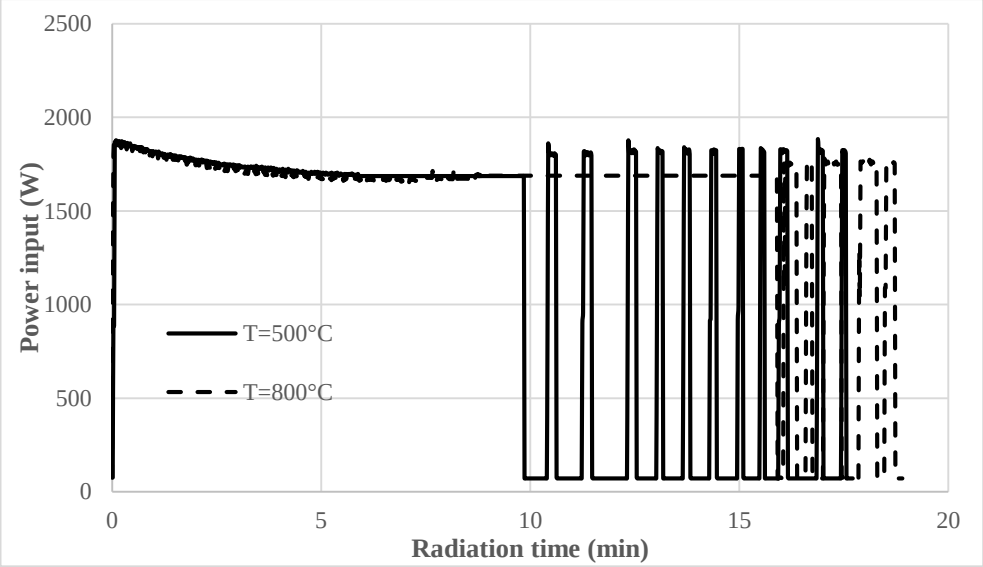

Figure 4-20: Power input during microwave pyrolysis

A major difference is observed during microwave pyrolysis, where the input power ranges between 79 W under normal operation to 1700 W during microwave heating. The former covers the energy used for lighting and ventilation of the microwave oven. It took around 10 minutes for biomass to reach 500ºC, in contrast to 40 minutes during conventional pyrolysis. Similarly, it took around 16 minutes during MP of biomass to reach 800ºC.

The power profiles show a typical cyclic load graph due to the ON/OFF of microwave power to maintain the sample at a set temperature. *Eq: 4-6* is used to measure the power consumption per unit of biomass.

$$Input\ power\ (kW/kg) = \frac{Power\ input^{2}}{Mass\ of\ biomass} \qquad \text{Eq: 4-6}$$

[2] Average power input over the course of pyrolysis

Energy consumed during the conventional and microwave pyrolysis of EFB and rice husk pellets is listed in *Table 4-12* and *Table 4-13*, respectively. The input power of CP ranges between 10.27 to 12.76 kW, as the reaction temperature is increased from 500 to 800ºC.

Table 4-12: Energy consumption during conventional and microwave pyrolysis of EFB pellets

	Conventional pyrolysis		**Microwave pyrolysis**	
Temperature (°C)	500	800	500	800
Input power (kW)	10.27	12.76	1.11	1.30
Mass (kg)	0.20	0.20	0.04	0.04
Input power (kW/kg)	51.35	63.80	27.75	32.50
Conversion efficiency	0.63	0.79	0.90	0.77
Radiation time (min)	70	120	30	36
Electricity consumption (kWh/kg)	59.91	127.70	13.88	19.50
Energy consumption (MJ/kg)	215.67	459.36	49.95	70.20

Table 4-13: Energy consumption during conventional and microwave pyrolysis of rice husk pellets

	Conventional pyrolysis		**Microwave pyrolysis**	
Temperature (°C)	500	800	500	800
Input power (kW)	10.27	12.76	1.25	1.43
Mass (kg)	0.20	0.20	0.04	0.04
Input power (kW/kg)	51.35	63.80	31.25	35.75
Conversion efficiency	0.63	0.79	0.80	0.70
Radiation time (min)	70	120	30	36
Electricity consumption (kWh/kg)	59.91	127.7	15.63	21.45
Energy consumption (MJ/kg)	215.67	459.36	56.25	77.22

Meanwhile, microwave pyrolysis of rice husk consumed a higher input power at around 1.25-1.43 kW, compared to 1.11-1.30 kW during EFB pyrolysis. The conversion efficiency from electrical to microwave energy in this study is found to be around 70-90%. The remainder is lost as heat. Conventional pyrolysis required a much greater energy input

per unit biomass, at around 51.35-63.80 kW/kg, compared to around 31-36 MJ/kg during microwave pyrolysis of rice husk. Higher nominal power and longer heating time greatly influence the total energy consumption in CP.

A greater energy saving has been successfully demonstrated via the microwave pyrolysis process. It only requires about 23-27% of the total energy used in CP, where this value decreases to about 15-17% at high temperature. It also reduces the pyrolysis time to about 10-20 minutes with a much simpler setup.

4.6.1 Energy Balance Analysis

An energy balance analysis of the pyrolysis system is presented in this section. A control volume is set to define the energy flowing into and leaving the system, as illustrated in *Figure 4-21*. Input energy includes the GCV of biomass (Q_b) and the electrical energy consumed during the pyrolysis process, Q_e. Meanwhile, output energy comprises of GCV of pyrolysed char (Q_c), bio oil (Q_{oil}) and pyrolysis gas (Q_g), heat of reaction (ΔH) and energy lost within the system, Q_{loss}. The conversion loss of microwave energy, latent heat of residual carbon, and heat taken by cooling water are lumped together under Q_{loss}. The calculation for energy balance follows *Eq: 4-7*.

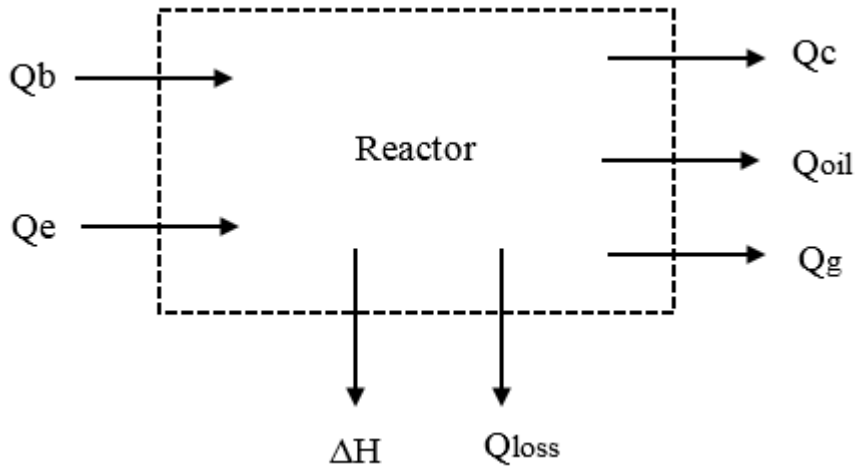

Figure 4-21: Pyrolysis system control volume

$$Qb + Qe = Qc + Qoil + Qg + Qloss + \Delta H$$ Eq: 4-7

These are listed in *Table 4-14* and *Table 4-15* for pyrolysis of EFB and rice husk pellets, respectively. Without taking Q_e into account, it can be seen that pyrolysis increases the energy density of biomass. This effect is greater with an increase in reaction temperature. This is especially true in the case of char and bio oil. CP at 800ºC has resulted in up to 45% increase in energy density of EFB pellets. Similarly, the MP process resulted in about 48% increase in energy density of rice husk pellets. However, GCV of pyrolysis gas is found to be much lower than the parent material. The analysis indicates no energy surplus when Q_e is taken into account. This is due to the higher electrical energy consumed to conduct the pyrolysis process, compared to energy recovered per kg of product.

Table 4-14: Energy balance of EFB pyrolysis

	Conventional pyrolysis		**Microwave pyrolysis**	
Temperature (°C)	500	800	500	800
Qin (MJ/kg)				
Qb	18.61	18.61	18.61	18.61
Qe	215.67	459.36	49.95	70.20
Qout (MJ/kg)				
Qchar	26.55	26.97	25.69	26.66
Qoil	25.21	25.58	25.68	26.00
Qgas	13.98	15.59	8.06	11.68
Q_{loss} + ΔH	168.54	409.83	9.13	24.47
Efficiency (η)	28.06	14.26	86.68	72.45

Table 4-15: Energy balance of rice husk pyrolysis

	Conventional pyrolysis		**Microwave pyrolysis**	
Temperature (°C)	500	800	500	800
Qin (MJ/kg)				
Qb	15.24	15.24	15.24	15.24
Qe	215.67	459.36	56.25	77.22
Qout (MJ/kg)				
Qchar	19.68	20.9	19.62	19.71
Qoil	21.33	21.46	22.61	22.44
Qgas	14.63	16.98	10.88	10.46
Q_{loss} + ΔH	175.27	415.26	18.38	39.85
Efficiency (η)	24.10	12.50	74.29	56.90

In terms of efficiency, MP is found to be more efficient than CP although this value decreases during high temperature pyrolysis. For example, the efficiency of the MP system is found to be between 57-87%, compared to about 12-29% during conventional pyrolysis. This indicates that around 71-88% of the input energy is lost in the CP system. Energy lost within MP system is much lower at around 18%, which can be attributed to poor heating associated with a bottom-feed waveguide microwave oven. This will be discussed in Chapter 5.

Since Q_e made up the largest fraction of the total energy input, an improvement in efficiency (η) can be achieved via economy of scale. This is particularly important in CP due to its capability to handle a large volume of load. Another way to increase the overall η is by direct combustion of char and pyrolysis gas in a boiler to cover a fraction of Q_e. This is practical in the context of an industrial process.

The minimum amount of biomass needed to achieve 80% efficiency is determined using the 'Goal-seek' tool in MS Excel. It is assumed that other parameters such as radiation time, Q_e, and Q_{loss} are kept constant under normal operating conditions. It was found that 0.68 kg is the minimum load that should be processed in the CP reactor at 500°C in order to achieve η = 80%. Similarly, the higher Q_{loss} during high temperature pyrolysis can be compensated by employing a larger volume of load at ≥ 1.38 kg.

4.6.2 Energy Yield

The energy yield of each pyrolysis system can be determined with the knowledge of product yield and its corresponding energy content. This is determined following *Eq: 4-8*. The results are presented in *Figure 4-22* and *Figure 4-23* for conventional and microwave pyrolysis of EFB pellets, respectively. Similarly, *Figure 4-24* and *Figure 4-25* correspond to the energy yield obtained from conventional and microwave pyrolysis of rice husk pellets, respectively.

$$Energy\ yield\ (\%) = Y_i \times \frac{E_i}{E_b} \qquad \text{Eq: 4-8}$$

Where *Yi* is the product yield (%), E_i is the GCV of pyrolysis product and E_b is the GCV of biomass (MJ/kg).

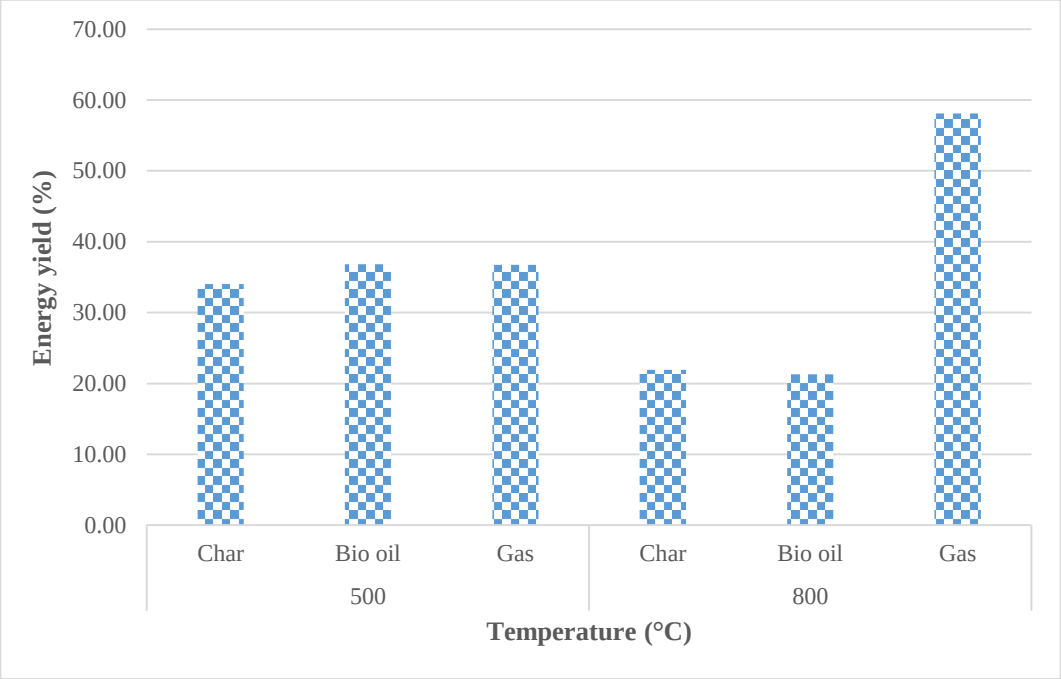

Figure 4-22: Energy yield from conventional pyrolysis of EFB pellets

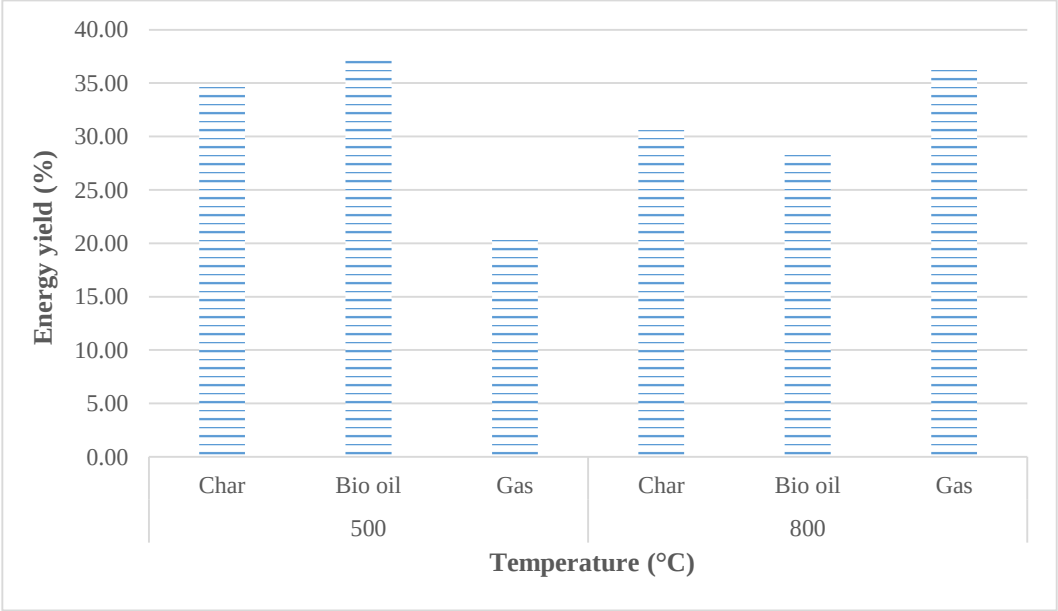

Figure 4-23: Energy yield from microwave pyrolysis of EFB pellets

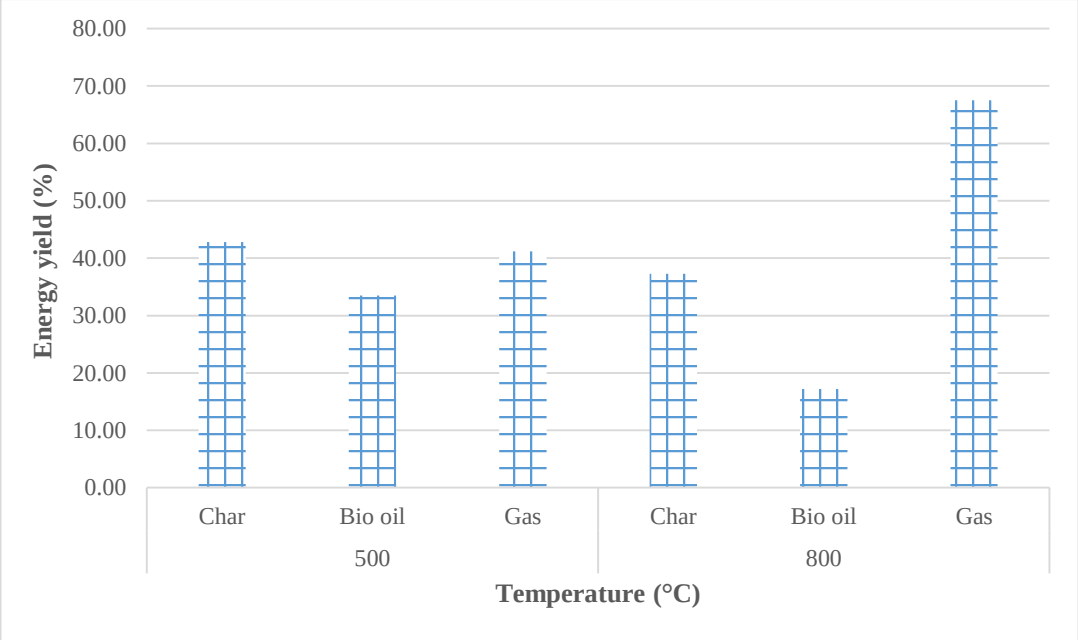

Figure 4-24: Energy yield from conventional pyrolysis of rice husk pellets

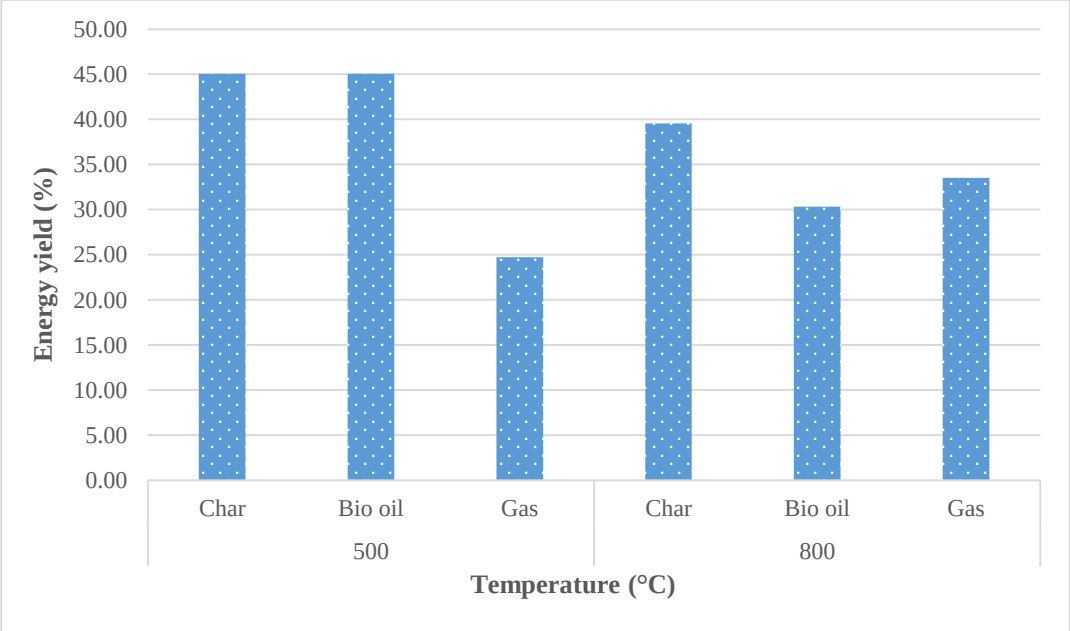

Figure 4-25: Energy yield from microwave pyrolysis of rice husk pellets

In general, the energy yield of char and bio oil decreases with an increase in pyrolysis temperature, regardless of pyrolysis method. Meanwhile, the energy yield of pyrolysis gas increases with temperature, particularly in CP. This is due to a higher gas production at an elevated temperature. For instance, switching from MP to CP has resulted in up to 54% increase in energy yield during EFB pyrolysis at 800ºC.

Meanwhile, the energy yield contribution from char and bio oil is higher in MP than CP for all samples. Up to 34% increase is observed in the energy yield from bio oil when EFB pellets are pyrolysed under microwave radiation at 500º. Similarly, it has resulted in up to 5.2% increase in the energy yield from char. This suggests the potential for process optimisation using MP for high quality char and bio oil production. Meanwhile, CP reactor is ideal for the production of high CV syngas.

4.7 Summary

This section explores the characteristics of biomass used in this study. In general, both biomass materials have around 5 wt.% moisture with 60-70 wt.% volatile content. The biomass materials were pyrolysed under both conventional and microwave pyrolysis equipment at two different temperatures. It was found that the yield of char and bio oil decrease while gas yield increases with rising temperature. Rice husk combustion revealed a higher percentage of ash at around 14 wt.%, where SiO_2 made up of the majority of inorganic species. Meanwhile, potassium is found in abundance in the EFB. The higher ash content in the rice husk contributes to its low calorific value compared to EFB.

Temperature, residence time, and particle size are found to play a significant role during the pyrolysis process. GC-MS analysis indicates no presence of Polycyclic Aromatic Hydrocarbons (PAH) with higher mono-aromatics compounds in MP oils relative to CP

oils. Meanwhile, the highest syngas production is recorded during MP EFB at 800°C at 77 vol. % dry. Surface imaging revealed the presence of deposits on the pores of CP chars, compared to the relatively clean pores observed in MP chars. The maximum surface area of 410 m^2/g is recorded during MP RH at 500°C. Wall fracture and sintering explain the poor surface area of pyrolysed chars at high temperature. The relative permittivity was observed to increase with increasing pyrolysis temperature, which gives exceptional advantage in the context of microwave processing of biomass. The microwave pyrolysis system used in this study has about 80% efficiency compared to just 28% from conventional pyrolysis. The higher energy yield indicates the potential of MP for large scale char and bio oil production while a conventional pyrolysis reactor can be optimised for syngas production.

5 Numerical Simulation of Microwave & Conventional Heating

This chapter outlines the governing equations used in the numerical simulation of microwave and conventional heating, with a detailed description of geometric models and input properties used in the simulation. Microwave heating simulation looks into the effects of variable input properties, load size, and waveguide position on the electromagnetic field and temperature distribution. The behaviour of a metallic thermocouple under microwave radiation is also investigated. Meanwhile, the second part of this chapter looks into transient heat conduction of a single biomass particle subjected to convective and radiant heating.

5.1 Microwave Heating Simulation

5.1.1 Governing Equations

Microwave radiation is governed by a set of Maxwell's equations which forms the basis for solving boundary condition problems in an electromagnetic model (Comsol, 2012). These equations are outlined as follows:

$$\nabla \times \mathrm{H} = -\mathrm{j}\omega\varepsilon_0\varepsilon'' E \qquad \text{Eq: 5-1}$$

$$\nabla \times E = j\omega\mu H \qquad \text{Eq: 5-2}$$

$$\nabla . E = 0 \qquad \text{Eq: 5-3}$$

$$\nabla . H = 0 \qquad \text{Eq: 5-4}$$

Where H is the magnetic field (A/m), E is the electric field (V/m), ω is the angular frequency (rad/s), ε_0 is the permittivity of free space at 8.85 x 10^{-12} F/m, ε'' is the dielectric loss, and μ is permeability (H/m). Although both electric and magnetic components make up the electromagnetic spectrum, the former is mainly responsible for the dielectric heating through conduction and dielectric polarisation. With the exception of metals, most dielectric materials have the magnetic permeability equivalent to the permeability of free space, μ_0.

Ampere's Law in *Eq: 5-1* states that the strength of magnetic field in a closed cavity is proportional to the net electric current flowing through its surface. Meanwhile, Faraday's Law in *Eq: 5-2* states that the electric field strength in a closed cavity is determined by net change in the magnetic flux density. *Eq: 5-3* is Gauss' Law for electric field which states that the total electric flux leaving the control volume must be proportional to the charges contained within it. Gauss' Law for magnetism in *Eq: 5-4* states that the net magnetic flux out of any closed volume must be equal to zero.

The wave equation is defined in *Eq: 5-5*, where k_o is the wave number in free space (rad/m) and n is the refractive index. Microwave power dissipation (P) in *Eq: 5-6* is proportional to the dielectric loss (ε'') and the square of electric field intensity. Meanwhile, the dielectric loss due to electrical conductivity, σ (S/m) is expressed as follows:

$$\nabla \times (\nabla \times E) - k_0^2 n^2 E = 0 \qquad \text{Eq: 5-5}$$

$$P = 2\pi f \varepsilon_0 \varepsilon'' E^2 \qquad \text{Eq: 5-6}$$

$$\varepsilon'' = \frac{\sigma}{2\pi\varepsilon_0 f} \qquad \text{Eq: 5-7}$$

Meanwhile, *Eq: 5-8* defines the impedance boundary condition, where electric field is known to penetrate only a short distance outside the non-lossy boundary. This is under the assumption that the surface current flows due to skin effect. This reduces the amount of computational effort needed to solve the PDE, by neglecting the interior mesh.

$$\sqrt{\frac{\mu_0\mu_r}{\varepsilon_0\varepsilon_r - j\frac{\sigma}{\omega}}}\, n \times H + E - (n.E)n = (n.E_s)_n - E_s \qquad \text{Eq: 5-8}$$

5.1.2 Geometric Model

A 3D geometric model was developed for a multi-mode microwave oven rated at 1000W as illustrated in *Figure 5-1*. This model features an oven cavity, magnetron, waveguide, high temperature furnace, biomass bed, and nitrogen as carrier gas. Biomass

pellets in an actual setup are simulated as a biomass bed in order to minimise the computational time. The oven cavity is made from copper with an overall dimension of (330 x 330 x 205 mm). The load was placed in a porcelain crucible (ϕ 30 x 55 mm).

The biomass bed domain takes the shape of a cylinder as shown in *Figure 5-2*. It has a diameter of 29 mm, with bed height (h) variation between 10-130 mm in the z-direction. It is placed at z=15mm, at the centre of oven cavity where y=0 mm, between x= 136 mm and x= 194mm.The magnetron generates microwaves at 2.45 GHz in TE_{10} mode that travels along the rectangular waveguide (50 x 78 x 10 mm).

The microwaves are then broadcast through a thin sheet of mica, located at the bottom of the oven cavity. The rotating metallic mode stirrer described in **Section 3.3.1** is not taken into account due to complexity during simulation.

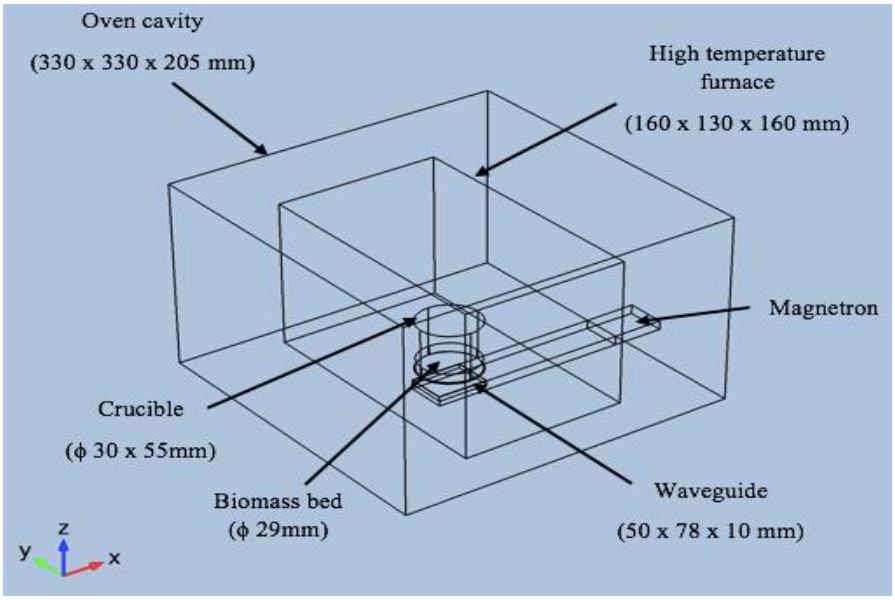

Figure 5-1: Geometric model of microwave oven

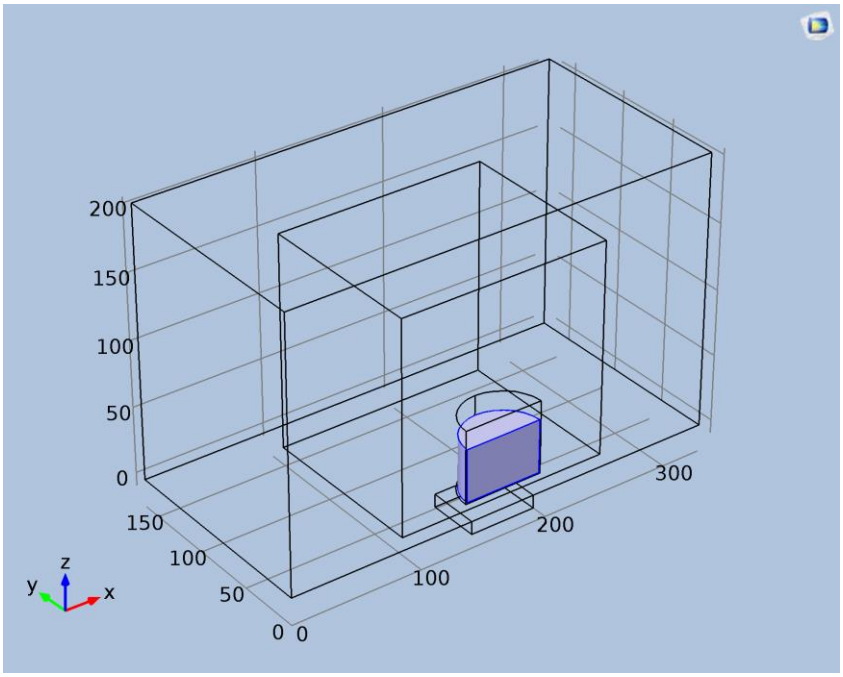

Figure 5-2: Biomass bed domain

The numerical simulation is solved for half of the model under the condition of symmetry. Under this assumption, the standing waves and temperature of the biomass bed on one side of the boundary is a mirror image of what is happening on the other side.

The simulation was carried out using a multi-physics software package. This is done by coupling the radio frequency field and the heat transfer model. The solution from Maxwell's equations serves as an input to predict the temperature distribution within biomass bed in a time-dependent solver. All domains; *i.e.*: oven cavity, furnace, crucible, waveguide, and biomass bed are included in the Maxwell's solution. However, only the biomass bed is solved for Fourier's conduction heat transfer, where its position within the Cartesian plane is illustrated in *Figure 5-3*.

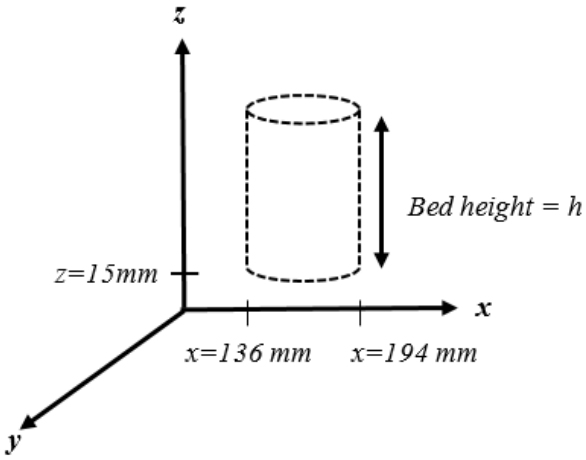

Figure 5-3: Biomass bed domain in a Cartesian plane. (Illustration not drawn to scale)

The electrical and thermal properties of biomass materials used in this study are listed in *Table 5-1***.** The thermal conductivity (k) and specific heat capacity at constant pressure (C_p) of biomass are taken as a function of temperature. Meanwhile, density (ρ) and relative permittivity (ε_r) are assumed to be independent of T. The temperature-dependent properties are updated at each time step and fed into Maxwell's equations to predict the new temperature distribution. This process is solved using a Backward Differentiation Formula (BDF) until the solution converges. *Table 5-2* highlights the size of meshing elements used for the computational work. A fine mesh size between 0.58041-19.35 mm is chosen to increase the simulation accuracy.

Table 5-1: Material properties used in this study

Properties	**Biomass**[3]	**Porcelain crucible**[4]	**Copper**[5]
Electrical conductivity, σ [S/m]	0	0	5.998×10^7
Relative permittivity, ε_r	$1.6-0.06*j$[4] [(0.0051T+1.1052) - (0.005T+0.0077) *j][6]	4.2	1
Relative permeability, μ_r	1	1	1
Thermal conductivity, k [W/m. K]	$0.13 \times 0.0003T^2$ 0.03	1.1	400
Density, ρ [kg/m^3]	1420	2200	8700
Specific heat capacity at constant pressure, C_p [J/kg. K]	$0.0431 + 0.0015T^2 + 2x10^{-5}T^2$ 1150	480	385

Table 5-2: Domain mesh defined in this model

Maximum element size (mm)	19.35
Minimum element size (mm)	0.5804
Maximum element growth rate	1.4
Curvature factor	0.4
Resolution of narrow regions	0.7
Initial time step (s)	0.001
Maximum time step (s)	0.1

This study aimed to investigate the effect of thermal properties, load size and waveguide position on the electric field and temperature distribution within the biomass bed. The simulations were performed on a Dell Precision Tower 5810 workstation with 16 GB RAM and 3.5 GHz processor.

[3] Data taken from Reference (Salema & Afzal, 2015)
[4] Data taken from COMSOL library
[5] Data taken from COMSOL library
[6] Data in this study

The following assumptions are made:

- The oven cavity is perfectly insulated and no heat is lost through the wall.
- Conduction is the primary mode of heat transfer, neglecting the effect of internal convection.

5.1.3 Boundary Conditions

Boundary conditions associated with this type of problem are listed as follows. Symmetry boundary in *Figure 5-4* is taken along the y-axis. The location where microwaves entered the cavity is defined as port boundary, as shown in *Figure 5-5*. This boundary changes with waveguide position, as discussed in **Section 5.2.3**. Meanwhile, an impedance boundary condition depicted in *Figure 5-6* is defined for the metallic surfaces, *i.e.*: oven cavity.

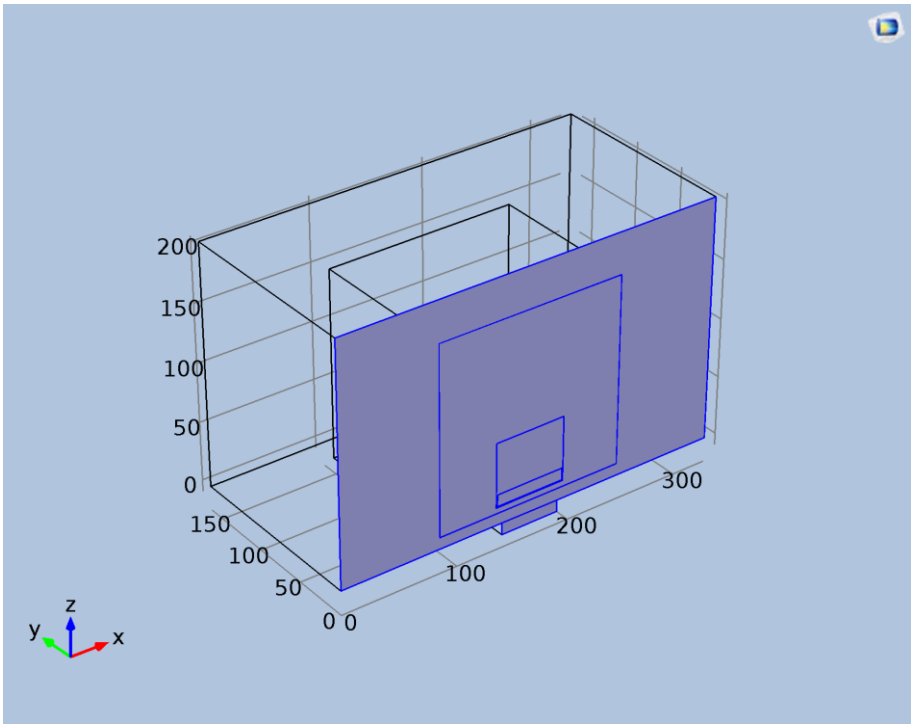

Figure 5-4: Symmetry boundary

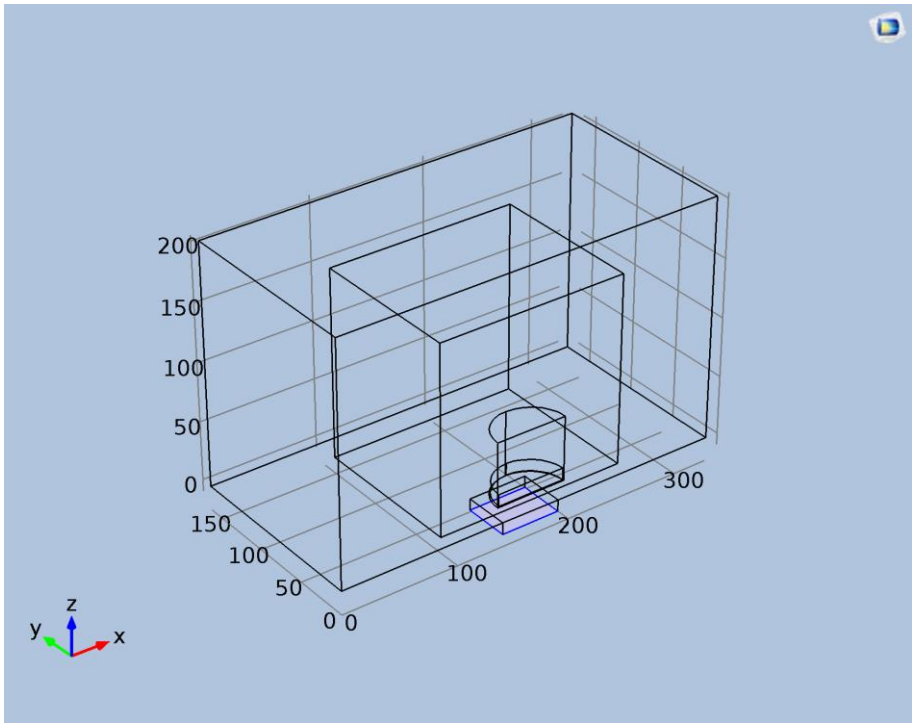

Figure 5-5: Port boundary

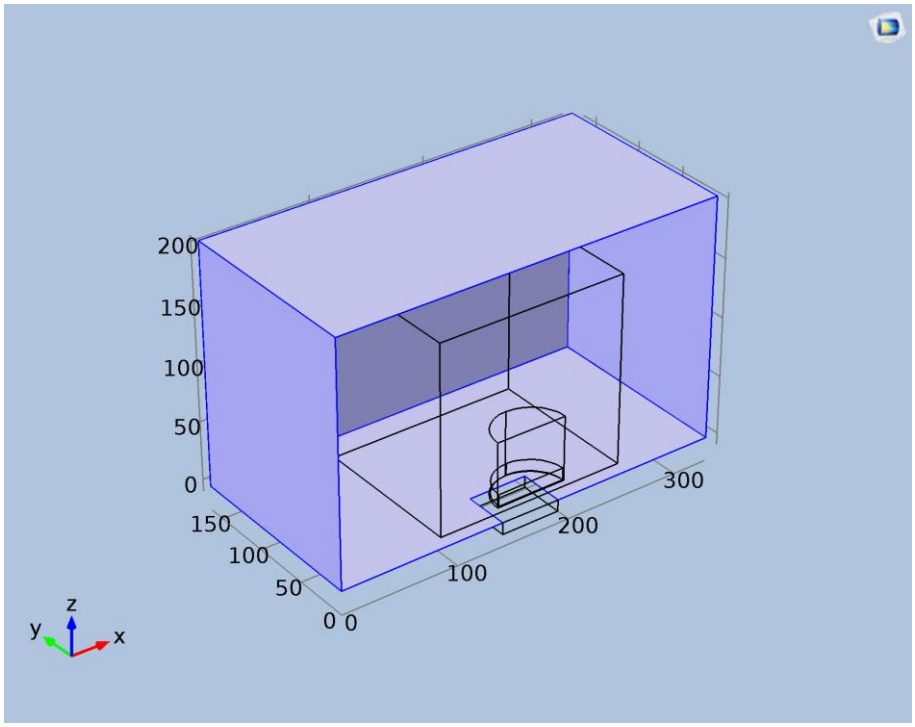

Figure 5-6: Impedance boundary

5.2 Results and Discussion of Microwave Heating Simulation

5.2.1 The Effect of Input Properties

The effect of thermal properties on load heating is investigated in this section. The thermal properties taken into account are Cp, k, and ε_r. These properties are taken as independent of temperature in Case 1. In the second case, Cp and k are taken as a function of temperature while keeping ε_r constant. In the third case, all thermal properties are taken as dependent on temperature.

Their effects on load heating are shown in *Figure 5-7*. A linear increase in temperature over time is observed for constant thermal properties (case 1). The graph then takes the shape of a polynomial when Cp and k are taken as a function of temperature. Poor heating of biomass can be attributed its low thermal diffusivity, $\alpha = \frac{k}{\rho C_p}$ where α is taken as 1.837 x 10^{-8} m^2/s.

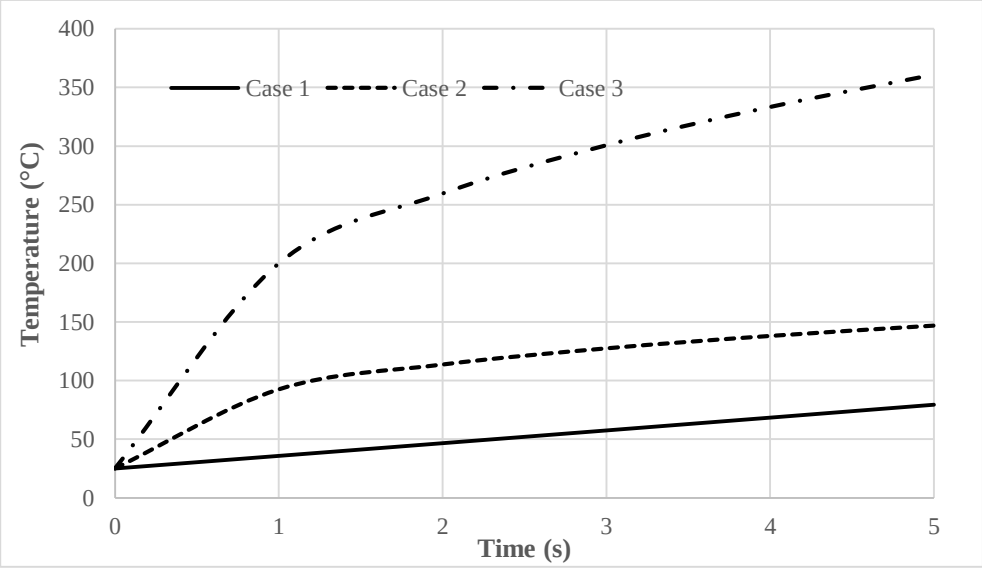

Figure 5-7: Influence of thermal properties on the rate of heating. Bed height, h=50mm

This causes slower transfer of heat within the biomass structure. Meanwhile, case 3 proves that ε_r plays a huge role in the context of microwave heating. Biomass is turned into char as pyrolysis progresses with temperature, with higher relative permittivity than initial feedstock. Maximum heating rate of 67 ºC/s is achieved when ε_r is taken as a function of temperature.

5.2.2 The Effect of Load Size

Figure 5-8 shows the standing waves pattern in an unloaded cavity at a nominal frequency of 2.45 GHz. It can be seen that the maximum and minimum nodes occur at a different location along longitudinal axis. However, these waves experienced slight perturbation when a load was introduced into the cavity, as indicated by the occurrence of hot spot just below the biomass bed in *Figure 5-9*. This indicates the ability of standing waves to respond to any changes with respect to load geometry, size, position within cavity, and load properties as suggested by (Pedreño-Molina et al., 2007).

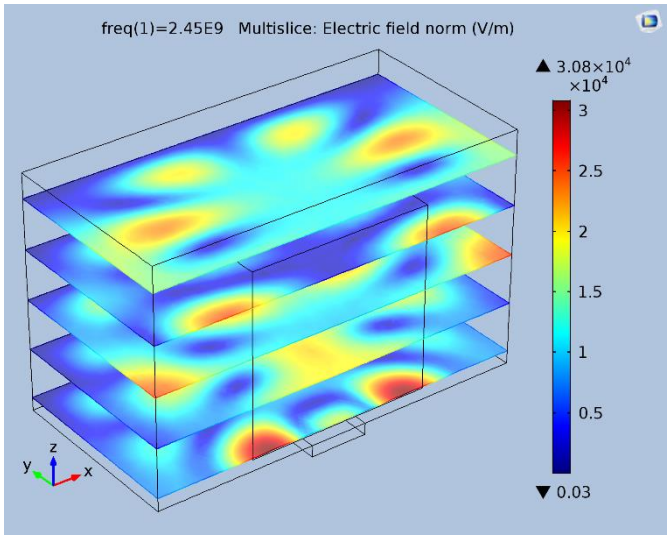

Figure 5-8: Electric field distribution in an unloaded cavity at f= 2.45 GHz

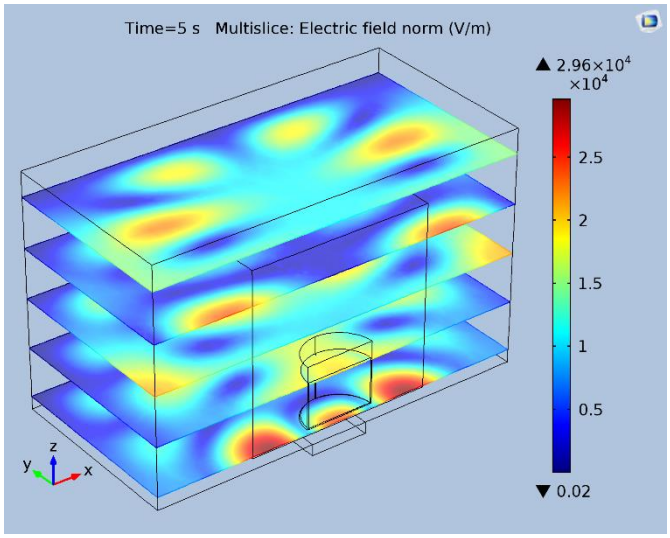

Figure 5-9: Electric field distribution in a loaded cavity at f=2.45 GHz. Load size: (ϕ 29 x 40mm)

Moreover, a slight decrease in the maximum electric field from 3.08 x 10^4 to 2.96 x 10^4 V/m suggests microwave absorption by the load. These waves would otherwise be reflected towards the oven cavity and magnetron in the absence of load. This could damage the magnetron and shorten its operating life

Figure 5-10 shows the electric field just above the biomass bed together with its corresponding temperature distribution. Consistent with the findings in the previous section, maximum electric field decreases from 2.73 x 10^4 to 1.96 x 10^4 V/m as the load size is increased from 10 to 50mm. The minimum and maximum nodes are scattered throughout the oven cavity, where their intensities change with load size. These hotspots are concentrated on the biomass bed at h=30-40mm and diminish outward at h=50mm. Maximum temperature is also recorded at these locations. The location of maximum temperature changes from around edge in h=10mm towards the centre of the biomass bed at h=40mm.

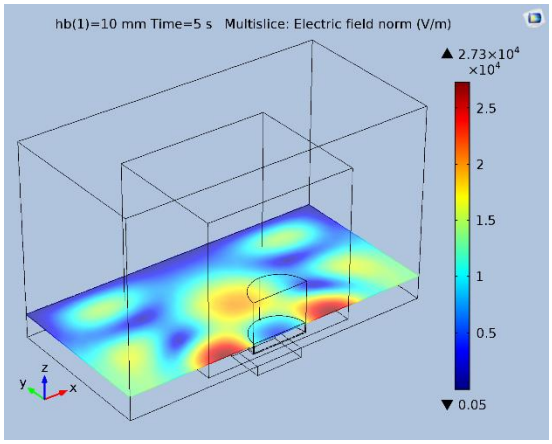
hb(1)=10 mm Time=5 s Multislice: Electric field norm (V/m)
▲ 2.73×10^4
×10^4
2.5
2
1.5
1
0.5
▼ 0.05
z
y
x

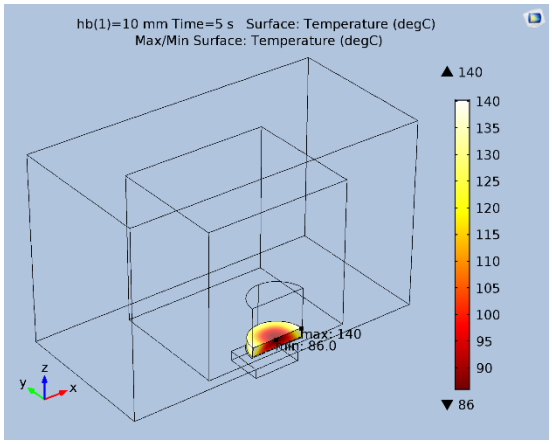
hb(1)=10 mm Time=5 s Surface: Temperature (degC)
Max/Min Surface: Temperature (degC)
▲ 140
140
135
130
125
120
115
110
105
100
95
90
▼ 86
max: 140
min: 86.0
z
y
x

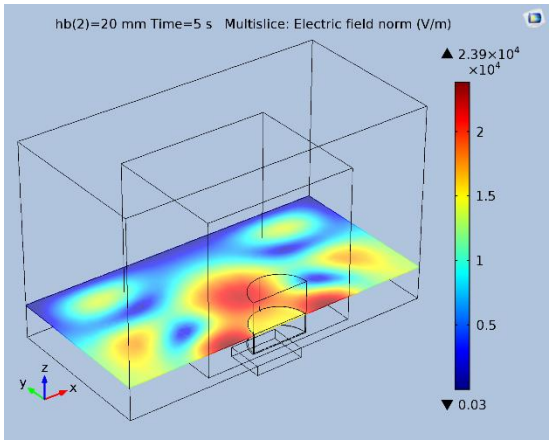
hb(2)=20 mm Time=5 s Multislice: Electric field norm (V/m)
▲ 2.39×10^4
×10^4
2
1.5
1
0.5
▼ 0.03
z
y
x

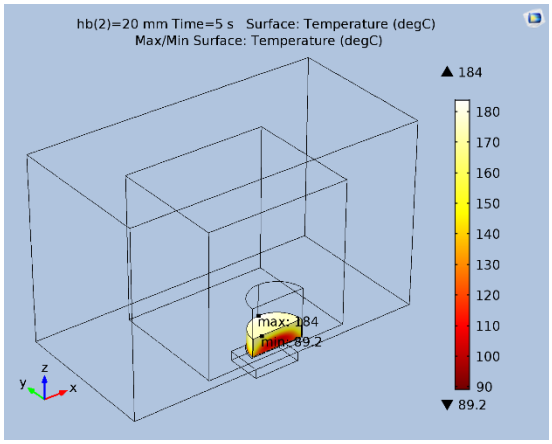
hb(2)=20 mm Time=5 s Surface: Temperature (degC)
Max/Min Surface: Temperature (degC)
▲ 184
180
170
160
150
140
130
120
110
100
90
▼ 89.2
max: 184
min: 89.2
z
y
x

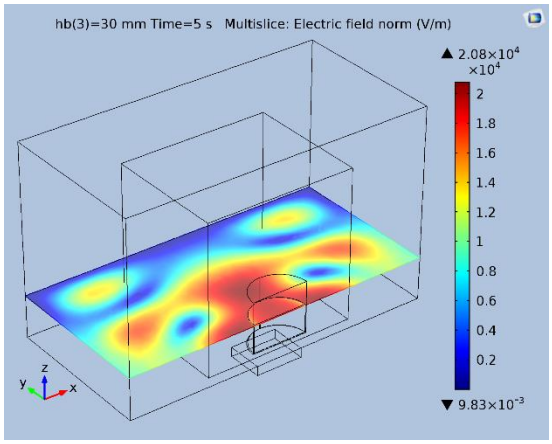
hb(3)=30 mm Time=5 s Multislice: Electric field norm (V/m)
▲ 2.08×10^4
×10^4
2
1.8
1.6
1.4
1.2
1
0.8
0.6
0.4
0.2
▼ 9.83×10^-3
z
y
x

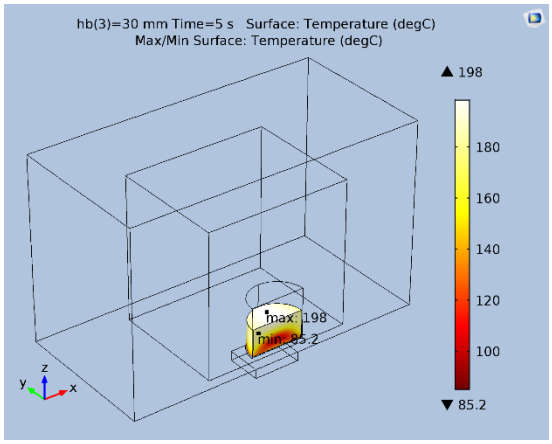
hb(3)=30 mm Time=5 s Surface: Temperature (degC)
Max/Min Surface: Temperature (degC)
▲ 198
180
160
140
120
100
▼ 85.2
max: 198
min: 85.2
z
y
x

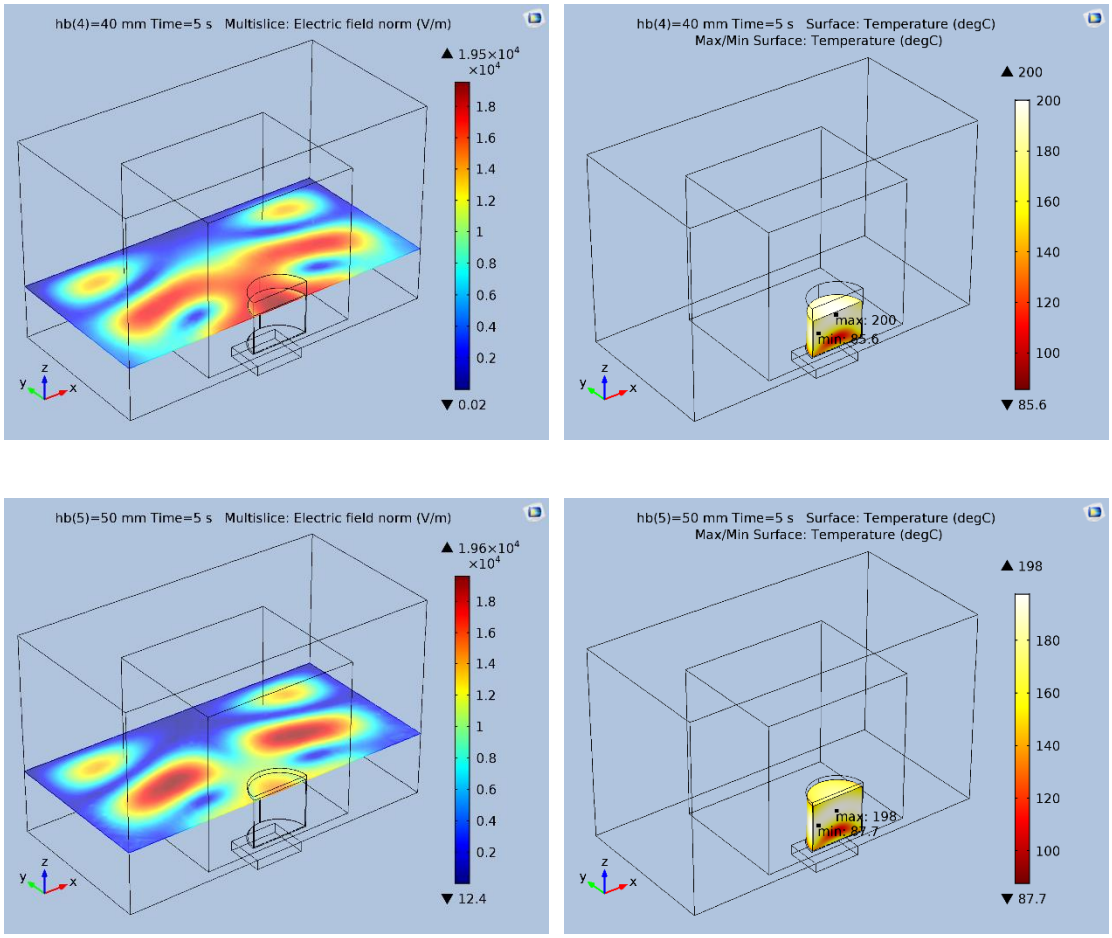

Figure 5-10: Standing wave pattern and temperature distribution of biomass at a different bed height

Bed temperature is also seen to increase with an increase in load size. For example, local temperature increases from 140 to 200ºC, when the load size is increased from 10 to 40mm. This suggests that there is a minimum load for efficient microwave heating. More microwave power is deposited within larger load, which explains its higher temperature. This also confirms the theory of microwave heating where the heating starts from within. This is characterised by an inverse temperature gradient, where temperature at the centre of load is higher than the surface temperature.

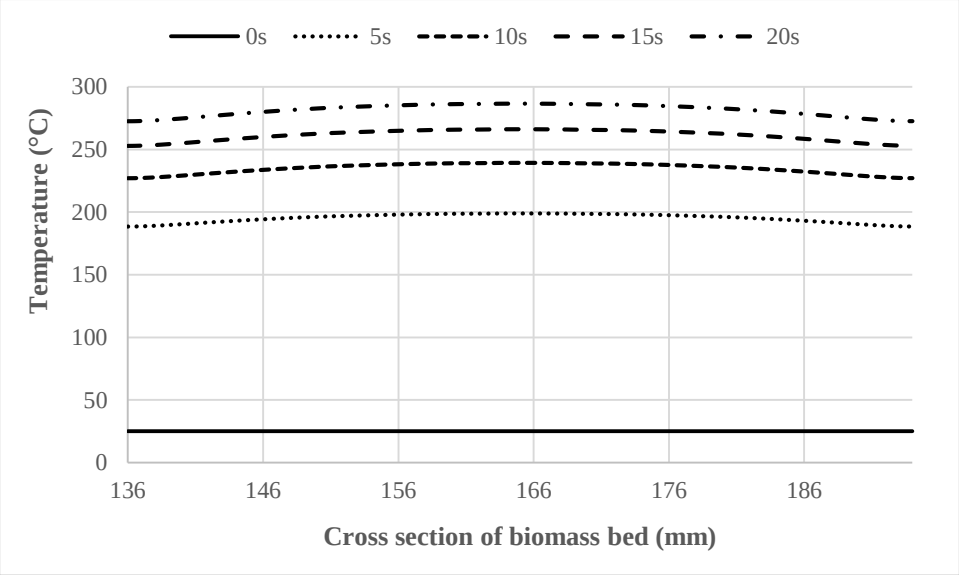

Figure 5-11: Temperature profile across biomass bed at different radiation time. Load size: (ϕ= 29 x 50 mm).

Figure 5-11 shows the temperature profile across the biomass bed under prolonged radiation. At t=0s, a uniform temperature distribution is set throughout the biomass bed at 25ºC. When the microwave power is applied, the temperature inside biomass registered an increase up to 200ºC at the centre, and much lower around the surface. Lower temperature is obtained on the surface as heat is lost to the surroundings. Further increase in temperature is recorded across biomass bed as radiation time is increased. After 20s, the centre of the biomass bed reached a maximum temperature of 286ºC, compared to 274ºC on the surface. High temperature attainable under a short period of time proves the efficiency of microwave, especially in the processing of a large-sized load. This is contrary to conventional heating which requires small-sized load for efficient heat transfer.

5.2.3 The Effect of Waveguide Location

Standing waves pattern, electric field intensity, and heating efficiency are unique to each oven configuration. They are influenced by cavity dimension, building material, power settings, and waveguide position to name a few. Most microwave ovens are equipped with the waveguide feed on the top or right-side of the cavity wall. However, in this study microwaves are being fed from the bottom of the oven cavity, which could lead to different performance. The effect of the waveguide position on the heating behaviour is investigated in this section. *Figure 5-12* shows the waveguide position in this microwave oven.

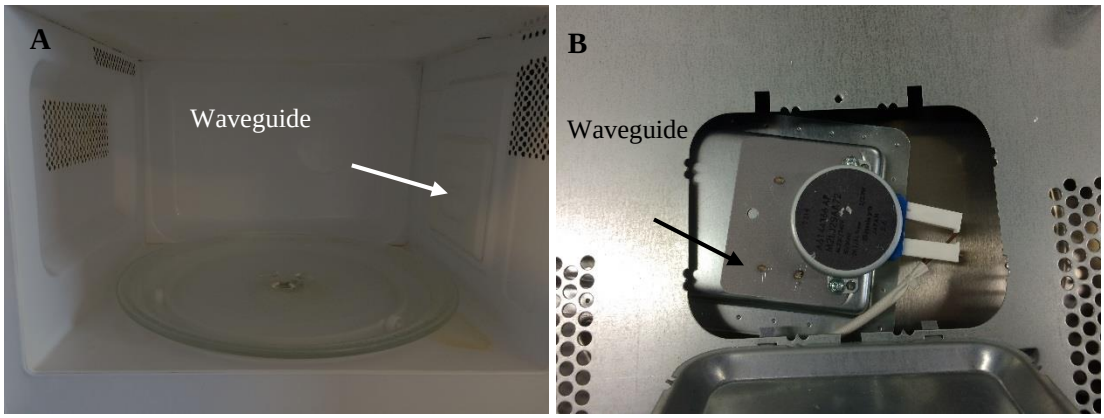

Figure 5-12: Waveguide position in a) Daewoo 500 W microwave oven, b) microwave oven in this study

Biomass bed h=130 mm is simulated when the microwaves enter the oven cavity at a different position, *i.e.*: bottom, right, and top. The standing waves and temperature within the biomass after 5s radiation are shown from *Figure 5-13* to *Figure 5-15*. The difference in standing waves pattern is observed, which implies that the position of the waveguide plays a significant role in the efficiency of microwave heating. The maximum and minimum nodes also occur at a different position. It can be seen that the right-side

waveguide is good for heating a small load (up to h=30 mm), as evidenced by a region of maximum temperature.

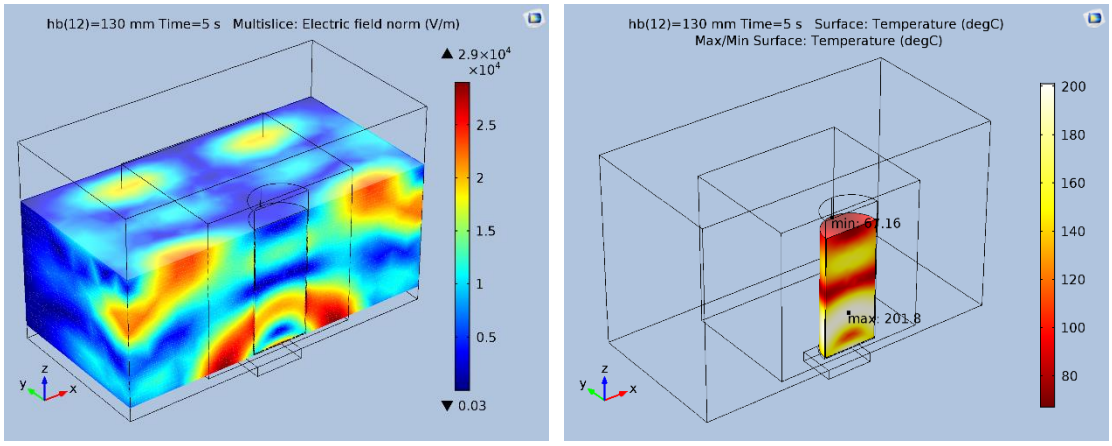

Figure 5-13: Bottom-side waveguide

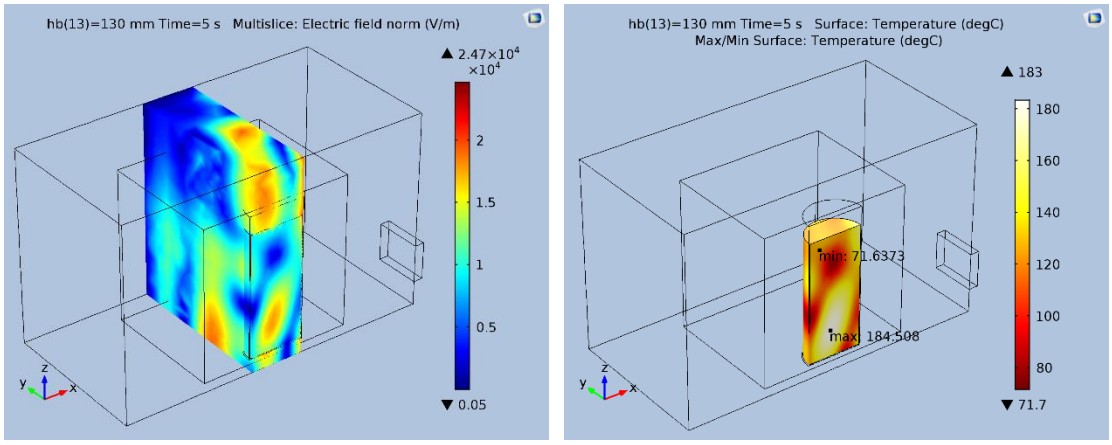

Figure 5-14: Right-side waveguide

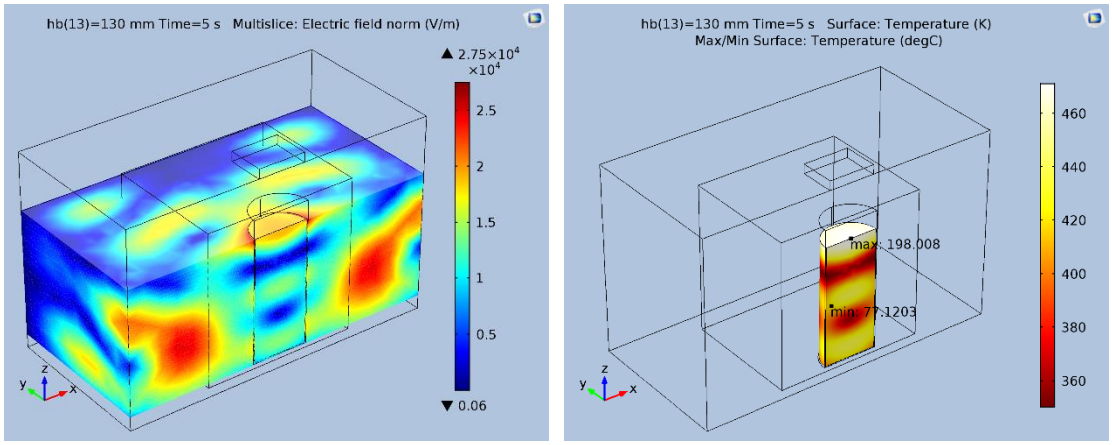

Figure 5-15: Top-side waveguide

Meanwhile, two regions of minimum field are observed in the case of a top or bottom-side waveguide, although these occur at a different bed height. *Figure 5-16* shows the microwave power absorbed at a different bed height. This is translated into internal heat generation during microwave heating. These values are found to increase steadily with load size, regardless of waveguide position. However, the heating behaviour is found to be dependent on the waveguide position. Microwave ovens equipped with top and right-side waveguides are found to be very efficient in heating up small load, up to 23 and 30 mm, respectively.

Meanwhile, a bottom-side waveguide is more efficient in processing a large load. It reaches a maximum of 192 W at h=130 mm. This is about 19.2% of the input power supplied. It increases steadily from h=10mm and reaches a plateau at around 60 and 120 mm. 60 mm is about half-wavelength (1/2λ) of the microwave, which also corresponds to the minimum nodes. The total heat source from the right-side waveguide increases steadily from around 20 to 147 W, as the bed height is increased from 10 to 130 mm. Meanwhile, as expected the graph for a top-side waveguide is seen as a mirror image of bottom-side. The regions of cold spots are identified at around h=30 and 80 mm.

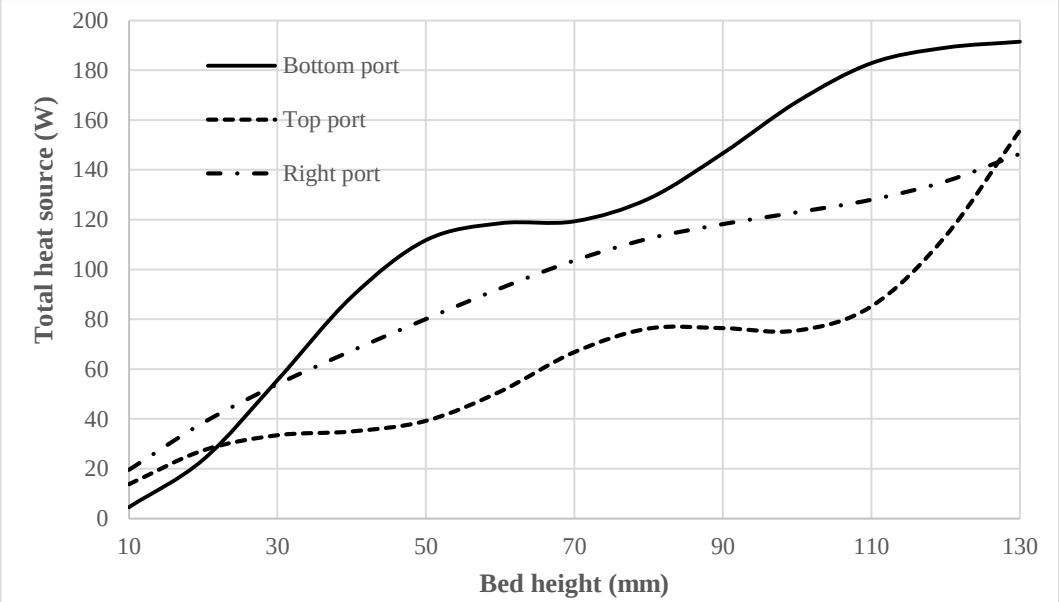

Figure 5-16: Microwave power absorbed at a different bed height

5.2.4 Modelling Microwave Thermocouple Effect

In this section, a metallic thermocouple is simulated as a ϕ=3 mm, 160 mm long cylindrical rod. It was fitted from the top of oven cavity, with its tip touching the biomass bed, as shown in *Figure 5-17*. Other parameters were kept constant. The temperature distribution inside biomass bed with and without the presence of thermocouple is compared. It can be seen that the biomass registered a much higher temperature of 216°C under the presence of thermocouple compared to the maximum of 200°C without the thermocouple, as depicted in *Figure 5-18* and *Figure 5-19*. Moreover, on a closer look it was revealed that the location of maximum temperature is found to be around the circular edge of the thermocouple tip, as shown in *Figure 5-20*.

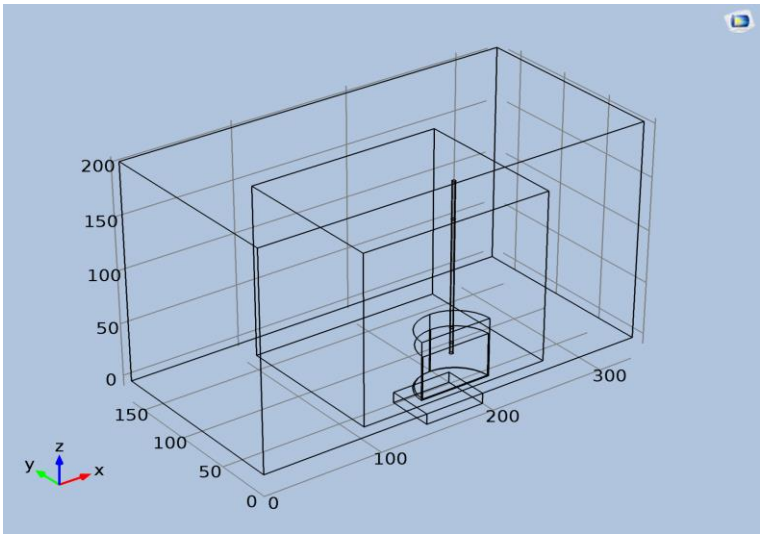

Figure 5-17: Geometric model

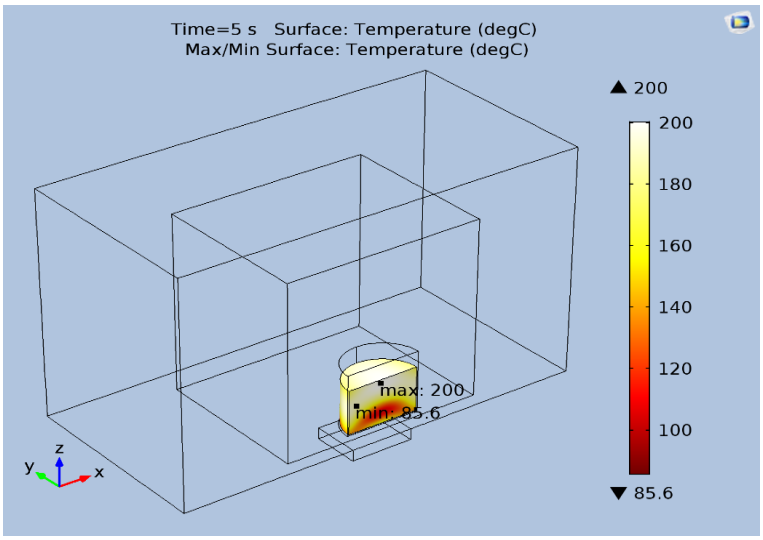

Figure 5-18: Temperature distribution inside biomass bed without thermocouple

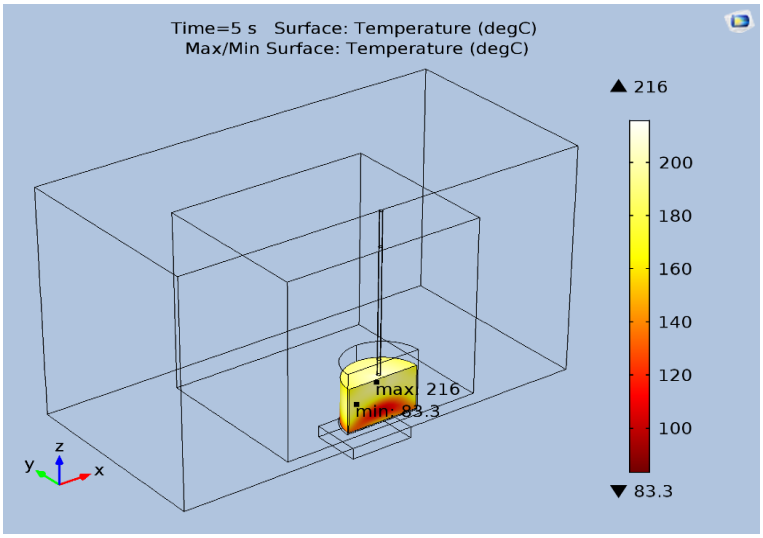

Figure 5-19: Temperature distribution inside biomass bed fitted with thermocouple

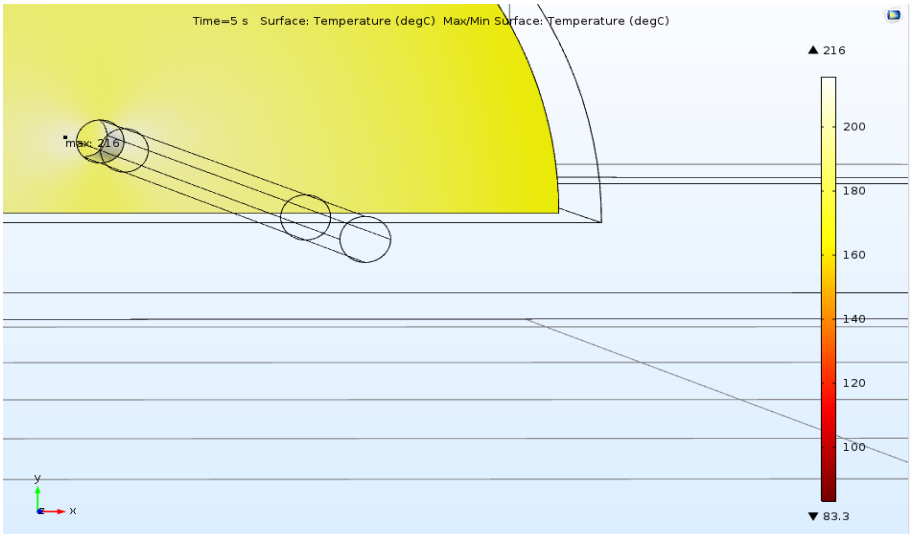

Figure 5-20: Magnified view

Thermocouple acts as an antenna that attracts the microwaves, causing an increased concentration of electric field. This might induce a localised heating and thus, a higher local temperature. Although precautionary steps have been taken to minimise the electromagnetic interference on the thermocouple, discrepancy in temperature reading still exists. For this reason, it is recommended to employ a non-contact optical fibre temperature sensor to mitigate the problems associated with contact, metallic thermocouple such as slow response time and possible EM interference.

5.3 Conventional Heating Simulation

The transient heat conduction within biomass is studied numerically. A cylindrical shaped particle with diameter ranging between 8-9 mm is subjected to a radiative and convective environment. This is representative of EFB and rice husk pellets. However, in order to demonstrate the effect of particle size on transient heating, Bi numbers of 0.64 and 1 are chosen. The effect of particle size and time taken for the particle to reach equilibrium with bulk temperature (T_∞) are studied . This problem is approached using Fourier's heat equation with its corresponding initial and boundary conditions. The ratio of L/r of biomass pellets in this is well above 10, which permits the use of transient heat conduction in infinite bodies. Under this assumption, heat conduction occurs in a radial direction. Several assumptions are made:

- No internal heat generation.
- Thermal and physical properties are indepenedent of temperature.
- The volatiles leave the solid as they are formed. Heat transfer analysis is limited to primary pyrolysis, neglecting the role of secondary reactions between gas and char inside biomass particle.
- Particle undergoing pyrolysis have a constant volume throughout experiment, with no particle shrinkage or thermal swelling. $V = V_s\,(t) + V_g\,(t) = \text{constant}$
- There is no temperature gradient at the centre line at (r=0) of the solid particle $(\frac{\partial T}{\partial r} = 0)$

Input properties used during numerical simulation are tabulated in *Table 5-3*.

Table 5-3: Input properties used during simulation

Input properties	**Value**	**References**
Thermal conductivity, k (W/mK)	0.1256	(Pyle & Zaror, 1984)
Thermal diffusivity of wood, α (m^2/s)	1.79 x 10^{-7}	(Jalan & Srivastava, 1999)
Initial temperature of biomass, T_0 (K)	300	-
Final temperature of reactor, T_∞ (K)	773, 1073	-
Convection heat transfer coefficient, h (W/m^2K)	20	(Babu & Chaurasia, 2004)
Specific heat capacity. C_p (J/kgK)	1670	(Pyle & Zaror, 1984)
Stefan-Boltzmann constant, σ (W/m^2K^4)	5.67 x 10^{-8}	-
Emissivity, ε	0.95	(Pyle & Zaror, 1984)
Biot number, Bi	0.64, 1	-
Density of biomass, ρ (kg/m^3)	1420	(Salema & Afzal, 2015)

5.3.1 Governing Equations

Where k is the thermal conductivity (W/m. K), C_p is the specific heat capacity at constant pressure (J/kg. K), ρ is density (kg/m^3) and r is the radial position (m). Meanwhile, thermal diffusivity, α (m^2/s) is defined as:

$$\frac{k}{\rho C_p} = \alpha \qquad \text{Eq: 5-9}$$

Substituting α into Eq: 3-1 yields the new heat equation:

$$\frac{dT}{dt} = \frac{\alpha}{r}\frac{d}{dr}\left(r\frac{dT}{dr}\right) \qquad \text{Eq: 5-10}$$

This partial differential equation (PDE) provides the variation of temperature with space and time; *i.e.*: $T(r, t)$. The initial condition is set as follows:

$$t = 0, \quad T(r, 0) = T_0 \qquad \text{Eq: 5-11}$$

The biomass particle is subjected to a combination of convection and radiation heat transfer to the surface, where r= R. The boundary conditions are defined as follows:

$$t > 0,\ r = 0,\ \frac{dT}{dr} = 0 \qquad \text{Eq: 5-12}$$

$$t > 0,\ r = R, \left(-k\ \frac{dT}{dr}\right)_{r=R} = h(T_\infty - T) + \in \sigma(T_\infty^4 - T^4) \qquad \text{Eq: 5-13}$$

Where T_∞ is the bulk temperature (K), h is the convection heat transfer coefficient (W/m^{2}K), ϵ is emissivity, and σ is the Stefan-Boltzmann constant (5.67 x 10^{-8} W/m^2 K^4). The problem can be solved numerically by transforming the heat equation, initial condition, and boundary conditions into the non-dimensional forms. The following dimensionless parameters are introduced:

$$x = \frac{r}{R} \quad \text{Eq: 5-14}$$

$$\theta = \frac{T_\infty - T}{T_\infty - T_0} \quad \text{Eq: 5-15}$$

$$\tau = \frac{\alpha t}{R^2} \quad \text{Eq: 5-16}$$

Where x is the dimensionless distance, θ is the dimensionless temperature, T_0 is the initial temperature of biomass (K), and τ is the dimensionless time. Substituting these parameters into *Eq: 5-10* yields a new dimensionless heat equation:

$$\frac{d^2\theta}{dx} = \frac{d\theta}{d\tau} \quad \text{Eq: 5-17}$$

The new initial and boundary conditions are described as follows:

$$\tau = 0,\ \theta(x,0) = 1 \quad \text{Eq: 5-18}$$

$$\tau > 0, at\ x = 0,\ \frac{d\theta}{dx} = 0 \quad \text{Eq: 5-19}$$

$$\tau > 0, at\ x = 1,\ \frac{d\theta}{dx} = -\theta Bi_m \quad \text{Eq: 5-20}$$

Where Bi_m is a modified Biot number expressed as:

$$Bi_m = \frac{R}{k}\left[h + \in \sigma\left(T^3 + T^2 T_\infty + T_\infty^2 T + T_\infty^3\right)\right] \quad \text{Eq: 5-21}$$

The governing equations are solved using an exact solution to predict the transient heat conduction inside a single biomass particle. This solution takes form of an infinite series, for Fo > 0.

$$\theta = \sum_{n=1}^{\infty} C_n \exp(-\zeta_n^2 Fo) J_0(\zeta_n x) \quad \text{Eq: 5-22}$$

$$C_n = \frac{2}{\zeta_n} \frac{J_1(\zeta_n)}{J_0^2(\zeta_n) + J_1^2(\zeta_n)} \quad \text{Eq: 5-23}$$

$$\zeta_n \frac{J_1(\zeta_n)}{J_0(\zeta_n)} = Bi \quad \text{Eq: 5-24}$$

$$Jn(x) = xJ_1(x) - BiJ_0(x) = 0 \quad \text{Eq: 5-25}$$

Where ζ_n are the eigenvalues or roots of the characteristic equation in Eq: 3-16. In this case, $Bi = \frac{hr}{k}$ and J_0 and J_1 are Bessel functions of the first kind. The method of finding solution to transient heat conduction in a cylindrical particle is outlined below.

- Find Biot and Fourier number.
- Look for eigenvalues (ζ_n) based on the Bi value. Bessel functions, J_0 and J_1 are determined using the function BESSELJ (ζ_n, n) in MS Excel.
- Dimensionless temperature distribution (θ) can be determined by solving the series, Cn.

Once the spatial temperature distribution T(r,t) is known, SOLVER tool is used to perform iteration to determine the time it takes for the centre of the particle to reach equilibrium with bulk temperature. The iteration process stops once the value of t converges.

5.4 Results and Discussion of Conventional Heating Simulation

5.4.1 Effect of Particle Size

Biot number provides the measure of internal resistance to conduction within material. Under the assumption of constant thermal properties, Bi number is taken as a function of a particle size. The radial temperature distribution at a different Bi number is presented in *Figure 5-21* and *Figure 5-22*. A stark contrast can be seen with material having high Bi has a large temperature gradient between the surface and centre of the particle. This large temperature variation means that the heat transfer to a particle is internally controlled,

while heat transfer is externally controlled in the case of small particle which results in approximately uniform temperature distribution.

For particle with high Bi number, the surface temperature (x=1) is always equal to the bulk temperature T∞, while this value appears to vary with time for smaller particle. In both cases, the temperature profiles get flattened over time and eventually the centre temperature reaches equilibrium with reactor temperature; *i.e.*: T=T∞.

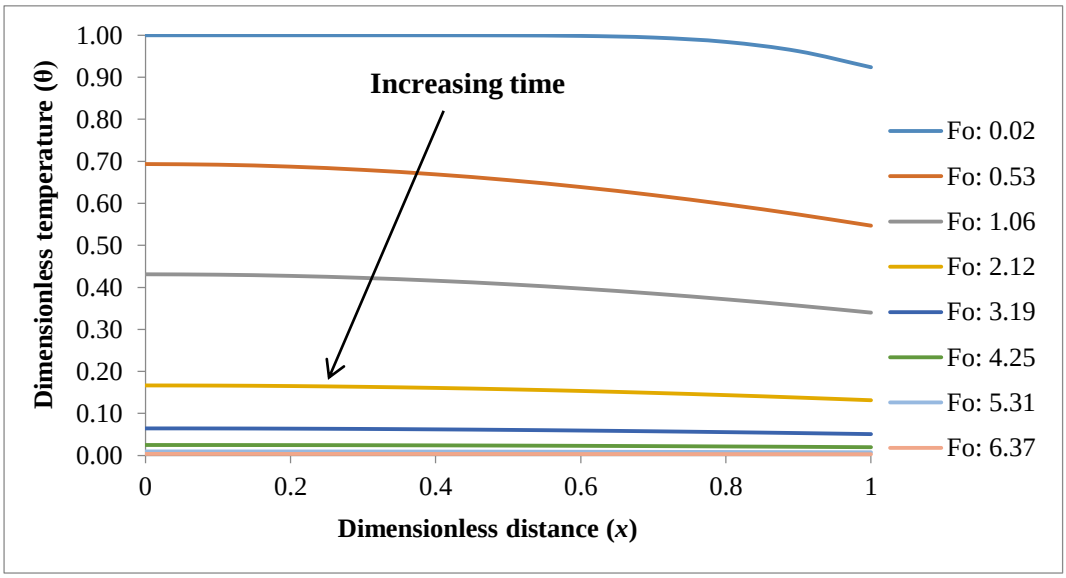

Figure 5-21: Temperature profile at Bi= 0.64

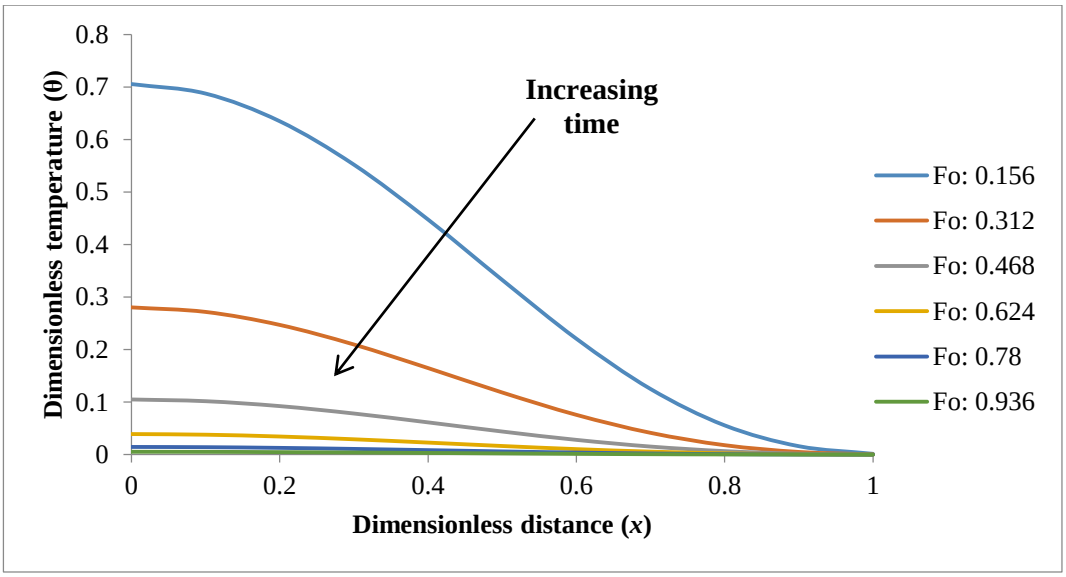

Figure 5-22: Temperature profile at Bi= 1

Table 5-4: Time taken for centre of particle to reach equilibrium with T∞

Biot number	Bulk temperature, T_∞ (°C)	Time (min)
	500	13.18
0.64	800	13.87
	500	19.38
1	800	21.49

With a known Biot number, the time taken for centre of the particle to reach equilibrium with T_∞ can be determined using a series of iteration process, where $T(0,t)= T_\infty$. This is presented in *Table 5-4.* Small particle, *e.g.*: Bi= 0.64 requires 13.18 minutes to reach thermal equulibrium, compared to around 20 minutes for larger particle. High pyrolysis temperature (T_∞ = 800°C) is expected to reduce the time it takes for centre of particle to reach equilbrium due to greater pyrolysis rate. However, this is not the case. It takes around 14 minutes for a particle to reach equilibrium with T_∞.

5.5 Summary

This chapter analysed the effect of variable thermal properties, load size, and waveguide position on the electric field and temperature distribution within the biomass bed. It gives prediction results for the standing waves pattern which are specific to oven dimension and waveguide location. By knowing the regions of minimum and maximum field, one can position the load for efficient microwave heating. A closer match to experimental values is predicted when using thermal properties that are temperature-dependent. Meanwhile, load size is found to exert a significant influence the microwave power deposited. It serves as an internal heat generation to increase the temperature of the biomass bed. Greater microwave power is deposited in a larger load, although heating efficiency is subject to a specific oven configuration.

This simulation also confirms the theory of microwave heating where the centre temperature is higher than the surface temperature. The effect of modelling mode stirrer rotation on the standing waves is beyond the scope of this research. However, from the results presented above, it is clear that the electrical fields will then move about so that each location will tend to receive an average field strength thus resulting in a more uniform heating. Nevertheless, the internal heat diffusion within the load will typically result in a higher temperature at the load centre. A more accurate representation can be obtained if kinetics parameters and chemical reactions are included in the biomass pyrolysis model.

A simple heat transfer model is generally adequate to model the pyrolysis process. It can be concluded that heat conduction in a single biomass particle subjected to a combination of convection and radiation heat transfer mechanism is generally much slower. It is primarily governed by particle size that influences the heat transfer efficiency, unlike microwave heating.

6 Challenges and Opportunities of Pyrolysis Process

This chapter discusses some issues associated with the potential scale-up of microwave pyrolysis process. It also highlights the potential of biomass pyrolysis and the market for pyrolysis products.

6.1 Issues Associated with the Scale-Up of Microwave Pyrolysis

Scaling up microwave pyrolysis technologies from laboratory scale to pilot or industrial scale requires a lot of thought in terms of reactor design, selecting appropriate materials for fabrication, and sample throughput, to name a few. However, progress in computational modelling allows process optimisation with respect to reactor geometry prior to fabrication. This enables the researcher to determine the region of maximum and minimum power density. So far, small scale microwave processing of biomass has shown tremendous benefits in terms of higher oil yield and better quality fuels in terms of aromatics and the absence of PAHs compounds.

However, batch processing is practically not feasible due to variation in dielectric properties with localised temperature and the magnitude of absorbed power as the biomass is pyrolysed under microwave radiation. These brought along the issue of process control, i.e.: how to keep the reaction temperature within the pyrolysis temperature range of below 500 °C to avoid potential thermal runaway, which further induces char gasification. This essentially limits the production of bio oil.

Sample throughput is another concern in microwave processing of biomass. Most of the microwave power will end up being reflected if the sample size is too small. However, when processing hundreds of kilograms of biomass, the amount of microwaves being

absorbed into the sample diminishes due to the effect of penetration depth. This could lead to surface overheating that is pretty similar to those obtained by conventional heating.

For this reason, it is recommended to utilise a continuous flow reactor with single-mode microwave applicator. The region of high peak power density is easily established in this type of reactor, in contrast to multi-mode configuration with its inherent low peak power density and large power density distribution. Region of peak power density is recorded at the centre and diminishes towards zero at the wall, which implies uneven heating of load across the cavity. This has been demonstrated in a pilot scale demonstration by Microwave Process Engineering research group at the University of Nottingham. It uses tunnel type applicator where the load is travelling on a microwave-transparent conveyor belt. In order to avoid uneven power density distribution, the tunnel applicator is equipped with self-cancelling reflection step (Robinson et al., 2010).

Another issue of concern during the scale up process is selection of materials. The materials commonly used in lab scale demonstration such as PTFE and quartz glass are no longer compatible for large scale reactor. Factors such as pressure and maximum handling temperature should be taken into consideration when choosing the construction materials.

6.2 Market for Pyrolysis Products

There are potential markets for wide range of pyrolysis products. For example, the market price for pyrolysis oil was valued at € 218/tonne in 2015, compared to heavy fuel oil which was valued at between € 400-600/tonne (Riedewald & Sousa-Gallagher, 2016) . This competitive pricing allow pyrolysis bio oil to compete with conventional fuels in a global market. However, pyrolysis bio oil is badly affected by a recent plummet in global

oil price. In order for pyrolysis bio oil to be competitive, the global oil price needs to be above $ 55 per barrel (Bauer, 2017).

Direct combustion of bio oil in an engine is practically impossible due to its highly oxygenated and acidic nature. This requires modifications in parts of internal combustion engine that can handle biofuels. On the other hand, pyrolysis bio oil can be blended with biodiesels and other liquid fuels. Moreover, high formation of phenol and other aromatics in bio oil made it an interesting prospect as chemicals precursor in petro-chemical industry. Thus reduces the reliance on petroleum-based chemicals. Bio oil treatments include catalytic upgrading, hot vapour filtration, and biomass leaching to remove ash.

Meanwhile, char produced from pyrolysis process still has a relatively low surface area than most adsorbents such as activated carbon. For this reason, it is recommended to utilise the chars as feed in the gasification process to increase their reactivity. Other uses of bio chars include being used as additive in soil rehabilitation or simply used as feed in combined heat and power (CHP) plant and domestic cooking due to their high energy value.

Gases evolved during biomass pyrolysis include hydrogen, carbon monoxide, carbon dioxide, and methane. The calorific values of pyrolysis gas range between 13-17 MJ/m^3 during conventional pyrolysis and between 8-12 MJ/m^3 during microwave pyrolysis. Lower CV in the latter can be attributed to a smaller amount of CH_4 emitted during microwave pyrolysis. Nevertheless, these gases can be used directly in an internal combustion engine or co-fired with natural gas in a Combined Heat and Power (CHP) cycle.

Moreover, steam reforming of methane can be employed to produce a rich energy carrier such as H_2 under the presence of catalyst. The reaction proceeds in two stages;

initially CH_4 reacts with steam under exothermic process to produce syngas, *i.e.*: CO and $3H_2$ at a temperature between 750-800°C. The heat for steam generation is normally supplied by process heat or flue gases. This is followed by water-gas shift reaction, where the CO produced in the first reaction is reacted with steam (H_2O) under the presence of catalyst to yield H_2 and CO_2 (New York State Energy Research and Development Authority, 2017). These gases can also be subjected to Fischer-Tropsch processing for conversion into liquid hydrocarbons and other chemical intermediates such as methanol and ammonia.

6.3 Potential for Biomass Pyrolysis

The initial characterisation of biomass in **Section 4.1** indicates the good potential of empty fruit bunch (EFB) and rice husk pellets for energy recovery via the pyrolysis process. Lignocellulosic biomass constitutes the majority of this waste biomass. Pyrolysis emerges as a solution towards circular economy by turning these wastes into a wide range of valuable products. The high composition of volatiles, up to 73 wt.% can be utilised for the production of bio oil and gas emitted during inert thermal decomposition of biomass. Moreover, the presence of alkali-earth metals can be beneficial during pyrolysis as they increase the devolatilisation rate and lower the initial degradation temperature.

The potential for large-scale biomass processing in Malaysia is endless. With a huge area dedicated to palm oil plantation, this will ensure a guaranteed supply of palm oil wastes to a processing facility. The same can be said for the waste biomass produced from a rice mill. The total area of plantation expands every year to accommodate a rising demand for food. This ensures a minimal problem on the supply side as to date, there is no competing needs of rice husk and EFB other than for use as fuels.

This is reinforced by the energy policies that support the move towards clean, renewable energy and reduce the heavy reliance on fossil fuels. The policy will award the independent power producers (IPP) who obtain their energy from renewable sources including biomass, solar photovoltaic, and hydro. These include financial incentives such as tax rebate for imported equipment and a guaranteed payment via the Feed in Tariff (FIT) system.

However, this raises a question of sustainability. If the new plantation crops are grown on the area of virgin land, this could defeat the notion of zero carbon cycle. The gases emitted during transportation of waste biomass from plantation to processing facility might offset the benefits. Another matter of concern is the cost of operating pyrolysis plant in terms of fuel processing and electrical power. For instance, sample size is one of the critical aspects in a conventional pyrolysis plant. Biomass has to undergo drying process and grinding to smaller particle size for maximum heat transfer efficiency. In order to increase the energy density of fuel and ease of fuel handling and storage, the biomass have to be compacted.

On top of that, electricity could be the single major operating cost in any pyrolysis plant. Hence, plant operator should look into potential buyers and be able to generate a steady stream of pyrolysis products to offset this cost. It has been successfully demonstrated that pyrolysis process could yield a wide range of high-value added chemicals.

7 Conclusions and Suggestions for Future Work

The aims and objectives defined at the start of this PhD research programme have been achieved successfully. This chapter outlines the conclusions derived from this innovative study and presents suggestions for future work.

7.1 Conclusions

- Pyrolysis raised the energy density of the biomass tremendously. Microwave pyrolysis was found to give greater bio oil and syngas yield than conventional pyrolysis at similar temperature. This system has resulted in up to 8.40% increase in bio oil as observed in the case of MP RH at 800ºC. A higher amount of mono-aromatics and phenolic were also recorded in MP oils, compared to heavier tar compounds or PAH in CP oils. Up to 44% increase in phenol formation was observed in MP oils. Similarly, microwave pyrolysis has resulted in up to 29% increase in syngas (H_2+CO) evolution and about 42% lower greenhouse gases (CO_2+CH_4) than conventional pyrolysis. The highest specific surface area of 410 m^2/g was recorded during MP of rice husk. This can be attributed to its cleaner pore structure, compared to the presence of secondary chars deposited on the pores of CP chars. In this respect, microwave pyrolysis can be optimised for the production of high quality char and bio oil, while conventional pyrolysis can be optimised to enhance syngas production.
- Out of two temperatures tested in this study, 500ºC is found to be the optimum temperature for maximum bio oil production. An increase in temperature would result in a greater gas production due to intensified secondary reactions. Moreover,

conducting pyrolysis at high temperature caused sintering and the destruction of cell wall structure, which gives it lower surface area.

- Maximum efficiency, η of 81% is observed during microwave pyrolysis compared to around 29% recorded during conventional pyrolysis. Microwave pyrolysis resulted in time and energy savings due to lower energy input required to conduct the pyrolysis process.
- Numerical simulation also revealed non-uniform heating during microwave pyrolysis due to the existence of local minimum and maximum electric field strength within the microwave oven cavity. Microwave power absorbed by the load is translated into internal heat generation which governed the biomass temperature distribution. The relative permittivity of microwave pyrolysed chars was higher than the parent biomass, where this value increases with an increase in pyrolysis temperature. This shows that pyrolysis char on its own could sustain the microwave pyrolysis process, without any addition of microwave absorber. An increase in localised heating was also reported when a metallic thermocouple was modelled into the simulation. This proves the extent of microwave thermocouple effect.

7.2 Suggestions for Future Work

- 3D rotation of the mode stirrer should be incorporated into the numerical modelling of microwave pyrolysis. This provides a more realistic representation of electric field within a microwave oven.
- BET analysis on the remaining chars should be used to characterise the specific surface area.
- Pyrolysis tests should be carried out at a wide range of temperature covering low and high temperature pyrolysis. By doing this, better understanding can be achieved on the influence of temperature on product yield and distribution.
- A non-contact, optical temperature sensor could be employed to measure the temperature during microwave pyrolysis to avoid the electromagnetic interference. This might provide a more accurate temperature reading than the thermocouple. Some examples include an infrared pyrometer and fibre optic probe.

8 References

Acierno, D., Barba, A. A. & D'Amore, M. (2004). Heat Transfer Phenomena during Processing Materials with Microwave Energy. *Heat and Mass Transfer/Waerme- und Stoffuebertragung*, 40(5), 413–420.

Antal Jr, M. J., Várhegyi, G. & Jakab, E. (1998). Cellulose Pyrolysis Kinetics: Revisited. *Industrial and Engineering Chemistry Research*, 37(4), 1267–1275.

Araszkiewicz, M., Koziol, A., Lupinska, A. & Lupinski, M. (2007). Microwave Drying of Various Shape Particles Suspended in an Air Stream. *Transport in Porous Media*, 66(1), 173–186.

Babu, B. V. (2008). Biomass Pyrolysis: A State-of-the-Art Review. *Biofuels, Bioproducts and Biorefining*, 2(5), 393–414.

Babu, B. V & Chaurasia, A. S. (2004). Pyrolysis of Biomass: Improved Models for Simultaneous Kinetics and Transport of Heat, Mass and Momentum. *Energy Conversion and Management*, 45(9–10), 1297–1327.

Basu, P. (2010a). *Biomass Gasification and Pyrolysis: Practical Design and Theory*. United States: Academic Press.

Basu, P. (2010b). Chapter 2 – Biomass Characteristics, in: *Biomass Gasification and Pyrolysis*, (pp. 27–63). Massachusetts: Academic Press.

Basu, P. (2010c). Chapter 3 - Pyrolysis and Torrefaction, in: *Biomass Gasification and Pyrolysis*, (pp. 65–96). Massachusetts: Academic Press.

Bauer, L. (2017). Biomass Pyrolysis Comes of Age. *Biofuels Digest*. Retrieved July 30, 2017, from http://www.biofuelsdigest.com/bdigest/2017/06/08/biomass-pyrolysis-comes-of-age/

Beneroso, D., Berm??dez, J. M., Arenillas, A. & Men??ndez, J. A. (2013). Microwave

Pyrolysis of Microalgae for High Syngas Production. *Bioresource Technology*, 144, 240–246.

Bharadwaj, A., Wang, Y., Sridhar, S. & Arunachalam, V. S. (2004). Pyrolysis of Rice Husk. *Current Science*, 87(7), 981–986.

Bridgwater, A. V. (2012). Review of Fast Pyrolysis of Biomass and Product Upgrading. *Biomass and Bioenergy*, 38, 68–94.

Bu, Q., Lei, H., Ren, S., Wang, L., Holladay, J., Zhang, Q., et al. (2011). Phenol and Phenolics from Lignocellulosic Biomass by Catalytic Microwave Pyrolysis. *Bioresource Technology*, 102(13), 7004–7007.

Bu, Q., Lei, H., Ren, S., Wang, L., Zhang, Q., Tang, J., et al. (2012). Production of Phenols and Biofuels by Catalytic Microwave Pyrolysis of Lignocellulosic Biomass. *Bioresource Technology*, 108, 274–279.

Budarin, V. L., Clark, J. H., Lanigan, B. A., Shuttleworth, P., Breeden, S. W., Wilson, A. J., et al. (2009). The Preparation of High-Grade Bio-Oils through the Controlled, Low Temperature Microwave Activation of Wheat Straw. *Bioresource Technology*, 100(23), 6064–6068.

Chamchong, M. & Datta, a K. (1999). Thawing of Foods in a Microwave Oven: II. Effect of Load Geometry and Dielectric Properties. *The Journal of microwave power and electromagnetic energy : a publication of the International Microwave Power Institute*, 34, 22–32.

Chang, S. H. (2014). An Overview of Empty Fruit Bunch from Oil Palm as Feedstock for Bio-Oil Production. *Biomass and Bioenergy*, 62, 174–181.

Chen, M., Wang, J., Zhang, M., Chen, M., Zhu, X., Min, F., et al. (2008). Catalytic Effects of Eight Inorganic Additives on Pyrolysis of Pine Wood Sawdust by

Microwave Heating. *Journal of Analytical and Applied Pyrolysis*, 82(1), 145–150.

Cheng, J. J. (2010). Biological Process for Ethanol Production, in: Cheng, J. (Ed.), *Biomass to Renewable Energy Processes*, (p. 209). Boca Raton: CRC Press.

Childs, N. (2016). Rice Outlook - June 2016. , 7. Retrieved June 22, 2016, from http://www.ers.usda.gov/media/2102912/rice-outlook-june-2016.pdf

Clarke, S. & Preto, F. (2011). Biomass Densification for Energy Production. *Ontario Ministry of Agriculture, Food and Rural Affairs*. Retrieved December 28, 2016, from http://www.omafra.gov.on.ca/english/engineer/facts/11-035.htm

Comsol. (2012). RF Module User's Guide, v4.3. Retrieved January 9, 2017, from https://is.muni.cz/el/1431/podzim2013/F7061/um/RFModuleUsersGuide.pdf

Dai, X., Wu, C., Li, H. & Chen, Y. (2000). The Fast Pyrolysis of Biomass in CFB Reactor. *Energy and Fuels*, 14(3), 552–557.

Daioglou, V., Stehfest, E., Wicke, B., Faaij, A. & van Vuuren, D. P. (2016). Projections of the Availability and Cost of Residues from Agriculture and Forestry. *GCB Bioenergy*, 8(2), 456–470.

Datta, A. K. & Ni, H. (2002). Infrared and Hot-Air-Assisted Microwave Heating of Foods for Control of Surface Moisture. *Journal of Food Engineering*, 51(4), 355–364.

Datta, A. K. & Rakesh, V. (2013). Principles of Microwave Combination Heating. *Comprehensive Reviews in Food Science and Food Safety*, 12(1), 24–39.

Demirbas, A. (2004). Effects of Temperature and Particle Size on Bio-Char Yield from Pyrolysis of Agricultural Residues. *Journal of Analytical and Applied Pyrolysis*, 72(2), 243–248.

Demirbaş, A. (2001). Yields of Hydrogen-Rich Gaseous Products via Pyrolysis from Selected Biomass Samples. *Fuel*, 80(13), 1885–1891.

Department of Energy & Climate Change. (2012). Electricity Generation Costs. , 27. Retrieved July 29, 2016, from https://www.gov.uk/government/uploads/system/uploads/attachment_data/file/65713/6883-electricity-generation-costs.pdf

Diebold, J. P. (1994). A Unified, Global Model for the Pyrolysis of Cellulose. *Biomass and Bioenergy*, 7(1–6), 75–85.

Diebold, J. P. & Czernik, S. (1997). Additives To Lower and Stabilize the Viscosity of Pyrolysis Oils during Storage. *Energy Fuels*, 11(10), 1081–1091.

Doman, L. E. (2016). International Energy Outlook 2016. , 7. Retrieved June 16, 2016, from http://www.eia.gov/forecasts/ieo/pdf/0484(2016).pdf

Domínguez, A., Menéndez, J. A. A., Inguanzo, M. & Pis, J. J. J. (2005). Investigations into the Characteristics of Oils Produced from Microwave Pyrolysis of Sewage Sludge. *Fuel Processing Technology*, 86(9), 1007–1020.

Domínguez, A., Menéndez, J. A., Fernández, Y., Pis, J. J., Nabais, J. M. V, Carrott, P. J. M., et al. (2007). Conventional and Microwave Induced Pyrolysis of Coffee Hulls for the Production of a Hydrogen Rich Fuel Gas. *Journal of Analytical and Applied Pyrolysis*, 79(1–2 SPEC. ISS.), 128–135.

Du, J., Liu, P., Liu, Z., Sun, D. & Tao, C. (2010). Fast Pyrolysis of Biomass for Bio-Oil with Ionic Liquid and Microwave Irradiation. *Journal of Fuel Chemistry and Technology*, 38(5), 554–559.

Du, Z., Li, Y., Wang, X., Wan, Y., Chen, Q., Wang, C., et al. (2011). Microwave-Assisted Pyrolysis of Microalgae for Biofuel Production. *Bioresource Technology*, 102(7), 4890–4896.

Engineering, O. (2017). Thermocouple Response Time. *Omega Engineering*. Retrieved

January 17, 2017, from http://www.omega.com/techref/ThermocoupleResponseTime.html

Fahmi, R., Bridgwater, A. V., Darvell, L. I., Jones, J. M., Yates, N., Thain, S., et al. (2007). The Effect of Alkali Metals on Combustion and Pyrolysis of Lolium and Festuca Grasses, Switchgrass and Willow. *Fuel*, 86(10–11), 1560–1569.

Fernandez, Y., Arenillas, A. & Menendez, J. A. (2011). Microwave Heating Applied to Pyrolysis (S. Grundas, Ed.). *Advances in Induction and Microwave Heating of Minerals and Organic Materials*.

Ferrera-Lorenzo, N., Fuente, E., Bermúdez, J. M., Suárez-Ruiz, I. & Ruiz, B. (2014). Conventional and Microwave Pyrolysis of a Macroalgae Waste from the Agar–Agar Industry. Prospects for Bio-Fuel Production. *Bioresource Technology*, 151, 199–206.

Geedipalli, S. S. R., Rakesh, V. & Datta, A. K. (2007). Modeling the Heating Uniformity Contributed by a Rotating Turntable in Microwave Ovens. *Journal of Food Engineering*, 82(3), 359–368.

Hoogwijk, M., Faaij, A., van den Broek, R., Berndes, G., Gielen, D. & Turkenburg, W. (2003). Exploration of the Ranges of the Global Potential of Biomass for Energy. *Biomass and Bioenergy*, 25(2), 119–133.

Horne, P. A. & Williams, P. T. (1996). Influence of Temperature on the Products from the Flash Pyrolysis of Biomass. *Fuel*, 75(9), 1051–1059.

Hu, Z., Ma, X. & Chen, C. (2012). A Study on Experimental Characteristic of Microwave-Assisted Pyrolysis of Microalgae. *Bioresource Technology*, 107, 487–493.

Huang, Y. F., Kuan, W. H., Lo, S. L. & Lin, C. F. (2008). Total Recovery of Resources and Energy from Rice Straw Using Microwave-Induced Pyrolysis. *Bioresource*

Technology, 99(17), 8252–8258.

India Brand Equity Foundation. (2016). Steel Industry in India. *India Brand Equity Foundation*. Retrieved July 27, 2016, from http://www.ibef.org/industry/steel.aspx

Jahirul, M., Rasul, M., Chowdhury, A. & Ashwath, N. (2012). Biofuels Production through Biomass Pyrolysis —A Technological Review. *Energies*, 5(12), 4952–5001.

Jalan, R. K. & Srivastava, V. K. (1999). Studies on Pyrolysis of a Single Biomass Cylindrical Pellet—kinetic and Heat Transfer Effects. *Energy Conversion and Management*, 40(5), 467–494.

Jameel, H., Keshwani, D. R., Carter, S. F. & Treasure, T. H. (2010). Thermochemical Conversion of Biomass to Power and Fuels, in: Cheng, J. J. (Ed.), *Biomass to Renewable Energy Processes*, (pp. 437–490). Boca Raton: CRC Press.

Jenkins, B. ., Baxter, L. ., Miles, T. . & Miles, T. . (1998). Combustion Properties of Biomass. *Fuel Processing Technology*, 54(1), 17–46.

Krieger-Brockett, B. (1994). Microwave Pyrolysis of Biomass. *Research of Chemical Intermediates*, 20(1), 39–49.

Kurniawan, H., Alapati, S. & Che, W. S. (2015). Effect of Mode Stirrers in a Multimode Microwave-Heating Applicator with the Conveyor Belt. *International Journal of Precision Engineering and Manufacturing-Green Technology*, 2(1), 31–36.

Lam, S. S., Russell, A. D., Lee, C. L. & Chase, H. A. (2012). Microwave-Heated Pyrolysis of Waste Automotive Engine Oil: Influence of Operation Parameters on the Yield, Composition, and Fuel Properties of Pyrolysis Oil. *Fuel*, 92(1), 327–339.

Lehto, J., Oasmaa, A., Solantausta, Y., Kytö, M. & Chiaramonti, D. (2014). Review of Fuel Oil Quality and Combustion of Fast Pyrolysis Bio-Oils from Lignocellulosic Biomass. *Applied Energy*, 116, 178–190.

Lei, H., Ren, S. & Julson, J. (2009). The Effects of Reaction Temperature and Time and Particle Size of Corn Stover on Microwave Pyrolysis. *Energy and Fuels*, 23(11), 3254–3261.

Lei, H., Ren, S., Wang, L., Bu, Q., Julson, J., Holladay, J., et al. (2011). Microwave Pyrolysis of Distillers Dried Grain with Solubles (DDGS) for Biofuel Production. *Bioresource Technology*, 102(10), 6208–6213.

Leonelli, C. & Veronesi, P. (2015). Chapter 2: Microwave Reactors for Chemical Synthesis and Biofuels Preparation, in: *Production of Chemicals and Biofuels with Microwave*, (pp. 17–40). Springer Science + Business Media Dordrecht.

Li, C. & Suzuki, K. (2009). Tar Property, Analysis, Reforming Mechanism and Model for Biomass Gasification-An Overview. *Renewable and Sustainable Energy Reviews*, 13(3), 594–604.

Li, X. T., Grace, J. R., Lim, C. J., Watkinson, A. P., Chen, H. P. & Kim, J. R. (2004). Biomass Gasification in a Circulating Fluidized Bed. *Biomass and Bioenergy*, 26(2), 171–193.

Lim, J. S., Abdul Manan, Z., Wan Alwi, S. R. & Hashim, H. (2012). A Review on Utilisation of Biomass from Rice Industry as a Source of Renewable Energy. *Renewable and Sustainable Energy Reviews*, 16(5), 3084–3094.

Long, J., Song, H., Jun, X., Sheng, S., Lun-shi, S., Kai, X., et al. (2012). Release Characteristics of Alkali and Alkaline Earth Metallic Species during Biomass Pyrolysis and Steam Gasification Process. *Bioresource Technology*, 116, 278–284.

Van Loo, S. & Koppejan, J. (2008). *The Handbook of Biomass Combustion and Co-Firing* (S. Van Loo and J. Koppejan, Eds.). London: Earthscan.

Lua, A. C. & Guo, J. (1998). Preparation and Characterization of Chars from Oil Palm

Waste. *Carbon*, 36(11), 1663–1670.

Malaysian Palm Oil Berhad. (2015). Oil Palm Planted Area by State. Retrieved June 21, 2016, from http://bepi.mpob.gov.my/images/area/2015/Area_summary.pdf

McKendry, P. (2002). Energy Production from Biomass (Part 1): Overview of Biomass. *Bioresource Technology*, 83(1), 37–46.

Menéndez, J. A., Arenillas, A., Fidalgo, B., Fernández, Y., Zubizarreta, L., Calvo, E. G., et al. (2010). Microwave Heating Processes Involving Carbon Materials. *Fuel Processing Technology*, 91(1), 1–8.

Miura, M., Kaga, H., Sakurai, A., Kakuchi, T. & Takahashi, K. (2004). Rapid Pyrolysis of Wood Block by Microwave Heating. *Journal of Analytical and Applied Pyrolysis*, 71(1), 187–199.

Mohan, D., Pittman, C. U. & Steele, P. H. (2006). Pyrolysis of Wood/Biomass for Bio-Oil: A Critical Review. *Energy & Fuels*, 20(3), 848–889.

Motasemi, F. & Afzal, M. T. (2013). A Review on the Microwave-Assisted Pyrolysis Technique. *Renewable and Sustainable Energy Reviews*, 28, 317–330.

Mushtaq, F., Abdullah, T. A. T., Mat, R. & Ani, F. N. (2015). Optimization and Characterization of Bio-Oil Produced by Microwave Assisted Pyrolysis of Oil Palm Shell Waste Biomass with Microwave Absorber. *Bioresource Technology*, 190, 442–450.

Namazi, A. B., Allen, D. G. & Jia, C. Q. (2016). Benefits of Microwave Heating Method in Production of Activated Carbon. *Canadian Journal of Chemical Engineering*, 94(7), 1262–1268.

Natarajan, E. & Ganapathy, S. E. (2009). Pyrolysis of Rice Husk in a Fixed Bed Reactor. *World Acedemy of Science, Engineering and Technolgy*, 3(8), 467–471.

Neves, D., Thunman, H., Matos, A., Tarelho, L. & G??mez-Barea, A. (2011). Characterization and Prediction of Biomass Pyrolysis Products. *Progress in Energy and Combustion Science*, 37(5), 611–630.

New York State Energy Research and Development Authority. (2017). Hydrogen Production-Steam Methane Reforming. *Hydrogen Fact Sheet*. Retrieved January 23, 2017, from www.amiqweb.es/app/download/.../6hydrogenproductionsteammethanereforming.pdf

Nowakowski, D. J., Jones, J. M., Brydson, R. M. D. & Ross, A. B. (2007). Potassium Catalysis in the Pyrolysis Behaviour of Short Rotation Willow Coppice. *Fuel*, 86(15), 2389–2402.

Olsson, J. G., Ja, U. & Pettersson, J. B. C. (1997). Alkali Metal Emission during Pyrolysis of Biomass. *Energy & Fuels*, 11(7), 779–784.

Omar, R., Idris, A., Yunus, R., Khalid, K. & Aida Isma, M. I. (2011). Characterization of Empty Fruit Bunch for Microwave-Assisted Pyrolysis. *Fuel*, 90(4), 1536–1544.

Onay, O. & Kockar, O. M. (2003). *Slow, Fast and Flash Pyrolysis of Rapeseed*.

Van Paasen, S. V. B., Kiel, J. H. A. & Biomass, E. (2004). Tar Formation in a Fluidised-Bed Gasifier: Impact of Fuel Properties and Operating Conditions. Retrieved June 15, 2016, from https://www.ecn.nl/docs/library/report/2004/c04013.pdf

Pavia, D. L., Lampman, G. M., Kriz, G. S. & Vyvyan, J. R. (2009). Infrared Spectroscopy, in: *Introduction to Spectroscopy*, (pp. 15–73). California: Brooks/Cole Cengage Learning.

Pedreño-Molina, J. L., Monzó-Cabrera, J. & Catalá-Civera, J. M. (2007). Sample Movement Optimization for Uniform Heating in Microwave Heating Ovens.

International Journal of RF and Microwave Computer-Aided Engineering, 17(2), 142–152.

Peyre, F., Datta, A. & Seyler, C. (1997). Influence of the Dielectric Property on Microwave Oven Heating Patterns: Application to Food Materials. *The Journal of microwave power and electromagnetic energy : a publication of the International Microwave Power Institute*, 32(1), 3–15.

Pitchai, K., Chen, J., Birla, S., Jones, D., Gonzalez, R. & Subbiah, J. (2015). Multiphysics Modeling of Microwave Heating of a Frozen Heterogeneous Meal Rotating on a Turntable. *Journal of Food Science*, 80(12).

Plaza-González, P., Monzó-Cabrera, J., Catalá-Civera, J. M. & Sánchez-Hernández, D. (2004). New Approach for the Prediction of the Electric Field Distribution in Multimode Microwave-Heating Applicators with Mode Stirrers. *IEEE Transactions on Magnetics*, 40(3), 1672–1678.

Popescu, S., Misawa, T., Ohtsu, Y., Fujita, H. & Sanematsu, S. (2008). New Microwave Reactor for Paper-Based Waste Neutralization. *Resources, Conservation and Recycling*, 52(4), 671–677.

Pyle, D. L. & Zaror, C. A. (1984). Heat Transfer and Kinetics in the Low Temperature Pyrolysis of Solids. *Chemical Engineering Science*, 39(1), 147–158.

QM Consultants. (2016). Empty Fruit Bunch (EFB). Retrieved June 22, 2016, from http://qmconsultants.com.my/?page_id=395

Raveendran, K., Ganesh, A. & Khilar, K. C. (1996). Pyrolysis Characteristics of Biomass and Biomass Components. *Fuel*, 75(8), 987–998.

Ren, S., Lei, H., Wang, L., Bu, Q., Chen, S., Wu, J., et al. (2012). Biofuel Production and Kinetics Analysis for Microwave Pyrolysis of Douglas Fir Sawdust Pellet. *Journal*

of Analytical and Applied Pyrolysis, 94, 163–169.

Riedewald, F. & Sousa-Gallagher, M. (2016). Technological and Economical Feasibility of a 40,000 T/y Tyre Pyrolysis Plant: Results of a H2020 SME Phase 1 Study. Retrieved July 30, 2017, from http://crlltd.com/wp-content/uploads/2016/05/09-Tyre-presentation-ETRA-2016.pdf

Robinson, J. P., Kingman, S. W., Snape, C. E., Bradshaw, S. M., Bradley, M. S. A., Shang, H., et al. (2010). Scale-up and Design of a Continuous Microwave Treatment System for the Processing of Oil-Contaminated Drill Cuttings. *Chemical Engineering Research and Design*, 88(2), 146–154.

Saidur, R., Abdelaziz, E. A., Demirbas, A., Hossain, M. S. & Mekhilef, S. (2011). A Review on Biomass as a Fuel for Boilers. *Renewable and Sustainable Energy Reviews*, 15(5), 2262–2289.

Salema, A. A. & Afzal, M. T. (2015). Numerical Simulation of Heating Behaviour in Biomass Bed and Pellets under Multimode Microwave System. *International Journal of Thermal Sciences*, 91(0), 12–24.

Salema, A. A. & Ani, F. N. (2011). Microwave Induced Pyrolysis of Oil Palm Biomass. *Bioresource Technology*, 102(3), 3388–3395.

Salema, A. A. & Ani, F. N. (2012). Pyrolysis of Oil Palm Empty Fruit Bunch Biomass Pellets Using Multimode Microwave Irradiation. *Bioresource Technology*, 125, 102–107.

Shafizadeh, F. (1982). Introduction to Pyrolysis of Biomass. *Journal of Analytical and Applied Pyrolysis*, 3(4), 283–305.

Sheng, C. & Azevedo, J. L. T. (2005). Estimating the Higher Heating Value of Biomass Fuels from Basic Analysis Data. *Biomass and Bioenergy*, 28(5), 499–507.

Stern, N. (2006). STERN REVIEW: The Economics of Climate Change. , 4. Retrieved August 8, 2016, from http://webarchive.nationalarchives.gov.uk/20130129110402/http://www.hm-treasury.gov.uk/media/9/9/CLOSED_SHORT_executive_summary.pdf

Stylus. (2016). Rice Husk Electrodes. Retrieved June 22, 2016, from http://www.stylus.com/ccfflh

Sutton, D., Kelleher, B. & Ross, J. R. H. H. (2001). Review of Literature on Catalysts for Biomass Gasification. *Fuel Processing Technology*, 73(3), 155–173.

The Swedish Bioenergy Association. (2016). Bioenergy Facts. *The Swedish Bioenergy Association*. Retrieved July 19, 2016, from https://www.svebio.se/english/bioenergy-facts

The World Bank. (2016). CO2 Emissions (Kt). *The World Bank*. Retrieved July 27, 2016, from http://data.worldbank.org/indicator/EN.ATM.CO2E.KT

Tian, Y., Zuo, W., Ren, Z. & Chen, D. (2011). Estimation of a Novel Method to Produce Bio-Oil from Sewage Sludge by Microwave Pyrolysis with the Consideration of Efficiency and Safety. *Bioresource Technology*, 102(2), 2053–2061.

Tripathi, M., Sahu, J. N., Ganesan, P. & Dey, T. K. (2015). Effect of Temperature on Dielectric Properties and Penetration Depth of Oil Palm Shell (OPS) and OPS Char Synthesized by Microwave Pyrolysis of OPS. *Fuel*, 153, 257–266.

U.S Energy Information Administration. (2016). What Drives Crude Oil Prices? Retrieved July 28, 2016, from https://www.eia.gov/finance/markets/spot_prices.cfm

United Nations Environment Programme. (2016). Climate Change Mitigation : Energy. Retrieved June 15, 2016, from http://www.unep.org/climatechange/mitigation/Energy/tabid/104339/Default.aspx

United Nations Framework Convention on Climate Change. (2014a). Global Warming Potentials. *UNFCC*, 2014. Retrieved July 27, 2016, from http://unfccc.int/ghg_data/items/3825.php

United Nations Framework Convention on Climate Change. (2014b). Kyoto Protocol. Retrieved August 8, 2016, from http://unfccc.int/kyoto_protocol/items/2830.php

United States Department of Agriculture. (2016). China on the Path to Become Major Peanut Importer. , 1–36. Retrieved June 21, 2016, from http://apps.fas.usda.gov/psdonline/circulars/oilseeds.pdf

Varhegyi, G. & Jakab, E. (1994). Is the Broido-Shafizadeh Model for Cellulose Pyrolysis True? - Energy & Fuels (ACS Publications). *Energy & Fuels*.

Vassilev, S. V., Baxter, D., Andersen, L. K. & Vassileva, C. G. (2010). An Overview of the Chemical Composition of Biomass. *Fuel*, 89(5), 913–933.

Vilayannur, R. S., Puri, V. M. & Anantheswaran, R. C. (1998). Size and Shape Effect on Nonuniformity of Temperature and Moisture Distributions in Microwave Heated Food Materials: Part1 Simulation. *Journal of Food Process Engineering*, 21(3), 209–233.

Wan, Y., Chen, P., Zhang, B., Yang, C., Liu, Y., Lin, X., et al. (2009). Microwave-Assisted Pyrolysis of Biomass: Catalysts to Improve Product Selectivity. *Journal of Analytical and Applied Pyrolysis*, 86(1), 161–167.

Wang, X. H., Chen, H. P., Ding, X. J., Yang, H. P., Zhang, S. H. & Shen, Y. Q. (2009). Properties of Gas and Char from Microwave Pyrolysis of Pine Sawdust. *BioResources*, 4(3), 946–959.

White, J. E., Catallo, W. J. & Legendre, B. L. (2011). Biomass Pyrolysis Kinetics: A Comparative Critical Review with Relevant Agricultural Residue Case Studies.

Journal of Analytical and Applied Pyrolysis, 91(1), 1–33.

Williams, P. T. & Horne, P. A. (1994). The Role of Metal Salts in the Pyrolysis of Biomass. *Renewable Energy*, 4(1), 1–13.

Yang, H., Yan, R., Chen, H., Lee, D. H., Liang, D. T. & Zheng, C. (2006). Pyrolysis of Palm Oil Wastes for Enhanced Production of Hydrogen Rich Gases. *Fuel Processing Technology*, 87(10), 935–942.

Yang, H., Yan, R., Chen, H., Zheng, C., Lee, D. H. & Liang, D. T. (2006). Influence of Mineral Matter on Pyrolysis of Palm Oil Wastes. *Combustion and Flame*, 146(4), 605–611.

Yin, C. (2012). Microwave-Assisted Pyrolysis of Biomass for Liquid Biofuels Production. *Bioresource Technology*, 120, 273–284.

Yu, F., Deng, S., Chen, P., Liu, Y., Wan, Y., Olson, A., et al. (2007). Physical and Chemical Properties of Bio-Oils from Microwave Pyrolysis of Corn Stover, in: *Applied Biochemistry and Biotechnology*, (pp. 957–970).

Yu, F., Steele, P. H. & Ruan, R. (2010). Microwave Pyrolysis of Corn Cob and Characteristics of the Pyrolytic Chars. *Energy Sources, Part A: Recovery, Utilization and Environmental Effects*, 32(5), 475–484.

Zhang, H. & Datta, A. K. (2005). Heating Concentrations of Microwaves in Spherical and Cylindrical Foods. *Food and Bioproducts Processing*, 83(1), 6–13.

Zhao, X., Wang, M., Liu, H., Li, L., Ma, C. & Song, Z. (2012). A Microwave Reactor for Characterization of Pyrolyzed Biomass. *Bioresource Technology*, 104(0), 673–678.

Zhao, X., Zhang, J., Song, Z., Liu, H., Li, L. & Ma, C. (2011). Microwave Pyrolysis of Straw Bale and Energy Balance Analysis. *Journal of Analytical and Applied Pyrolysis*, 92(1), 43–49.

Zhou, J., Xu, W., You, Z., Wang, Z., Luo, Y., Gao, L., et al. (2016). A New Type of Power Energy for Accelerating Chemical Reactions: The Nature of a Microwave-Driving Force for Accelerating Chemical Reactions. , 6, 25149.